

# Inter-city infections and the role of size heterogeneity in containment strategies

Viktor Bezborodov <sup>\*</sup> Tyll Krueger <sup>†</sup> Cornelia Pokalyuk <sup>‡</sup> Piotr Szymański <sup>§</sup>  
Aurélien Velleret <sup>¶</sup>

## Abstract

This study examines the effectiveness of regional lockdown strategies in mitigating pathogen spread across regional units, termed cities hereinafter. We develop simplified models to analyze infection spread across cities within a country during an epidemic wave. Isolation of a city is initiated when infection numbers within the city surpass defined thresholds. We compare two strategies: strategy ( $P$ ) consists in prescribing thresholds proportionally to city sizes, while the same threshold is used for all cities under strategy ( $U$ ). Given the heavy-tailed distribution of city sizes, strategy ( $P$ ) may result in more secondary infections from larger cities than strategy ( $U$ ).

Random graph models are constructed to represent infection spread as a percolation process. In particular, we consider a model in which mobility between cities only depends on city sizes. We assess the relative efficiency of the two strategies by comparing the ratios of the number of individuals under isolation to the total number of infections by the end of the epidemic wave under strategy ( $P$ ) and ( $U$ ). Additionally, we derive analytical formulas for disease prevalence and basic reproduction numbers.

Our models are calibrated using mobility data from France, Poland and Japan, validated through simulation. The findings indicate that mobility between cities in France and Poland

---

<sup>\*</sup>Wrocław University of Science and Technology, Faculty of Information and Communication Technology, ul. Janiszewskiego 11/17, 50-372 Wrocław, Poland; E-mail: [viktor.bezborodov@pwr.edu.pl](mailto:viktor.bezborodov@pwr.edu.pl)

<sup>†</sup>Wrocław University of Science and Technology, Faculty of Information and Communication Technology, ul. Janiszewskiego 11/17, 50-372 Wrocław, Poland; E-mail: [tyll.krueger@pwr.edu.pl](mailto:tyll.krueger@pwr.edu.pl)

<sup>‡</sup>University of Lübeck, Institute for Mathematics, Ratzeburger Allee 160, D-23562, Lübeck, Germany; E-mail: [cornelia.pokalyuk@uni-luebeck.de](mailto:cornelia.pokalyuk@uni-luebeck.de)

<sup>§</sup>Wrocław University of Science and Technology, Department of Computational Intelligence, Wrocław, Poland; E-mail: [piotr.szymanski@pwr.edu.pl](mailto:piotr.szymanski@pwr.edu.pl)

<sup>¶</sup>Université Paris-Saclay, Université d'Evry Val d'Essonne, CNRS, LaMME, UMR 8071 91037 Evry, France; E-mail: [aurelien.velleret@nsup.org](mailto:aurelien.velleret@nsup.org), corresponding author

is mainly determined by city sizes. However, a poor fit was observed with Japanese data, highlighting the importance to include other factors like e.g. geography for some countries in modeling. Our analysis suggest similar effectiveness for both strategies in France and Japan, while strategy ( $U$ ) demonstrates distinct merits in Poland.

**Keywords:** Epidemic spreading; Stochastic processes; SIR epidemic model; Random graphs; Containment strategies; Transportation networks; Lockdowns.

**AMS Subject Classification:** 92D30, 05C80, 05C82, 60J80, 60G55

## 1 Introduction

The spread of Sars-CoV-2 in early 2020 and the subsequent invasions of more pathogenic mutants of the original strain made the necessity of effective methods to control a pandemic strikingly clear. Since neither drugs nor vaccines were available at the beginning of the pandemic, non-pharmaceutical interventions were arranged to restrict contacts between infected and uninfected individuals and slow down the pace of the epidemic.

In China and New Zealand with regional containment strategies the first epidemic wave could essentially be stopped, Maier and Brockmann (2020). These countries followed so called zero-COVID strategies where a regional lockdown was already imposed when only a small number of individuals got infected. For example in China, the application of this strategy resulted in approximately 60 million people (the residents of Hubei province) being under a very strict lockdown during the first wave in 2020, see Wilder-Smith and Freedman (2020). Some precaution measures, like mandatory mask wearing and certain social distancing controls, were in addition applied outside Hubei province, partially even if there were no detected cases.

In Europe many countries coupled the level of regional, non-pharmaceutical interventions to relative incidences calculated from the daily number of individuals tested positive in counties, see e.g. Jarvis et al. (2021) and Bundesregierung (Hrsg.) for respective rules in England and Germany and Hale et al. (2021) for a general overview on the pandemic policies applied in different countries. These strategies have been only partially successful and quickly ended in national lockdowns.

In general, population sizes differ greatly between counties. Heavy-tailed distributions, like the Zipf law or a log-normal distribution, fit very well the distribution of the county population sizes for many countries, for France, Poland and Japan see e.g. Figure 1. As a consequence, when mitigation strategies are based on relative incidences, many individuals need to be tested positive in counties with large population sizes until measures are applied, while sizes thresholds for interventions are already exceeded in counties with small population when only a relatively small number of individuals gets tested positive. This is particularly problematic, since pathogens often start to spread first within metropolitan areas with large population sizes and only afterwards hit the rural countryside which typically

## Estimation of the power-law coefficient

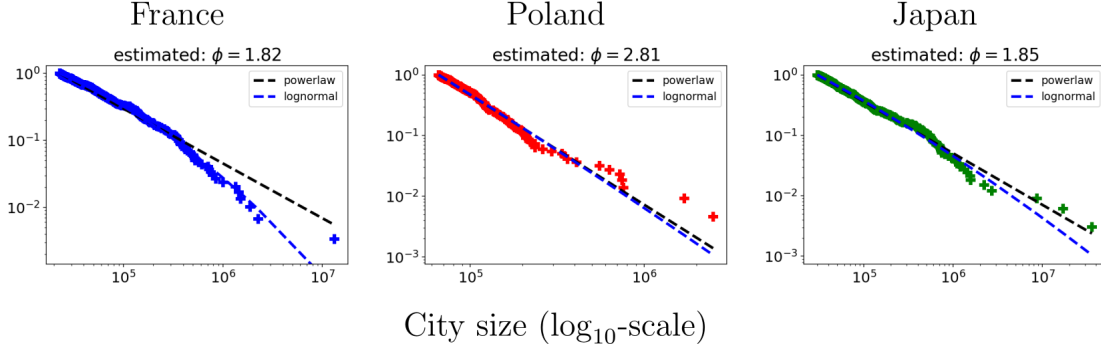


Figure 1: Heavy-tailed distributions were fitted to the size distributions of areas of attraction in France and Poland as well as of prefectures in Japan.

make up counties with relatively small or intermediate population sizes, see for example for the initial spread of COVID-19 in the US Stier et al. (2020).

To compare the consequences of the two types of mitigation strategies applied during the COVID-19 pandemic, we consider in this paper two different criteria at which interventions are imposed, either when a certain fixed number (later called strategy ( $U$ )) or when a certain proportion of individuals (later called strategy ( $P$ )) gets tested positive in a regional unit, from now on called city.

Specifying thresholds that are determined solely by city sizes is not merely a simplification for modeling purposes; it mirrors the actual measures implemented during the COVID-19 pandemic (e.g. in Germany and New Zealand), where authorities often relied on city population metrics to guide intervention strategies. Such a choice was driven more by the convenience of implementing them on a national scale instead of being based on a firm basis for their superiority in regulating propagation.

We build a simplified model in which cities are represented as the vertices of a random graph. We only follow the spread of the infection between cities and not within a city. The infection spreads according to a SIR model between cities in the sense that each city can participate in the epidemic only once and is isolated (put under lockdown) till the end of the epidemic after a certain number of citizens get infected. A description of preventive measures in this way greatly simplifies the analysis. Even though complete isolation of a city is a rather extreme scenario, it is a common pattern that the spread of an arising pathogen occurs in waves. Successive waves may occur if preventive measures are applied that slow down pathogen propagation and/or if the newly arising pathogen causes at least temporal immunity. Here, we consider a single wave and for simplicity approximate this wave by a SIR-process.

From an infected city, the disease is transmitted to other cities depending on the connectivity between the cities. We consider here two model variants, which we term transportation graph (abbreviated as TG) and kernel graph (abbreviated as KG) in the following. For the transportation graph, for each pair of cities  $(i, j)$  the probability of transmitting the disease from city  $i$  to city  $j$  is based on the strength of mobility from city  $i$  to city  $j$ . We estimate the strength of mobility between pairs of cities for France, Poland and Japan using commuting data from these countries. For the kernel graph we simplify the model further. We assume that the transmission probability of the infection from city  $i$  to city  $j$  depends only on the sizes  $x_i$  and  $x_j$  of the two cities. More precisely, we assume that the transmission probability can be expressed in terms of a kernel function  $\kappa_{a,b}(x_i, x_j)$  with parameters  $a$  and  $b$ . This function  $\kappa_{a,b}$  expresses the (country-wide) relationship between the size of a city and the probability of traveling to and out of that city. The parameters  $a$  and  $b$  are estimated for France, Japan and Poland, with commuting data from these countries (as for the transportation graph).

A primary objective of this study is to compare the effectiveness of the two regulation strategies and also to judge the adequacy of model reduction in this scope. We measure the effectiveness of a strategy by calculating the number of people subject to isolation in relation to a prescribed number of individuals affected by the disease. The smaller this ratio the more efficient the strategy, since less persons need to be isolated. We analytically benchmark the two containment strategies ( $U$ ) and ( $P$ ) against each other in the scenario where cities have an equal chance of being contaminated by infected visitors or by inhabitants who got infected during travel (corresponding to the parameter choice  $a = 1 + b$ ). In that case, we can determine under reasonable and simple conditions on the parameters which strategy performs best when assuming that the numbers of individuals who get infected are under both strategies the same, see Section 4.3. In the general case, we calculate numerically the theoretical infection probabilities to compare the two strategies.

We, surprisingly, find that, according to the estimated best fit parameters for France and Japan, both strategies perform almost equally well, while strategy ( $U$ ) is preferred over strategy ( $P$ ) for Poland. To validate our approximation of the empirical mobility matrix by an (at most) rank-2- kernel matrix, we simulated epidemics according to the fitted kernel model as well as with the fitted TG model. When comparing for the two types of simulations several statistics like the probability that a city gets during an epidemic infected or the probability that a city of a certain size generates an outbreak, we find overall for France a pretty large correspondence. For Poland, the correspondence is in general weaker. For Japan, pretty large difference can be observed. A possible explanation could be that the geographic structure between the cities of Japan plays a significant role, which is neglected in the kernel model.

Before we introduce our model in detail in Section 3 we give an overview of our key findings, summarize the essential insights and illustrate them with simulations.



## 2 Overview on the main results

By presenting several key findings in this section, we aim at emphasizing some essential take-aways without requiring the reader to engage with the underlying mathematical framework or the data calibration processes, which will be described in the subsequent sections.

As mentioned in the introduction we build simplifying models that mimic the spread of an infection between cities, see Section 3 for details. The epidemic spread is encoded by a directed random graph, termed the epidemic graph, where the nodes of the graph are the cities. The set of cities that would eventually get infected if an infection process starts in city  $i$  is given by the forward connected component of city  $i$ , which is the set of cities  $j$  for which there is a directed path going from  $i$  to  $j$ .

The probability for an edge between city  $i$  and  $j$  to be present in this graph depends essentially on two quantities: the number of individuals that get infected in city  $i$  (from its infection till its isolation) and the travel from city  $i$  to city  $j$  and back.

We consider two city isolation strategies, reflecting different criteria on the number of people infected in the city before the lockdown is implemented. Under strategy  $(U)$ , the number of people that get infected in an infected city is for all cities the same. Under strategy  $(P)$ , the number of infected persons is proportional to the city size. So we assume that the number of infected individuals in an infected city until isolation is in total  $L(x) = L$  under strategy  $(U)$  and  $L(x) = px$  under strategy  $(P)$ .

Each infected person (from city  $i$ ) can directly transmit the disease to city  $j$  by traveling there and infecting citizens of that city. On the other hand people from city  $j$  can catch the disease in city  $i$  during travel, when meeting an infected person. We use commuting data to estimate the number of individuals traveling from city  $i$  to city  $j$  and back and store this information in a matrix  $(M_{i,j})_{i,j}$ . So if city  $i$  is infected the number of individuals bringing the disease to city  $j$  is on average

$$k_C \frac{L(x_i)}{x_i} (M_{i,j} + M_{j,i}) \quad (1)$$

where  $k_C$  is reflecting the intensity of travel, contact and virulence of the pathogen. The first summand is accounting for infected citizens from city  $i$  who travel to city  $j$  and the second summand for citizens from city  $j$  who travel to city  $i$  and contract the disease from infected individuals there.

Whenever epidemic graphs are based on matrices  $(M_{i,j})_{i,j}$  which respect the pairwise estimates of mobility between cities, we call them transportation graphs (TG, for short), see also Section 3 and in particular Subsection 3.1.1.

Infection processes based on transportation graphs can be simulated, but they are in general too complex to be analyzed theoretically. Hence, we reduce the model further by assuming that the travelling probabilities to and from a city both depend only on the city size. In Figure 2, inbound and outbound travel counts are plotted for France, Poland and

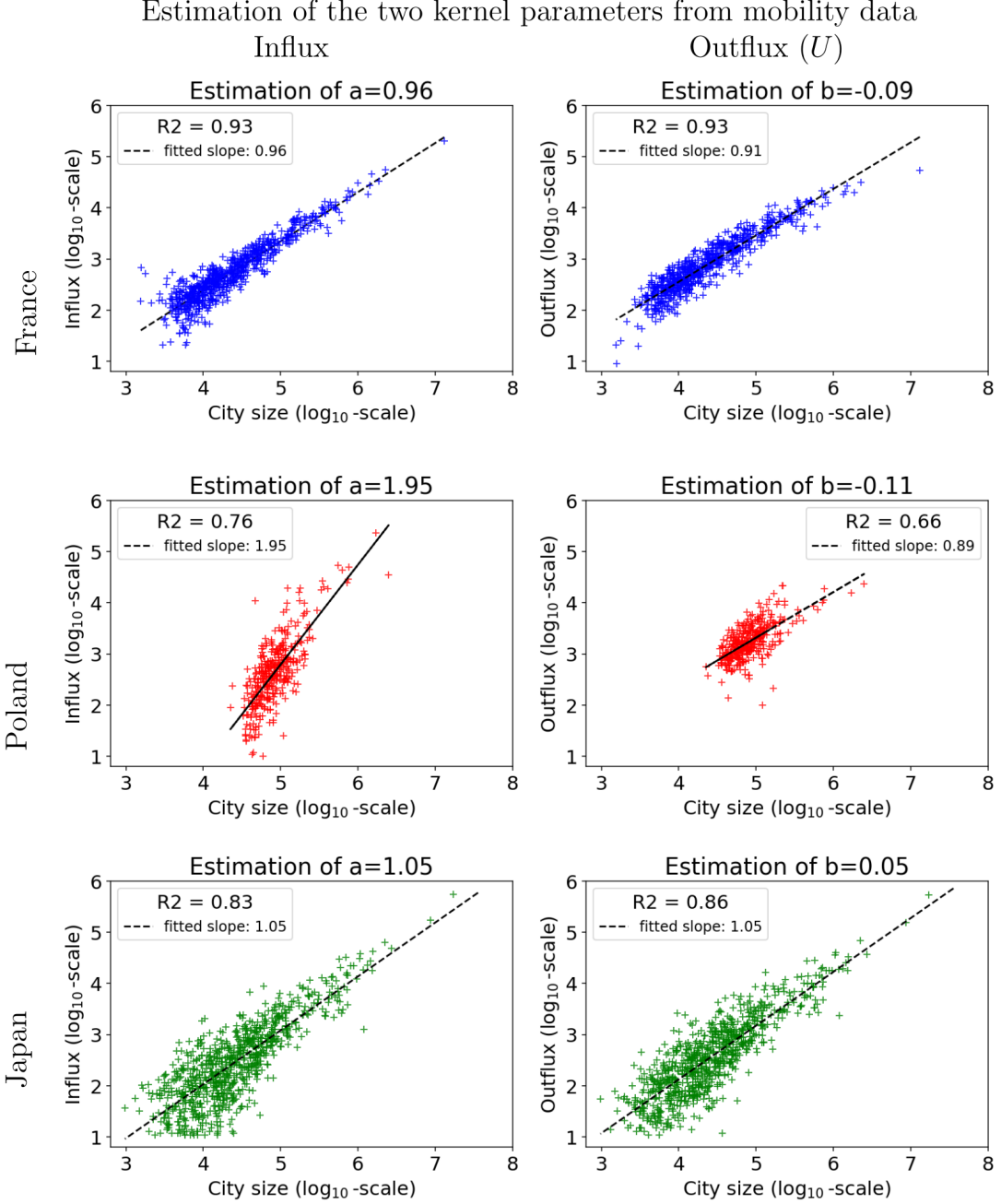


Figure 2: Inbound travel counts (left column) and outbound travel counts for the estimation of  $a$  and  $b$ , resp., for France, Poland and Japan.

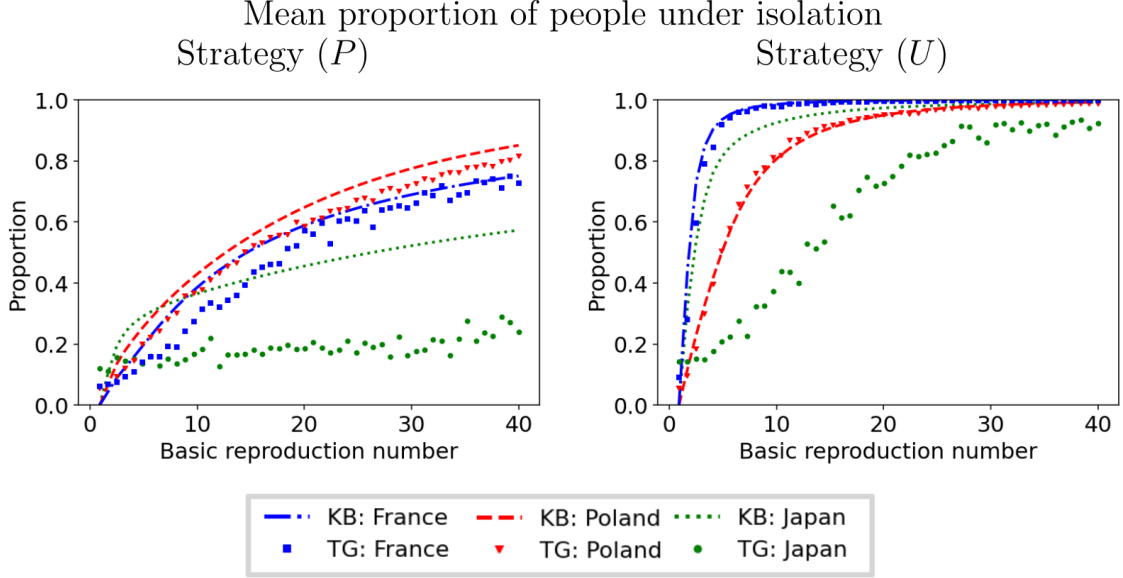


Figure 3: Comparison of the mean TG and KB proportions of people under isolation depending on the basic reproduction number. Dashed lines show proportions when simulations are performed according to the transportation graph (TG), and scatter plots when proportions are calculated with KB approximations, for France (in blue), Poland (in red) and Japan (in green), under strategy ( $P$ ) on the left and strategy ( $U$ ) on the right.

Japan. We see in these plots that it is very natural to consider in the kernel a power-law relation between inbound travels and city size and similarly for the relation between outbound travels and city size. We thus consider mobility matrices of the form

$$M_{i,j} = k_M x_i^{1+b} x_j^a,$$

for some  $a, b \in \mathbb{R}$  and some constant  $k_M$ , scaling the traveling intensity appropriately. Here  $x_i^b$  is (asymptotically) proportional to the probability that an individual of city  $i$  leaves the city (when the city is infected) and  $x_j^a$  is (asymptotically) proportional to the probability that an individual that is traveling chooses city  $j$  as a destination. So the average number of people that are traveling from city  $i$  to a city  $j$  is (asymptotically) proportional to  $x_i x_i^b x_j^a = x_i^{1+b} x_j^a$ .

The chosen kernel greatly synthesizes the migration data. The two parameters  $a$  and  $b$  can be estimated separately from respectively the inbound and the outbound travel counts, as presented in Figure 2. We call the epidemic graphs that are based on this model kernel graph (KG, for short).

We use branching process approximations to analyze the probability that a city gets infected during a (large) outbreak (in the following termed infection probability) and the probability that a city initiates an outbreak (in the following termed outbreak probability), see Sections 4.1 and 4.2 for more details. On the basis of these probabilities, we compare the efficiency of the two strategies ( $U$ ) and ( $P$ ), see Section 4.3 for the criterion. In the case where  $a = b + 1$ , we find that Strategy ( $U$ ) is more effective than Strategy ( $P$ ) if  $a > 1$ , that strategies ( $U$ ) and ( $P$ ) perform equally well if  $a = 1$  (and  $b = 0$ ) and that Strategy ( $P$ ) outperforms Strategy ( $U$ ) otherwise, see Proposition 4.3.1. For a general pair  $(a, b)$ , we compare the two strategies numerically, see Section 5.5. Since for France and Japan  $a \approx 1 + b$  and  $a \approx 1$ , see Figure 2, we conclude that both strategies perform roughly equally well for these countries. For Poland, however,  $a \approx 2$  and  $b \approx 0$ . Our numerical analysis suggests that in this case Strategy ( $U$ ) is preferred, see Section 5.5 and in particular Figure 8.

To check whether the alignment of the TG and KG infection and outbreak probabilities is robust for varying epidemic strength, there are two natural summary statistics, namely the proportion of people (resp. cities) under isolation. We compare the analytically derived proportions with the corresponding simulated proportions, that can be calculated from epidemics generated on the basis of TG and KG graphs for France, Poland and Japan, see Figure 3. In the figures, we abbreviate the analytical derived curves by KB (K for kernel and B for branching), since they are based on the branching processes approximations. In the following, we refer to the mean proportion of people under isolation calculated from simulations based on the transportation graph (resp. the kernel graph) by the abbreviated notations of TG (resp. KG) proportion under isolation.

For Poland and France, we find an agreement of the TG proportion under isolation with the KG proportion of isolation which is surprisingly good given the high level of reduction to arrive at the KG graph. The correspondence is almost perfect under strategy ( $U$ ). Under strategy ( $P$ ), we observe a downward shift for Poland. For France under strategy ( $P$ ), the KG proportion under isolation displays a more regular shape that appears to interpolate between the TG proportion under isolation for resp. small (less than 5) and large values (more than 20) of the  $R_0$ . For Japan however, the correspondence between KG and TG proportions under isolation is very weak, which shows that it is not appropriate for every country to neglect the geometric structure of a country and base the mobility matrix solely on city sizes.

In the following plots, we compare the infection and outbreak probabilities calculated on the basis on the transportation graph (TG), kernel graph (KG) and the kernel branching process approximation (KB). For France, the TG infection probabilities are in very good agreement with KB and KG infection probabilities, see Figure 4. For Poland, the correspondence is actually worse, despite the better agreement observed in Figure 3. For Japan, TG infection probabilities deviate from KG and KB infection probabilities over a broad

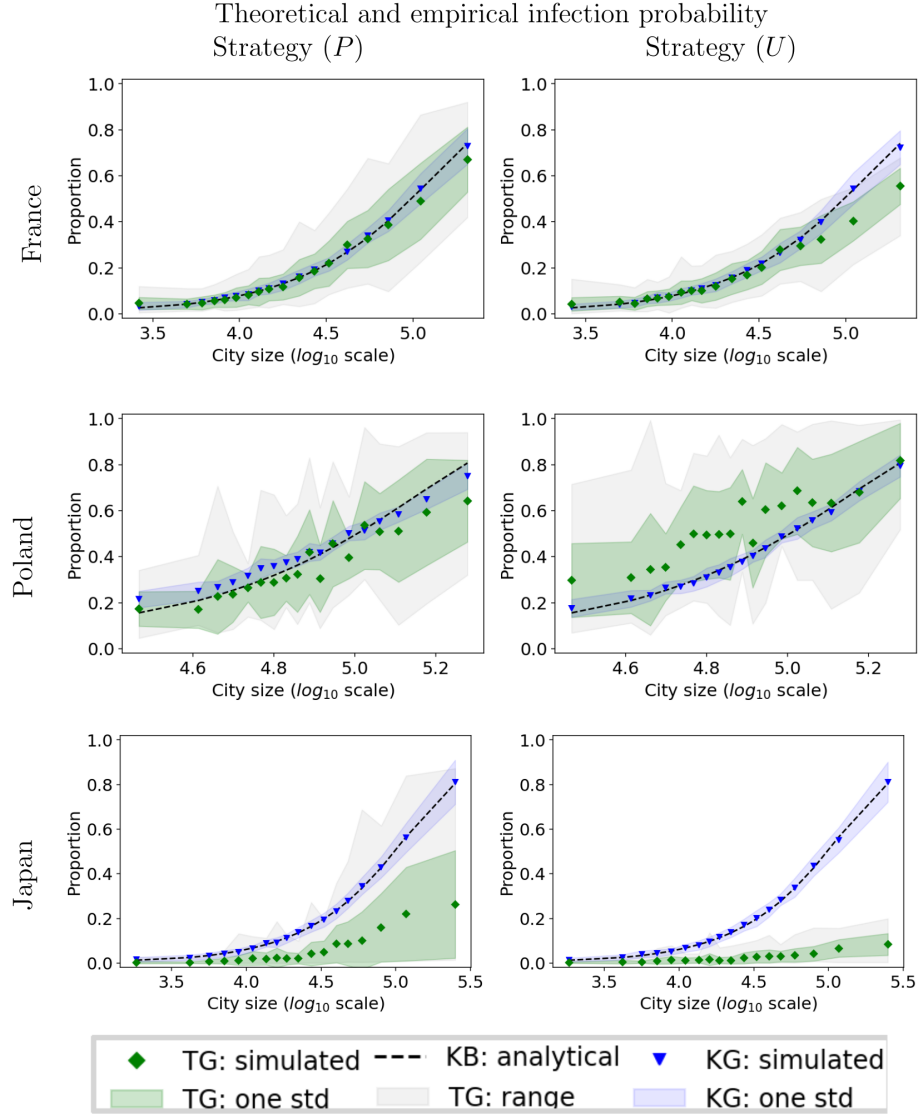


Figure 4: Comparison of simulated and theoretical infection probabilities, on the left for strategy ( $P$ ) and on the right for strategy ( $U$ ) for mobility data from Poland and Japan in the upper and lower row, resp. The  $R_0$  value is adjusted such that for cities of size  $10^5$  the theoretical infection probability of infection is 0.5, see Section 4.2.

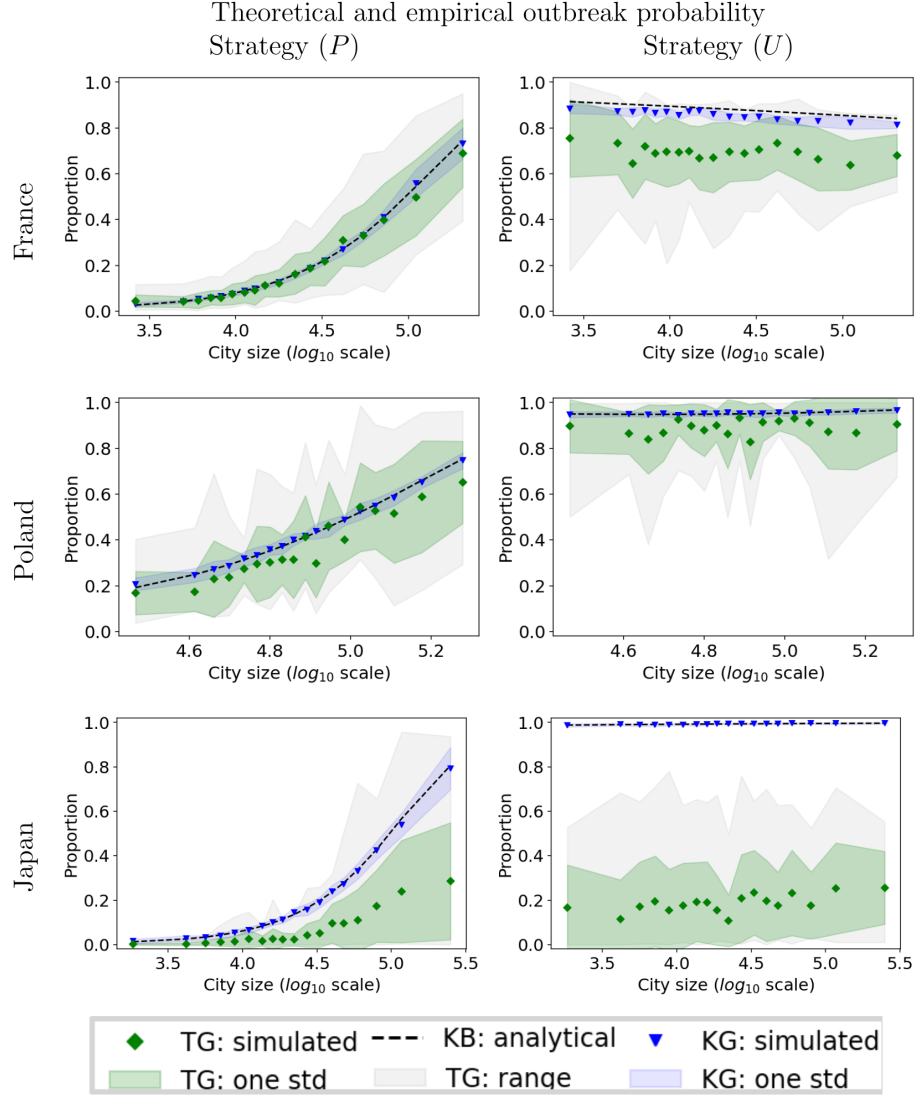


Figure 5: Comparison of empirical and theoretical outbreak probabilities, on the left for strategy ( $P$ ) and on the right for strategy ( $U$ ) for mobility data from France, Poland and Japan in the upper, middle and lower row, resp. The  $R_0$  value is adjusted such that for cities of size  $10^5$  the probability of infection is 0.5, see Section 4.2 for more details.

range of city sizes, with a more significant impact of the largest cities on the proportion of people under isolation. In contrast, KG and KB infection probabilities are in very good agreement whatever the country, which shows that the branching process approximation is appropriate at least for the considered cases.

Similarly, TG outbreak probabilities are in a very good agreement with KG and KB outbreak probabilities under strategy ( $P$ ) for both France and Poland, see Figure 5. This is expected, since under strategy ( $P$ ) infection and outbreak probabilities are symmetric.

On the other hand, we see that under strategy ( $U$ ), TG outbreak probabilities typically do not agree well with KB nor KG outbreak probabilities. The geographical structure has then a much stronger influence, leading to a reduced propagation of the disease as compared to a dissemination that would be global. A criterion for comparing mitigation strategies based on infection probabilities is therefore expected to provide more reliable comparisons with respect to the specifics of migration data in contrast to those based on outbreak probabilities.

The strong association between the TG proportions under isolation and infection probabilities as determined by the KG values for France and Poland argues for approximating the epidemic by the KB approximation. Consequently, it is also reasonable to use the KB approximation to infer numerically the relative advantage of one strategy over the other. We tested the efficiency of each strategy while looking at the dependency on the city size distribution and the two kernel parameters, see Figure 8 in Section 5.5. The findings indicate that for France both strategies would perform equally well under any scenario, while for Poland, strategy ( $U$ ) would generally outperform strategy ( $P$ ).

## 2.1 Structure of the remaining sections

The various models used in this study are described more extensively in the following Section 3. After the general framework is presented in Section 3.1, we make the distinction between the transportation model, given in Section 3.1.1 and at the basis of the transportation graph (TG), and the kernel approach, as explained in Section 3.2. This approach leads to the finite kernel graph (KG) as explained in Section 3.2.1, but also to possible generalizations to other city size distributions, see Section 3.2.2, and finally to the branching approximations, see Sections 3.2.3 and 3.2.4 for the forward and backward branching processes respectively. The analysis of the branching process conducted in Section 4 leads to analytical formulas from which the kernel branching (KB) estimates were derived, first for the outbreak probability, see Section 4.1, second for the infection probability, see Section 4.2, and third for the basic reproduction number, see Section 4.4. Our procedure to compare the efficiency of strategy ( $U$ ) over strategy ( $P$ ) is expressed within this framework in Section 4.3, with a general comparison result obtained in the specific case of rank-1 kernels. We also relate these two strategies in terms of basic reproduction number in Section 4.5. The data analysis is explained more extensively in Section 5, starting by the description of

the considered datasets in Section 5.1. The estimation leading to Figure 1 and of the kernel parameters are presented respectively in Sections 5.3, before we describe in Section 5.4 the evaluation of the prevalence, of the infection and outbreak probabilities from TG and KG epidemic simulations. The next Section 5.5 is dedicated to the numerical efficiency comparison of the two strategies. We place back these results in the context of regional lockdown strategies during COVID-19 pandemics in Section 5.6, leading to estimations of (city-wise) basic reproduction numbers. It seems out of reach to accurately assess such basic reproduction numbers based on the temporal increase in the number of infected cities, as demonstrated by the findings in Section 5.7. We close Section 5 by the comparison of transportation and kernel graphs in terms of in- and outdegree. Finally in Section 6, we discuss and summarize our results and give an outlook on possible future research directions.

### 3 Models

#### 3.1 A model for the spread of an infection between cities

The underlying mathematical foundation for our analysis is the relation between SIR epidemic models and inhomogeneous random directed graph from Cao and Olvera-Cravioto (2020), see also Bollobas et al. (2007) for the undirected case. The vertices of the random graph will be interpreted as cities, with a given ordering from 1 to  $N$ . In this epidemic graph, a directed edge  $(i, j)$  between city  $i$  and city  $j$  represents a potential infection event, in the sense that, if city  $i$  would get infected, it would spread the infection to city  $j$  (given that city  $j$  is not yet infected). Hence, the forward connected component of city  $i$  in such a random directed graph represents the set of cities that would eventually get infected if an infection process starts in city  $i$ . To generate the epidemic graph, we retain any directed edge  $(i, j)$  from the complete graph with some probability  $p_{ij}$ , akin to percolation processes, with an independent sampling of the edges.

From any choice of an initial epidemic source, it is possible to determine all the cities that become infected by analyzing the epidemic graph. These cities correspond to the vertices accessible by a path issued from the epidemic source, formed by the oriented edges of the graph. The relation of this conclusion to a discrete-time SIR epidemic model is well described, e.g. in Cao and Olvera-Cravioto (2020). For  $k \geq 1$ , the  $k$ -th generation of infected cities then consists of the vertices whose graph distance to the source of infection is exactly  $k$ .

We specify the probabilities  $p_{ij}$  by accounting first for mobility between cities, second for the effect of local restrictions and third for a transmission factor. We take as an input some mobility matrix  $(M_{ij})_{i,j \in \llbracket 1, N \rrbracket}$  that reflects the migration level of citizens from city  $i$  to city  $j$ . Local restrictions limit the number of infected individuals in a city. A function  $L : \mathbb{R}_+ \rightarrow \mathbb{R}_+$  that defines this number for any city size reflects the strategy of mitigating the epidemic (which is only based on city sizes). In an infected city of size  $x$ , a fraction



$L(x)/x$  of all citizens is infected. A scaling factor  $k_C > 0$  is considered in addition to adjust the strength of disease propagation. The following expression for  $p_{ij}$  is considered:

$$p_{ij} = 1 - \exp \left[ -\frac{k_C}{N} \cdot (M_{ij} + M_{ji}) \cdot \left( \frac{L(x_i)}{x_i} \right) \right]. \quad (2)$$

Note that the disease can disseminate to city  $j$  due to infected citizens of city  $i$  visiting  $j$ , which leads to the term proportional to  $M_{ij}L(x_i)/x_i$ , but also due to the citizen of city  $j$  visiting  $i$  and bringing back the disease. The later is represented by the term proportional to  $M_{ji}L(x_i)/x_i$ , with the assumption that any visited citizen would get infected in city  $i$  at a rate proportional to the incidence, thus proportional to  $L(x_i)/x_i$ . The latter transmission events are designated as infections from the inside (the inside of city  $i$ ) in contrast to the former events others considered to be from the outside (since infected citizens of  $i$  are traveling and transmit the disease outside of city  $i$ ).

The exponential form of  $p_{ij}$  is derived from an approximation based on large city sizes, see Section S.1 of the Supplementary material for more details. Furthermore, for values of  $(M_{ij} + M_{ji}) \cdot L(x_i)/x_i$  that would be comparable for any pairs  $(i, j)$ , a scaling of  $k_C$  with  $1/N$  (as assumed in (2)) would be the right one to arrive at a well-defined epidemic process also in the limit  $N \rightarrow \infty$ , see Cao and Olvera-Cravioto (2020). Recall however that both  $M_{ij}$  and  $x_i$  are typically expected to take very heterogeneous values in our modeling framework.

We consider two alternative choices of the function  $L$  that correspond to two different strategies for the epidemic containment. Strategy ( $U$ ) consists in prescribing a threshold  $L_V$  for isolation that is independent of the city size, i.e.  $L_U(x) := L_V$ . Strategy ( $P$ ) consists in prescribing a threshold for isolation that is proportional to the city size, thus given through a proportion  $p_V$ , i.e.  $L_P(x) := p_V \cdot x$ .

In an actual epidemic, it is in general not possible to know the number of infected individuals, due to e.g. the time-shift between the infection of an individual and the detection of its infection and since not all individuals can be tested at any time point. In particular, it is in general not possible to know with certainty, if a given threshold  $L$  has been reached. In our model, we neglect these uncertainties.

The migration matrix  $(M_{ij})_{i,j}$  and the city sizes  $(x_i)$  are to be fitted with data, that are taken in our analysis from France, Poland and Japan.

### 3.1.1 The transportation graph model

In the transportation model, the entries of the matrix are estimated separately according to the same procedure for any pair of cities.  $N \times N$  parameters are then to be inferred from migration data. This graph is expected to retain mobility patterns formed by other factors than the city sizes, e.g. by the spatial distribution of the cities. We call the corresponding epidemic graph the transportation graph (TG).

## 3.2 Reduction to a kernel depending solely on city sizes

### 3.2.1 The kernel graph model

We propose a reduction of the model through an alternative choice of the migration matrix that serves three purposes: first we want to have expressions as directly related to our focal feature, the city sizes, which we expect to be one of the determining factor of epidemic progression; second we look for more efficient numerical approaches; third we are interested to generate an epidemic graph that can scale with the number of vertices, by relating to the framework of Cao and Olvera-Cravioto (2020).

The reduction that we propose consists in assuming a specific form of the mobility matrix  $(M_{ij})_{i,j \in \llbracket 1, N \rrbracket}$ , namely that of a kernel function. The kernel denoted by  $\kappa_M$  receives as inputs the sizes  $x_i$  and  $x_j$  of respectively the source and the visited cities, i.e.  $M_{ij} = \kappa_M(x_i, x_j)$ . Several observations confirmed to us the interest of looking for non-symmetrical gravity type kernels of the following form:

$$\kappa_M(x, y) = x^{1+b} \cdot y^a, \quad (3)$$

where the two parameters  $a$  and  $b$  are to be fitted from the transportation matrix, for  $x, y \in \mathbb{R}_+$ . These observations include those of the influx and outflux, recalling Figure 2, but also of the transportation matrix, see Section 5.8 on the degree distribution of this random graph. While  $y^a$  corresponds to the bias towards a visit of a city of size  $y$ ,  $x^b$  refers to mobility of citizens of a city of size  $x$ . If  $a > 0$  there is a bias of travels being more often directed into large cities, while if  $b > 0$  there is a bias of inhabitants of large cities to travel more often abroad.

It is an essential property of  $\kappa_M$  that it takes a separable form: it is the product of two terms, namely  $x^{1+b}$  and  $y^a$ , which depend separately on  $x$  and  $y$ , the source and visited city sizes respectively. This property simplifies the analysis of the branching process and allows for very efficient numerical implementation of the epidemic process.

The probabilities  $(p_{ij})_{i,j \in \llbracket 1, N \rrbracket}$  are then computed according to (2) in order to produce the random sampling of the epidemic graph which we name the kernel graph (KG). Distinguishing the contribution of infections from the outside of  $i$  to those from the inside leads to consider the two kernels  $\kappa_O, \kappa_I : \mathbb{R}_+^2 \rightarrow \mathbb{R}_+$  defined respectively as:

$$\kappa_O(x, y) := k_C L(x) \cdot x^b \cdot y^a = k_C \frac{L(x)}{x} \kappa_M(x, y) \quad (4)$$

and as

$$\kappa_I(x, y) := k_C L(x) \cdot x^{a-1} \cdot y^{1+b} = k_C \frac{L(x)}{x} \kappa_M(y, x). \quad (5)$$

We deduce the following identity for the probabilities  $p_{ij}^\kappa$  involved in the kernel graph:

$$-N \cdot \ln(1 - p_{ij}^\kappa) := \kappa_O(x_i, x_j) + \kappa_I(x_i, x_j). \quad (6)$$

### 3.2.2 The limit of a large number of cities

We are interested moreover in a scaling of the kernel graph with the number  $N$  of vertices. The proposed form of the mobility matrix is directly extended for any set of vertices with city sizes as attributes, leading to a similar kernel graph between these vertices. For this scaling, we thus interpret the observed distribution of city sizes as the sampling of a probability distribution  $\beta$ . To obtain a kernel graph with  $N'$  vertices we can draw  $N'$  city size values independently according to  $\beta$ .

Basically  $\beta$  can simply be evaluated as the empirical distribution  $\sum_{i=1}^N \delta_{x_i}$ ,  $N$  being very large. Alternatively, empirical size distributions of large cities are generally well described by heavy-tailed distributions, like the log-normal distribution which density takes the form

$$\beta(x) := \frac{\mathbf{1}_{\{x>0\}}}{\sqrt{2\pi}\sigma x} \exp\left(-\frac{(\ln(x) - \mu)^2}{2\sigma^2}\right),$$

for the two parameters  $\mu \in \mathbb{R}$  and  $\sigma > 0$ , or power-law distribution with a density of the form

$$\beta(x) := \frac{\mathbf{1}_{\{x>x_L\}}}{Z} x^{-\phi}, \quad (7)$$

for some  $x_L > 0$  and  $\phi > 1$  and with an appropriate normalizing constant  $Z$ , as we have seen e.g. in Figure 1.

Because of the very significant and specific role of the few largest cities in the epidemic outcomes, we have chosen the empirical distribution as the baseline city size distribution, in particular to generate Figures 3-5. Power-law distributions have also been considered to test the robustness of our conclusions.

As  $N'$  tends to  $\infty$ , we want the secondary number of infection a.s. to be asymptotically finite. This is ensured by the formula we proposed in (6) in relation to  $N$ . For large  $N'$  the probability that there is an edge from  $i$  to  $j$  is then equivalent to  $\kappa(x_i, x_j)/N'$ , where

$$\kappa(x, y) := k_C \cdot (L(x) \cdot x^b \cdot y^a + L(x) \cdot x^{a-1} \cdot y^{1+b}). \quad (8)$$

In this setting, we will compare our model with some branching processes. In the limit where  $N' \rightarrow \infty$ , the random epidemic graph is locally a random tree generated by a branching process. This observation establishes a connection between large random graphs and branching processes Bollobas et al. (2007).

It shall be noted that such connections have been rigorously justified, for instance in Cao and Olvera-Cravioto (2020), under the assumption that  $\kappa \in L^1(\mathbb{R}_+ \times \mathbb{R}_+)$ . If  $\beta$  is a power-law distribution with exponent  $\phi$ , this assumption means for strategy  $(U)$  that

$$1 + b - \phi < -1 \quad \text{and} \quad a - \phi < -1, \quad (9)$$

while it means for strategy  $(P)$  that

$$2 + b - \phi < -1 \quad \text{and} \quad 1 + a - \phi < -1. \quad (10)$$

There are actually two types of branching processes that we introduce in the next two Subsections 3.2.3 and 3.2.4: One follows the epidemic forward in time and describes the initial spread of the infection. Outbreak probabilities are associated to this process. Backward in time, we follow potential routes according to which a city might get infected. The infection probability is derived in terms of the corresponding branching process approximation. We start with the forward in time process whose derivation is more straightforward.

### 3.2.3 Forward in time branching process

We write  $i \xrightarrow{O} j$  if there is an edge between  $i$  and  $j$  corresponding to an infection of  $j$  from the outside generated by a visitor from city  $i$ , and by  $i \xrightarrow{I} j$  if there is an edge between  $i$  and  $j$  corresponding to an infection of  $j$  from the inside initiated by a visit in city  $i$ . We consider the following random point process on  $\{O, I\} \times \mathbb{R}_+$

$$\xi_{i,\rightarrow}^{N'} := \sum_{i \xrightarrow{O} j} \delta_{(O, x_j)} + \sum_{i \xrightarrow{I} j} \delta_{(I, x_j)}.$$

The asymptotic property of  $\xi_{i,\rightarrow}^{N'}$  is expressed in terms of the following two functions  $K_{O,\rightarrow}$ ,  $K_{I,\rightarrow}$  and probability measures  $\nu_{O,\rightarrow}, \nu_{I,\rightarrow}$ . To simplify notations, we abbreviate  $\mathcal{Z}_\gamma := \int y^\gamma \beta(dy)$ , for  $\gamma > 0$ .

$$\begin{aligned} K_{O,\rightarrow}(x) &:= k_C L(x) x^b \mathcal{Z}_a, & \nu_{O,\rightarrow}(dy) &:= \frac{y^a \beta(dy)}{\mathcal{Z}_a}, \\ K_{I,\rightarrow}(x) &:= k_C \frac{L(x)}{x} \cdot x^a \mathcal{Z}_{1+b}, & \nu_{I,\rightarrow}(dy) &:= \frac{y^{1+b} \beta(dy)}{\mathcal{Z}_{1+b}}. \end{aligned} \quad (11)$$

The independence properties and (8) yield that  $\xi_{i,\rightarrow}^{N'}$  converges weakly in law as  $N'$  tends to infinity to a Poisson random measure (PRaMe)  $M_{i,\rightarrow}$  on the state space  $\{O, I\} \times \mathbb{R}_+$  with intensity  $K_{O,\rightarrow}(x_i) \cdot \delta_O \otimes \nu_{O,\rightarrow} + K_{I,\rightarrow}(x_i) \cdot \delta_I \otimes \nu_{I,\rightarrow}$ .

This is to be understood as follows. The number of cities that get *infected from the outside* by citizens of city  $i$  is Poisson distributed with mean  $K_{O,\rightarrow}(x_i)$ . In particular, this distribution depends only on  $x_i$ . The size distribution of any city infected from the outside is independently prescribed by the probability measure  $\nu_{O,\rightarrow}$ , which happens not to depend on  $i$ . Because of this independence property, we may refer to a city *typically infected from the outside* when we consider the randomness of sampling the city size according to  $\nu_{O,\rightarrow}$ .

Symmetrically, the number of cities that get *infected from the inside* by citizens of  $i$  is Poisson distributed with mean  $K_{I,\rightarrow}(x_i)$  and the size distribution of any city infected

from the inside is independently prescribed by the probability measure  $\nu_{I,\rightarrow}$ , which happens also not to depend on  $i$ . Because of this independence property, we may refer to a city *typically infected from the inside* when we consider the randomness of sampling the city size according to  $\nu_{I,\rightarrow}$ .

We can iteratively proceed this process and arrive at a discrete-time branching process  $\mathbf{V}^\infty$  associated to the infection process. Even though the branching process is not evolving on the actual graph of cities, we can view it as evolving on a random tree. We will call the nodes of the branching process infected cities, as we did for the infection process. The next generation of infected cities is generated by means of PRaMes with intensity measures  $K_{O,\rightarrow} \cdot \delta_O \otimes \nu_{O,\rightarrow} + K_{I,\rightarrow} \cdot \delta_I \otimes \nu_{I,\rightarrow}$  that are drawn independently for each infected city (of the previous generation). Above we have argued about the convergence as  $N'$  tends to infinity of the law of  $\xi_{i,\rightarrow}^{N'}$ , that is in particular we consider the very beginning of the infection process. Whether an approximation of the infection process by a branching process is reasonable also at later time points, we evaluate by means of simulations in Section 5.4 and in Section 5.7. In particular, we show simulation results that assess the impact of isolating (large) cities during the epidemic.

We are primarily interested in the number and sizes of the infected cities. However, distinguishing cities that get infected from the outside vs those that get infected from the inside will be simplifying the analysis. With this respect the following proposition will prove useful later. It is a direct consequence of the above conclusions.

**Proposition 3.2.1.** *The projection  $\mathbf{V}^{(2)}$  on the two-type space  $\{O, I\}$  of the process  $\mathbf{V}^\infty$  yields a two-type branching process with offspring generated as follows<sup>1</sup>. Assume in generation  $g-1$  that  $n_O^{g-1}$  cities are infected from the outside and that  $n_I^{g-1}$  cities are infected from the inside. Then first city sizes  $(x_i^O)_{i \in n_O^{g-1}}$  and  $(x_j^I)_{j \in n_I^{g-1}}$  are drawn independently according to the measure  $\nu_{O,\rightarrow}$  and  $\nu_{I,\rightarrow}$ , resp., for these cities. In the next generation  $g$ , the number  $n_O^g$  of cities infected from the outside is Poisson distributed with parameter  $\sum_{i \in n_O^{g-1}} K_{O,\rightarrow}(x_i^O) + \sum_{j \in n_I^{g-1}} K_{O,\rightarrow}(x_j^I)$  and the number  $n_I^g$  of cities infected from the inside is Poisson distributed with parameter  $\sum_{i \in n_O^{g-1}} K_{I,\rightarrow}(x_i^O) + \sum_{j \in n_I^{g-1}} K_{I,\rightarrow}(x_j^I)$ .*

We consider two different kinds of initial conditions. Either only the numbers  $n_O^0$  and  $n_I^0$  of cities infected from the outside and from the inside are specified or in addition to the numbers  $n_O^0$ ,  $n_I^0$  also the city sizes  $(x_i^{O,0})_{i \in n_O^0}$  and  $(x_j^{I,0})_{j \in n_I^0}$  are given in generation 0. In the latter case, city sizes are not resampled in generation 1. The number  $n_O^1$  of cities infected from the outside is Poisson distributed with parameter  $\sum_{i \in n_O^0} K_{O,\rightarrow}(x_i^{O,0}) + \sum_{j \in n_I^0} K_{O,\rightarrow}(x_j^{I,0})$  and the number  $n_I^1$  of cities infected from the inside is Poisson distributed with parameter  $\sum_{i \in n_O^0} K_{I,\rightarrow}(x_i^{O,0}) + \sum_{j \in n_I^0} K_{I,\rightarrow}(x_j^{I,0})$ .

---

<sup>1</sup>This is a consequence of the fact that the associated transfer operator projects on a two-dimensional subspace, as we discuss in Section S.4.

The fact that we have this projection to a two-state branching process originates from the separable form of the matrix kernel  $k_M$  in (6).

### 3.2.4 Backward in time branching process

Similarly as in the previous section, we can follow backwards in time potential infection routes along which a city can get infected. To infer (approximately) the infection probability for a city  $j$  of size  $x_j$  we approximate the backward infection chains also by a branching process. For a target city  $j$  we say that  $j'$  is an infector of  $j$  from the outside (resp. from the inside) if  $j' \xrightarrow{O} j$  (resp. if  $j \xrightarrow{I} j'$ ). Then the random variable

$$\xi_{j,\leftarrow}^{N'} := \sum_{j' \xrightarrow{O} j} \delta_{(O,x_{j'})} + \sum_{j' \xrightarrow{I} j} \delta_{(I,x_{j'})}.$$

gives the possible infectors of  $j$ , where  $O$  and  $I$ , resp., indicate if the infecting city introduced the infection from the outside or from the inside and  $x_{j'}$  denotes the size of the infecting city. In analogy to the process  $\xi_{j,\rightarrow}^{N'}$  and thanks to (8) and to the independence properties in the large population limit,  $\xi_{j,\leftarrow}^{N'}$  converges weakly to a PRaMe  $M_{j,\leftarrow}$  on the state space  $\{O, I\} \times \mathbb{R}_+$  with intensity  $K_{O,\leftarrow}(x_j) \cdot \delta_O \otimes \nu_{O,\leftarrow} + K_{I,\leftarrow}(x_j) \cdot \delta_I \otimes \nu_{I,\leftarrow}$ , where

$$\begin{aligned} K_{O,\leftarrow}(x) &:= k_C x^a \int_0^\infty L(z) \cdot z^b \beta(dz), \\ \nu_{O,\leftarrow}(dy) &:= \frac{L(y) \cdot y^b \beta(dy)}{\int_0^\infty L(z) \cdot z^b \beta(dz)}, \\ K_{I,\leftarrow}(x) &:= k_C x^{1+b} \int_0^\infty L(z) \cdot z^{a-1} \beta(dz), \\ \nu_{I,\leftarrow}(dy) &:= \frac{L(y) \cdot y^{a-1} \beta(dy)}{\int_0^\infty L(z) \cdot z^{a-1} \beta(dz)}. \end{aligned} \tag{12}$$

In the limit the number of infectors of  $j$  from the outside (resp. from the inside) is Poisson distributed with mean  $K_{O,\leftarrow}(x_j)$  (resp.  $K_{I,\leftarrow}(x_j)$ ). The sizes of the infectors of  $j$  from the outside (resp. from the inside) are independently prescribed by the probability  $\nu_{O,\rightarrow}$  (resp.  $\nu_I$ ), which happens not to depend on  $j$ .

The corresponding backward branching process we denote by  $\Lambda^\infty$ . In this discrete-time multitype branching process, an element with type  $x \geq 0$  is in the next generation replaced by elements drawn according to a Poisson random measure with intensity  $K_{O,\leftarrow}(x) \nu_{O,\leftarrow} + K_{I,\leftarrow}(x) \nu_{I,\leftarrow}$ .

In analogy to Proposition 3.2.1 we have the following result.

**Proposition 3.2.2.** *The projection  $\Lambda^{(2)}$  on the two-type space  $\{O, I\}$  of the process  $\Lambda^\infty$  started at the first generation generates a two-type branching process. Provided  $\Lambda^\infty$  starts*

with city  $i$  of size  $x_i$ , the initial condition of  $\Lambda^{(2)}$  is given by independent Poisson random numbers of cities infectors from the outside and from the inside respectively, with averages  $K_{O,\leftarrow}(x_i)$  and  $K_{I,\leftarrow}(x_i)$  respectively.

The separability of  $\kappa_M$  is again a crucial ingredient for this reduction.

## 4 Analysis of the branching approximation

### 4.1 Probability of generating an outbreak

In this section, we aim at an approximate formula for the probability that from a city of size  $x$  an outbreak is generated. As we approximated the infection process by the branching process  $\mathbf{V}^\infty$ , it is natural to approximate the outbreak probability by the probability of explosion of  $\mathbf{V}^\infty$  started with a single infected city of size  $x$  (see e.g. Theorem 3.11 in Cao and Olvera-Cravioto (2020) for a rigorous convergence result in this direction). It is well known that the explosion probability is equal to the survival probability for branching processes. Let us denote this probability by  $\eta(x)$ . According to Proposition 3.2.1  $\eta(x)$  coincides with the probability of survival of the two-type branching process  $\mathbf{V}^2$ . Thanks to Lemma 5.4 in Bollobas et al. (2007)  $\eta$  is the solution the following equation

$$\eta(x) = 1 - \exp \left[ -K_{I,\rightarrow}(x) \int_0^\infty \eta(y) \nu_{I,\rightarrow}(dy) - K_{O,\rightarrow}(x) \int_0^\infty \eta(y) \nu_{O,\rightarrow}(dy) \right]. \quad (13)$$

According to Lemma 5.6 in Bollobas et al. (2007) we can estimate  $(\eta(x))_x$  iteratively by setting

$$\eta^{k+1}(x) = 1 - \exp \left[ -K_{I,\rightarrow}(x) \int_0^\infty \eta^k(y) \nu_I(dy) - K_{O,\rightarrow}(x) \int_0^\infty \eta^k(y) \nu_{O,\rightarrow}(dy) \right] \quad (14)$$

and starting with  $\eta^0 \equiv 1$ .

The expression for  $\eta$  on the r.h.s. of (13) is a function of the two unknown parameters

$$\eta_I = \int_0^\infty \eta(y) \nu_{I,\rightarrow}(dy), \quad \eta_O = \int_0^\infty \eta(y) \nu_{O,\rightarrow}(dy). \quad (15)$$

We check the performance of the iterative procedure through the convergence of the associated sequences  $(\eta_I^k)_k$  and  $(\eta_O^k)_k$  with

$$\eta_I^k = \int_0^\infty \eta^k(y) \nu_{I,\rightarrow}(dy), \quad \eta_O^k = \int_0^\infty \eta^k(y) \nu_{O,\rightarrow}(dy), \quad (16)$$

which fulfill the recursions

$$\begin{aligned}\eta_I^{k+1} &= 1 - \int_0^\infty \exp \left[ -K_{I,\rightarrow}(x) \cdot \eta_I^k - K_{O,\rightarrow}(x) \cdot \eta_O^k \right] \nu_{I,\rightarrow}(dx), \\ \eta_O^{k+1} &= 1 - \int_0^\infty \exp \left[ -K_{I,\rightarrow}(x) \cdot \eta_I^k - K_{O,\rightarrow}(x) \cdot \eta_O^k \right] \nu_{O,\rightarrow}(dx).\end{aligned}$$

For our data these two sequences appear to converge quickly, see Figure S14. This suggests that a very accurate estimation of  $(\eta(x))_x$  is rapidly obtained.

Furthermore, the numerically calculated values of  $(\eta(x))_x$  appear to be close to the outbreak probabilities for simulated epidemics for strategy  $(P)$  for France, see Figure 5. For Japan and for Poland and under strategy  $(U)$ , theoretical outbreak probabilities fit less well, see also Figures S17 - S23 in the Supplemental Material.

## 4.2 Backward in time process and probability of infection

In this section, we give an approximation of the probability that a city (of size  $x$ ) eventually gets infected during an outbreak. Similarly as for the probability of an outbreak we approximate the probability of a city of size  $x$  eventually to be infected by the probability that the associated backward branching process introduced in Section 3.2.4 with initial state  $\delta_x$  survives.

Let us denote by  $\pi(x)$  the probability of survival of the backward process  $\mathbf{\Lambda}^\infty$  starting from a city of size  $x$ . According to Proposition 3.2.2 it coincides with the survival probability of the two-type branching process  $\Lambda^2$ . Thanks to Lemma 5.4 in Bollobas et al. (2007) and similarly as for  $\eta$ ,  $\pi$  is the solution the following equation.

$$\pi(x) = 1 - \exp \left[ -K_{O,\leftarrow}(x) \int_0^\infty \pi(y) \nu_{O,\leftarrow}(dy) - K_{I,\leftarrow}(x) \int_0^\infty \pi(y) \nu_{I,\leftarrow}(dy) \right]. \quad (17)$$

For large graphs under the condition that  $\kappa \in L^1(\mathbb{R}_+ \times \mathbb{R}_+)$  (recall (9), (10)), and conditionally on an outbreak, the relative size of the forward connected component is concentrated around the quantity  $\int \pi(x) \beta(dx)$  with a probability close to one whatever the initially infected city, see Theorem 3.11 in Cao and Olvera-Cravioto (2020) for more details.

We estimate  $\pi(x)$  iteratively, in analogy to the estimation procedure for  $\eta(x)$ . The performance of the iterative procedure is again checked through the convergence of the two summary parameters  $\pi_O$  and  $\pi_I$ , i.e. defined with  $\pi_O^0 = \pi_I^0 = 1$  and at step  $k \geq 0$ :

$$\begin{aligned}\pi_O^{k+1} &:= 1 - \int_0^\infty \exp \left[ -K_{O,\leftarrow}(x) \cdot \pi_O^k - K_{I,\leftarrow}(x) \cdot \pi_I^k \right] \nu_{O,\leftarrow}(dx), \\ \pi_I^{k+1} &:= 1 - \int_0^\infty \exp \left[ -K_{O,\leftarrow}(x) \cdot \pi_O^k - K_{I,\leftarrow}(x) \cdot \pi_I^k \right] \nu_{I,\leftarrow}(dx).\end{aligned}$$



In a few steps, it provides a very accurate estimation of  $\pi$  (see Figure S14).

By means of simulations we evaluate the suitability of the approximation with  $(\pi(x))$  in our context, in particular when the goodness of the branching approximation is at stake, see Section 5.4 and Section 5.7.

### 4.3 Comparison of the two strategies

In this section, we aim to compare the efficiency of the two strategies  $(U)$  and  $(P)$ . We recall that strategy  $(U)$  consists in prescribing a threshold  $L_V$  for isolation that is independent of the city size while under strategy  $(P)$  a city gets isolated when a certain proportion  $p_V$  of inhabitants of the city gets infected. To arrive at a comparison of the efficiency of the two strategies, we assume that after isolation of a city no further inhabitants get infected. In particular, at the end of an epidemic in an isolated city of size  $x$  under strategy  $(U)$  (under strategy  $(P)$ , resp.) there are  $L_V$  ( $p_V x$ , resp.) individuals that have been infected. Furthermore, we approximate the infection probabilities by the probabilities introduced in Section 4.2. Depending on the strategies, we denote these probabilities by  $\{\pi_U(x)\}_{x>0}$  and  $\{\pi_P(x)\}_{x>0}$ , resp. According to the results from the last section we have

$$\pi_P(x) = 1 - \exp \left[ -k_C p_V \left( x^a \int_0^\infty y^{b+1} \pi_P(y) \beta(dy) + x^{b+1} \int_0^\infty y^a \pi_P(y) \beta(dy) \right) \right], \quad (18)$$

and

$$\pi_U(x) = 1 - \exp \left[ -k_C L_V \left( x^a \int_0^\infty y^b \pi_U(y) \beta(dy) + x^{b+1} \int_0^\infty y^{a-1} \pi_U(y) \beta(dy) \right) \right]. \quad (19)$$

We measure the burden of the epidemic by the number  $I_\star$  of eventually infected people. Under our assumption for strategy  $(U)$  the number of eventually infected individuals is

$$I_U := \int_0^\infty L_V \cdot \pi_U(x) \beta(dx), \quad (20)$$

while for strategy  $(P)$  the number of eventually infected individuals is

$$I_P := \int_0^\infty p_V \cdot x \cdot \pi_P(x) \beta(dx). \quad (21)$$

Similarly, the number of individuals eventually under isolation is (under our assumptions) given by

$$\begin{aligned} Q_U &:= \int_0^\infty x \cdot \pi_U(x) \beta(dx), \\ Q_P &:= \int_0^\infty x \cdot \pi_P(x) \beta(dx). \end{aligned} \quad (22)$$

Assume that we adjust the parameters  $L_V$  and  $p_V$  such that  $I_*$  is the same under both strategies. Then, we regard the strategy for which less people need to be isolated as the more *efficient strategy*.

In the case of a rank-one kernel where  $a = 1 + b$ , we can rigorously identify which strategy outperforms the other, see Proposition 4.3.1. In the general case, for which  $a$  is not necessarily equal to  $1 + b$ , we do not have an analytical comparison of the two strategies. To arrive still at a comparison of the efficiency of strategy (U) and (P), we compare them by means of simulations, see Subsection 5.5.

### Comparison for rank-one kernels

In the specific case where  $a = 1 + b$ , the kernel of the (two-type)-branching process  $\Lambda^{(2)}$  is actually of rank-one, which clarifies the analysis. The next proposition states which strategy is more efficient depending on the value of  $a$ .

The probabilities  $\pi_U$  and  $\pi_P$  depend on  $k_C, a, \beta$ , and resp.  $L_V$  and  $p_V$ . To compare the two strategies, we fix  $k_C, a, \beta$  and a value  $I_*$  for the number of people that eventually get infected. We adjust the parameters  $L_V$  and  $p_V$  such that  $I_U = I_P = I_*$ .

**Proposition 4.3.1.** *Assume  $\beta$  is a non-Dirac probability measure,  $a, k_C$  and  $I_*$  are given and assume that  $a = b + 1$ .*

- i) If  $a = 1$ , then  $Q_U = Q_P$ , i.e. both strategies are equally efficient.*
- ii) If  $a < 1$ , then  $Q_U > Q_P$ , i.e. strategy (P) is more efficient.*
- iii) If  $a > 1$ , then  $Q_U < Q_P$ , i.e. strategy (U) is more efficient.*

As one can see in Section S.2 of the Supplementary Material, Proposition 4.3.1 is a consequence of Hölder's inequality.

### 4.4 Basic reproduction number

In this section, we define a basic reproduction number  $R_0$  for the branching process  $V^\infty$  (that approximates the transmission process between cities). We set

$$R_0 := \lim_{k \rightarrow \infty} \mathbb{E}_x[X_k]^{1/k}, \quad (23)$$

where  $X_k$  is the number of infected cities at the  $k$ -th generation.

We will deduce from Proposition 4.4.1 below that this definition actually does not depend on  $x$  and has an explicit form for this rank-2 kernel. We refer to Subsection 5.7 for the numerical study of this quantity for our datasets.

Proposition 4.4.1 exploits the following definition of the two-by-two matrix  $W$ :

$$W = \begin{pmatrix} \langle \nu_{I, \rightarrow} | K_{I, \rightarrow} \rangle & \langle \nu_{I, \rightarrow} | K_{O, \rightarrow} \rangle \\ \langle \nu_{O, \rightarrow} | K_{I, \rightarrow} \rangle & \langle \nu_{O, \rightarrow} | K_{O, \rightarrow} \rangle \end{pmatrix}. \quad (24)$$

The entry  $\langle \nu_{I,\rightarrow} | K_{I,\rightarrow} \rangle$  can be interpreted as the average number of cities that get infected from the outside from a typical city that got infected from the outside. A similar interpretation holds for the other entries.  $W$  is classically related to the long-time behavior of  $V^2$ , cf Kesten and P. Stigum (1966).

**Proposition 4.4.1.**  *$R_0$  as defined in (23) coincides with the dominant eigenvalue of the matrix  $W$ .*

In the Supplementary Material, we prove Proposition 4.4.1 as a direct consequence of Proposition S.4.2, see Section S.4 on the complete spectral analysis of the transfer operator related to  $V^\infty$ .  $R_0$  as an eigenvalue of this transfer operator has corresponding eigenvectors that are functions of the city size, as described in Subsection S.5 dedicated to eigenvector centrality. It is a measure for the number of infections that are triggered when city  $i$  gets infected and hence, allows to compare the relative importance of the different cities during the course of an epidemic. By targeting strict measures on cities with a high eigenvector centrality value, one wishes to target cities with a high potential for secondary infections.

## 4.5 Computation of the basic reproduction number

This subsection is dedicated to the computation of  $R_0$ , under the two strategies  $(P)$  and  $(U)$ . Recall that  $L(x) \equiv L_\vee$  under strategy  $(U)$  and  $L(x) = p_\vee \cdot x$  under strategy  $(P)$ . A crucial role is played by the moments  $Z_\gamma$  with exponent  $\gamma > 0$ , cf (11) and just above.

Under strategy  $(U)$  the entries of the two-type transmission matrix  $W$  defined in (24), here abbreviated as  $W^U$ , are the following:

$$\begin{aligned} W_{O,O}^U &:= \int_0^\infty \nu_{O,\rightarrow}(dx) k_C L_\vee x^b \int_0^\infty y^a \beta(dy) \\ &= k_C L_\vee Z_{a+b}, \\ W_{O,I}^U &:= k_C L_\vee \cdot \frac{Z_{2a-1} \cdot Z_{1+b}}{Z_a}, \\ W_{I,O}^U &:= k_C L_\vee \cdot \frac{Z_a \cdot Z_{1+2b}}{Z_{1+b}}, \\ W_{I,I}^U &:= k_C L_\vee Z_{a+b}. \end{aligned}$$

The largest eigenvalue of such a two-by-two matrix has an analytic expression, so that we deduce under strategy  $(U)$ :

$$R_0^{(U)} = k_C L_\vee r_0^U,$$

where

$$r_0^U = Z_{a+b} + \sqrt{Z_{2a-1} Z_{2b+1}}. \quad (25)$$

Under strategy  $(P)$  the entries of the corresponding two-type transmission matrix  $W^P$  are

$$\begin{aligned} W_{O,O}^P &= W_{I,I}^P := k_C p_V \mathcal{Z}_{1+a+b}, \\ W_{O,I}^P &:= k_C p_V \cdot \frac{\mathcal{Z}_{2a} \cdot \mathcal{Z}_{1+b}}{\mathcal{Z}_a}, \\ W_{I,O}^P &:= k_C p_V \cdot \frac{\mathcal{Z}_a \cdot \mathcal{Z}_{2+2b}}{\mathcal{Z}_{1+b}}. \end{aligned}$$

We deduce the following formula for the largest eigenvalue under strategy  $(P)$ :

$$R_0^{(P)} = k_C p_V r_0^P,$$

where

$$r_0^P = \mathcal{Z}_{1+a+b} + \sqrt{\mathcal{Z}_{2a} \mathcal{Z}_{2+2b}}. \quad (26)$$

### Elementary adjustment of the two strategies

A possibility to adjust the two strategies  $(U)$  and  $(P)$  to each other is to put  $R_0^{(U)}$  and  $R_0^{(P)}$  at the same level  $R_\star$  and compare the corresponding threshold values  $L_V$  and  $p_V$ . This is particularly useful, if one knows parameter regimes for which one of the two strategies leads to a subcritical epidemic and one wants to choose the threshold of the other strategy such that the corresponding epidemic is also subcritical. In the following proposition, we give conditions on the parameters  $a$  and  $b$  that enable to upper-bound  $p_V$  depending on  $L_V$ . It is proven in Section S.3 in the Supplementary Material.

**Proposition 4.5.1.** *Let us define  $\gamma := (2a) \vee (2+2b)$  and  $\delta \leq (2a-1) \wedge (2b+1)$ . For any  $\beta$  such that the moment  $\mathcal{Z}_\gamma$  is finite, it holds that  $\mathcal{Z}_{\delta+1} \cdot r_0^U \leq \mathcal{Z}_\delta \cdot r_0^P$ . Consequently, when  $R_0^{(U)}$  and  $R_0^{(P)}$  are put at the same level  $R_\star$ , it implies that  $p_V \leq L_V \cdot \mathcal{Z}_\delta / \mathcal{Z}_{\delta+1}$ .*

*In particular, it implies that*

$$p_V \leq L_V / \mathcal{Z}_1 \quad (27)$$

*provided  $a \geq 1/2$  and  $b \geq -1/2$ , and*

$$p_V \leq L_V \cdot \mathcal{Z}_1 / \mathcal{Z}_2 \quad (28)$$

*provided  $a \geq 1$  and  $b \geq 0$ .*

*In the case  $a = 1 + b$  we have*

$$p_V = L_V \cdot \mathcal{Z}_{1+2b} / \mathcal{Z}_{2+2b}. \quad (29)$$

The first inequality (27) means that the threshold for strategy ( $P$ ) must be smaller than  $L_V$  divided by the expected city size. For the second inequality (28) note that

$$p_V \frac{Z_2}{Z_1} = \int \frac{x}{\int y \beta(dy)} x p_V \beta(dx),$$

which can be interpreted as the average threshold number of infected people in the city of a randomly chosen individual. So Ineq. (28) means that  $p_V$  must be chosen such that this average threshold number is smaller than  $L_V$ .

In practice,  $\beta$  is often heavy-tailed. In this case, the two upper bounds can be very far apart. For the data from France (see Subsection 5.1 for the description of the dataset), the ratio  $Z_2/(Z_1)^2$  is actually close to 36, while for the Japanese data the ratio  $Z_2/(Z_1)^2$  is even larger than 80. Since  $a \approx 1$  and  $b \approx 0$  in both cases, only the second estimate of  $p_V$  by  $L_V \cdot Z_2/Z_1$  is thus relevant.

For heavy-tailed distributions  $\beta$  the right-hand side of (29) is very much affected by the value of  $b$ .

## 5 Data analysis and simulations

### 5.1 Datasets

We exploited mobility data from France, Poland and Japan for our analysis. The general data processing for the simulation consisted of: collecting population and travel flow data from original data sources and reaggregating data into regional units, as specified for the different countries in the following paragraphs.

Since mobility between nearby cities might be stronger influenced by proximity of the cities instead of the city sizes and we aim to depict with our model rather the spread of a disease on a nationwide level rather than on a regional level, we filtered the traveler counts by excluding mobility between municipalities closer to each other than 30 km. The rationale for this threshold is that the mean commuting time in European countries is roughly about 40 to 45 minutes per day, see Giménez-Nadal et al. (2022), and that e.g. in Germany more than 78% of all persons in employment have a distance of at most 25 km to work and roughly 5% travel more than 50 km or more to work Destatis (2022). To evaluate the effect of this filtering, we performed our data analysis also for non-filtered data as well as for data with a filtering that takes into account travels of distances of at least 50 km. In the following we will abbreviate the corresponding datasets by D1+, D30+ and D50+. The results of the D1+ and D50+ analysis can be found in the Supplemental Material, because our model generally fits worse to this data (see Figures S18-S23).

The French data was sourced from the main statistical office in France - INSEE. Populations INSEE (2021) and travel flows INSEE (2020) were extracted on a municipal level

and reaggregated in regions which represented the *areas of attraction* defined by INSEE Beck et al. (2023). The travel flow dataset represents workforce mobility (fr. *mobilités professionnelles*) from the area of living, to the area of work.

The Polish data was sourced from the Polish Statistical Office (rebranded recently as Statistics Poland Filas-Przybył and Stachowiak (2019)), more precisely from the 2016 dataset on workforce mobility based on a census from 2011. Both population and travel flows are provided per commune level (pl. *gmina*). In the case of Poland however, there is no established area of attraction division that would relate to the last fully published census of 2011. Instead, we reaggregated the data to the *powiat* level. In two cases, we reaggregated further a couple of *powiat*s into two regional units: the GZM, which is an interconnected region of around 5 mln inhabitants in Upper Silesia, and the Tricity, which is a region of three densely connected cities in the central northern Poland.

In Japan, we use the data from the inter-regional mobility study of 2015 MLIT (2015a,b). It is the largest census of public mobility in Japan, collected from railway companies - it encapsulates the complete mobility of a country on - among others - a working weekday. This is an important difference from how the previous two data sets were created, as this data set does not only include workforce mobility, but all railway mobility on a weekday - it is obviously heavily dominated by workforce mobility, but does include all other trip reasons. As there are as for Poland no predesigned areas of attraction for Japan, we first divided Japan in regional units according to municipalities. Based on the division created by OECD Dijkstra et al. (2019), we reaggregated the listed municipalities into 61 larger regional units, that correspond to the 61 Functional Urban Areas of Japan. Some of the municipalities among the remaining ones were additionally removed, because they were either not listed as origin or as destination in the mobility census (after the filtering by distance). The remaining municipalities were left as singular regional units.

Following the just prescribed procedure, we obtained empirical city size distributions of size 668 for France, 341 for Poland and 777 for Japan and for each country a mobility matrix that gives the (directed) travel counts between each pair of cities.

## 5.2 Estimating the city size distributions

To describe the tail of the city size distributions in France, Poland and Japan, as presented in Figure 1, we used the Python package “powerlaw” with a fit according to the Kuiper distance Alstott et al. (2014).

We found that the (tail of the) size distribution of French areas of attraction is well approximated by a log-normal distribution, while a power-law distribution with  $\phi = 2.81$  (respectively  $\phi = 1.85$ ), recalling Formula (7), can be fitted well to the size distribution of Polish (respectively Japanese) areas of attraction. The fit of French areas of attraction by a power-law distribution leads to an estimate of  $\phi = 1.82$ .

### 5.3 Estimating cities attractiveness and inhabitants mobility

We used the empirical number of inbound and outbound travels of work-related mobility in France, Japan and Poland to estimate the values of  $a$  and  $b$  in the different countries, see Figure 2.

According to our model we assume that the probability  $p_i(x)$  that a city of size  $x$  is chosen as a travel target is proportional to  $x^a$ . Based on the travel counts to a city we empirically estimate this probability by the ratio of the "number of travels to the city" to the "total number of travels". In case our model is good, we consequently assume that

$$cx^a \approx \frac{\# \text{ travels to the city}}{\text{total number of travels}}$$

and hence

$$\log(\text{number of travels to the city}) \approx a \cdot \log(x) + c'$$

for some appropriate constant  $c'$ . To arrive at an estimate of  $a$ , we fit a linear regression with least squares to the data points

$$(\log(x_i), \log(\text{number of travels to city } i))_i,$$

where  $x_i$  denotes the size of city  $i$  and set  $\hat{a}$  equal to the slope of this regression line.

Similarly we estimate  $b$ . According to our model we assume that the probability that an individual of a city of size  $x$  is traveling is proportional to  $x^b$ . Hence on average we assume that  $x \cdot cx^b$  many individuals will leave a city of size  $x$  for travel for some  $c > 0$ . Based on the outbound travel counts we estimate this number by the number of travels from the city of size  $x$ . In particular, we assume

$$\log(\text{number of outbound travels from the city}) \approx (1 + b) \log(x) + c'$$

for some appropriate constant  $c'$ . Consequently, we fit a linear regression with least squares to the data points

$$(\log(x_i), \log(\text{number of outbound travels from city } i))_i$$

to arrive at an estimate of  $b$ , and set  $\hat{b} + 1$  equal to the slope of this regression line.

Using the census data filtered according to D30+ described in Section 5.1, we estimate

$$\hat{a} = 0.96 \text{ and } \hat{b} = -0.09 \text{ for France,}$$

$$\hat{a} = 1.05 \text{ and } \hat{b} = 0.05 \text{ for Japan,}$$

and

$$\hat{a} = 1.95 \text{ and } \hat{b} = -0.11 \text{ for Poland,}$$

recall Figure 2. These estimates (as well as the estimates that are obtained when filtering the mobility data according to D1+ and D50+) are also added in Figure 8, where the efficiency of strategy  $(U)$  and  $(P)$  are compared for a range of  $a$  and  $b$  values.

## 5.4 Infection probabilities and probabilities to trigger an outbreak

In Sections 4.1 and 4.2, we derived analytical (implicit) formulas for the infection and outbreak probabilities that are based on branching process approximations. We showed in Section 2 already some figures, see Figures 3-5, that compare infection and outbreak probabilities based on the transportation graph with the analytically derived infection and outbreak probabilities. In this section, we provide a more thorough comparison of these probabilities.

For the transportation graph simulations, we recall that edge probabilities  $(p_{ij}^{(m)})_{i,j \leq N}$  are determined by the empirical mobility matrices (based on commuters data) given by

$$-N \cdot \ln(1 - p_{ij}^{(m)}) := k_C \frac{L(x_i)}{x_i} \cdot (m_{ij} + m_{ji}), \quad (30)$$

where  $L(x) = L_\vee$  under strategy  $(U)$  and  $L(x) = p_\vee x$  under strategy  $(P)$ , while  $m_{ij}$  denotes the number of travels from city  $i$  to city  $j$ , see Section 5.1 for the procedure leading to this mobility matrix for each country. In the case of the kernel graph, the value of  $m_{ij}$  is replaced by  $x_i^{1+b} \cdot x_j^a$ , as stated in (6) with the best fit estimates of  $a$  and  $b$  for each country as described in Section 5.3. The KB infection probability is evaluated as described in Section 4.2 with the empirical size distribution for  $\beta$ . We adjusted the free parameter  $k_C$ , such that the KB infection probability is equal to 0.5 for cities of size  $10^5$  for France, Poland and Japan.<sup>2</sup>

After the simulation of infection and outbreak probabilities for any city of the (finite) graph, we collect cities of similar size into 20 bins (such that every bin contains about 30 cities for France, 15 cities for Poland and 40 cities for Japan). For each bin, we calculate the average infection and outbreak probability. The plots concerning the infection probabilities can be found in Figure 4, and the plots concerning the outbreak probabilities in Figure 5. Additional figures (Figures S15-S23) can be found in the Supplemental Material to check the robustness of these numerical outcomes.

To illustrate the variation of the infection and outbreak probabilities within a bin, standard deviations are plotted, as well as minimal and maximal values of TG-based probabilities. Furthermore, we calculated coefficients of determination, that are denoted by  $R^2$  in the following and provided in Table 1, to evaluate how well the KB-based infection (resp. outbreak) probabilities predict TG-simulated infection (resp. outbreak) probabilities. More precisely, we use the following definition of  $R^2$  that is expressed in terms of the  $n$  data observations  $(y_i)_{i \leq n}$  (which are here the TG-simulated infection (resp. outbreak) probabilities),

---

<sup>2</sup>Additional figures are presented in the Supplementary Material where the fit to 0.5 for cities of size  $10^5$  is set to the outbreak probability instead of the infection probability, to investigate further the robustness of our results, see Figures S16 and S17.



Country	infection probability		outbreak probability	
	strategy ( $P$ )	strategy ( $U$ )	strategy ( $P$ )	strategy ( $U$ )
France	0.98	0.80	0.98	-28.81
Poland	0.78	0.04	0.80	-4.02
Japan	-5.17	-111.60	-4.28	-370.84

Table 1: Values of the coefficient of determination for TG simulations as samples and KB formulas as predictions for the infection (left panel) and outbreak (right panel) probability under strategy ( $U$ ) and ( $P$ ), for France, Poland and Japan. Values close to 1 (in white) indicate good performances of prediction, close to 0 (light-gray) similar performances as the simple average of TG observation. If the variance with respect to the prediction is larger than the corresponding variance with respect to TG averages, the value is negative (in gray).

their average  $\bar{y}$ , and the predictions  $(\hat{y}_i)_{i \leq n}$ :

$$R^2 = 1 - \frac{\sum_{i \leq n} (y_i - \hat{y}_i)^2}{\sum_{i \leq n} (y_i - \bar{y})^2}. \quad (31)$$

It is well known, that if the prediction is given by a regression, this coefficient of determination is necessarily non-negative and can be expressed as the fraction of the variance in the observation that is explained by the regression. In general, the prediction may be biased (on average over the  $n$  observations), therefore the numerator in (31) can a priori express both a variance and a squared bias over the residuals  $(y_i - \hat{y}_i)_{i \leq n}$ . Especially when the simulated outbreak/infection probabilities vary little with the city size (so that the denominator is small), the  $R^2$  value in the comparison with the theoretical outbreak/infection probabilities can be largely negative.

The coefficients of determination given in Table 1 confirm the goodness of fit for France, particularly under strategy ( $P$ ), but also under strategy ( $U$ ), and to a lesser extent for Poland under strategy ( $P$ ) for the infection probability. For Poland under strategy ( $U$ ), the TG infection probability values are not as regularly increasing as under strategy ( $P$ ), with quite concentrated values. That the fit by KG infection probability is as good as the mere average of TG infection probability values (in the sense of a  $R^2$  value close to 0) is a reasonable performance. For Japan on the contrary, KG infection probabilities provide a much worse prediction of the TG values as compared to their average.

Concerning the outbreak probabilities, we observe very similar  $R^2$  values under strategy ( $P$ ) as for the infection probabilities. This outcome is foreseeable, as the infection and outbreak probabilities coincide under strategy ( $P$ ). Under strategy ( $U$ ),  $R^2$  values for outbreak probability are largely negative. This can be explained by the fact that the variance of the TG values is very small, resulting in a very small denominator in (31) that amplifies

any prediction bias in the KG values.

Interestingly, KB infection probability functions appear to be extremely similar for strategy ( $U$ ) and strategy ( $P$ ) when adjusted at the reference size of  $10^5$  inhabitants, with the data from France, Poland and Japan. This implies that, for a prescribed expected number of infected individuals, the distribution of the city sizes placed under isolation shall be almost the same under strategy ( $U$ ) and strategy ( $P$ ), and similarly for a given expected number of people under isolation. This property can actually be proved whenever  $a = 1 + b$  (corresponding to the kernel  $\kappa$  in (8) being of rank-one). This observation is crucial for Proposition 4.3.1, implying then a robust comparison of efficiency between the two strategies.

To check whether the alignment of the TG and KB infection and outbreak probabilities is robust for varying epidemic strength, there are two natural summary statistics, namely the proportion of people (resp. cities) under isolation. On the other hand, the basic reproduction number provides a natural scale to compare variations in the virulence levels (or in the threshold value)<sup>3</sup>. Note that the proportion of infected people is linearly related to the proportion of people (resp. of cities) under isolation under strategy ( $P$ ) (resp. under strategy ( $U$ )) when the value of  $k_C$  is changed.

We already presented in Figure 3 the mean proportion of people under isolation for a range of basic reproduction numbers, where the analytical proportions are calculated according to the theoretical probabilities as defined in (17) and the corresponding in silico proportions are obtained from simulations of TG epidemics. In Figures 6 (and 7) we display analogous plots for the mean proportion of *cities* under isolation (respectively the mean proportion of people under isolation *conditionally on a large outbreak*, for France and Poland). In Figure S15 of the Supplementary Material, we show each country on a specific panel to better compare the proportions of people and of cities under isolation.

To be more precise, the TG- and KG- simulated values of proportions of cities as well as people under isolation are taken as the simple averages over replicates. For each replicate, the infection starts with a single infected city randomly chosen according to some distribution, which we set as  $\nu_{O,\rightarrow}$ . Concerning the analytical formulas, recall that for each considered basic reproduction number  $r$  a unique value of  $k_C$  is associated to, from which the corresponding infection probability function  $\pi^r : \mathbb{R}_+ \rightarrow [0, 1]$  (according to (17)) and outbreak probability function  $\eta^r : \mathbb{R}_+ \rightarrow [0, 1]$  (according to (13)) can be deduced. Conditionally on an outbreak, the expected proportion of people (resp. of cities) under isolation is given as  $\int_{\mathbb{R}_+} x \cdot \pi^r(x) \mu(dx)$  (resp. as  $\int_{\mathbb{R}_+} \pi^r(x) \mu(dx)$ ) and is to be compared to the average number of people under isolation in simulated epidemics with (relatively) large outbreaks (defined as to having at least 20 infected cities), see Figure 7. In Figures 3 and 6, the unconditioned averages on the other hand are compared to  $\int_{\mathbb{R}_+} \eta^r(y) \nu_{O,\rightarrow}(dy) \int_{\mathbb{R}_+} x \cdot \pi^r(x) \mu(dx)$

---

<sup>3</sup>Recalling (25) and (26), we observe that both  $r_0^U = R_0^{(U)}/(k_C L_\nu)$  and  $r_0^P = R_0^{(P)}/(k_C p_\nu)$  are directly expressed in terms of  $a$ ,  $b$  and the distribution  $\beta$ .

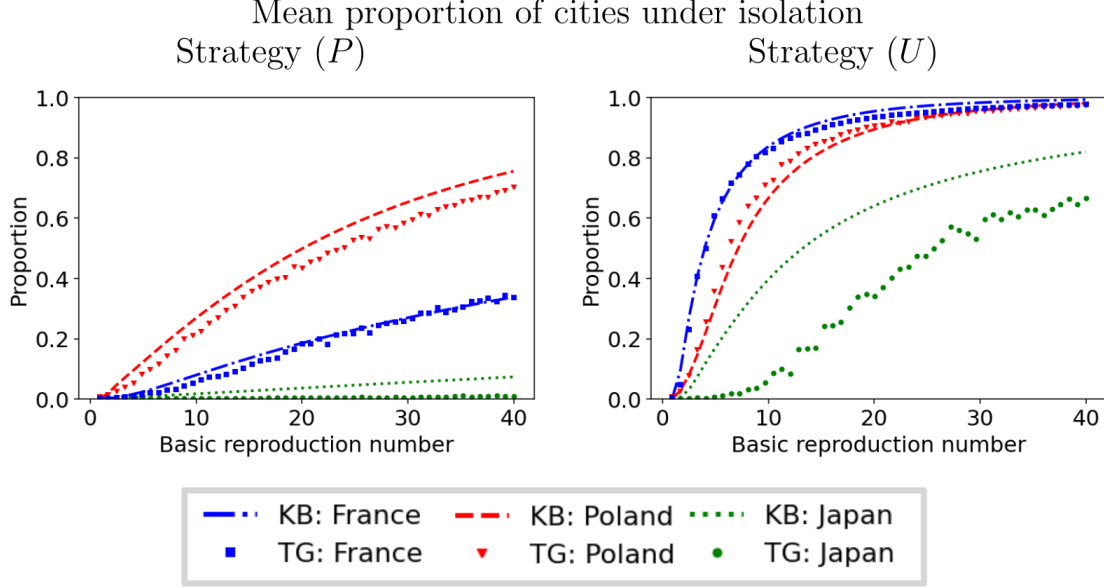


Figure 6: Comparison of the mean TG and KB proportions of cities under isolation depending on the basic reproduction number. Dashed lines show proportions when simulations are performed according to the transportation graph (TG), and scatter plots when proportions are calculated with KB approximations, for France (in blue), Poland (in red) and Japan (in green), under strategy ( $P$ ) on the left and strategy ( $U$ ) on the right.

(respectively to  $\int_{\mathbb{R}_+} \eta^r(y) \nu_{O,\rightarrow}(dy) \int_{\mathbb{R}_+} \pi^r(x) \mu(dx)$ ), where the factor  $\int_{\mathbb{R}_+} \eta^r(y) \nu_{O,\rightarrow}(dy)$  expresses the probability that the outbreak starts from a single city whose size is randomly chosen according to  $\nu_{O,\rightarrow}$ .

In Figures 6 and 7 similarly as in in Figure 3, we find a very good agreement for France and Poland of the TG proportion of cities under isolation (resp. of people under isolation conditional on an outbreak) with the KB such proportions.

More precisely concerning France, while the agreement is almost perfect of the TG and KB proportion of cities under isolation under both strategies, the slight downward shift that was visible in Figure 3 of the TG proportion of people under isolation as compared to the KB one under strategy ( $P$ ) is more pronounced and more regular when such proportions are evaluated conditional on a large outbreak. Concerning Poland on the other hand, the similar slight downward shift under strategy ( $P$ ) is observed for the TG proportion of cities under isolation equally as for the TG proportion of people under isolation, both in the unconditioned case and conditionally on a large outbreak. Under strategy ( $U$ ), the shift is rather upwards.

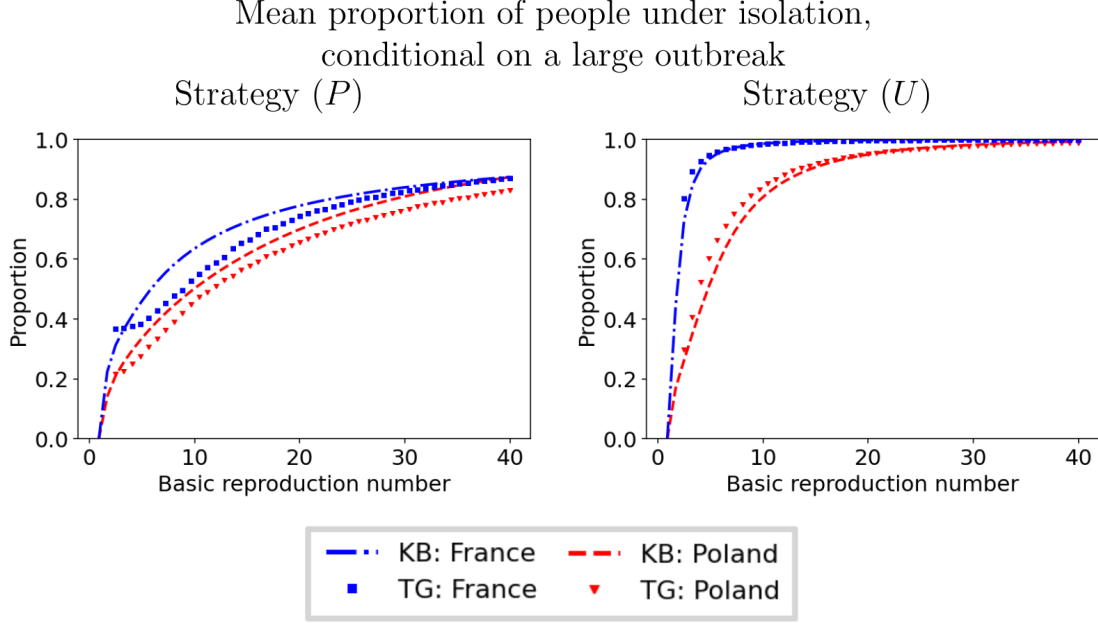


Figure 7: Comparison of the mean TG and KB proportions of people under isolation depending on the basic reproduction number conditional on an outbreak with more than 20 cities under isolation, for France (in blue), and Poland (in red), on the left under strategy ( $P$ ) and on the right-panel under strategy ( $U$ ). For Japan, especially under strategy ( $U$ ), the threshold of outbreak size by 20 is not associated to a relevant distinction in the final incidence, which is why the plot is not shown (the observed values do actually still largely disagree between KB and TG proportions).

Globally nonetheless, we mainly confirm the robustness of the alignment of TG and KB infection and outbreak probabilities for varying values of the basic reproduction number, for both France and Poland. In contrast for Japan, the TG proportion of cities (as the one of people) under isolation does not fit the KB corresponding proportion. Large outbreaks are only rarely observed for Japanese TG epidemics, which is why the plot is not shown in Figure 7.

Besides, due to the definition of the basic reproduction number, it was expected that the KB proportion under isolation should reflect the emergence of large outbreaks as soon as  $R_0$  would exceed 1. Despite the calibration of the virulence level in the transportation graph, it was less clear that the emergence of outbreaks when  $R_0 > 1$  would similarly be reflected by the TG proportion of people or cities under isolation, with outbreak sizes starting close to 0 for small  $R_0$  values. This is nonetheless what we observed, whatever the country or

the strategy, both for people and for cities.

It deserves to be noted as well that very large  $R_0$  values are associated with relatively intermediate TG and KG proportions of people under isolation, especially under strategy (P). This hints at the fact that most of the epidemic spread occurs within a few generations. This also suggests that it is not absolutely essential to be particularly accurate in determining the incidence threshold that serves as an isolation criterion (for an anticipated number of infected people).

As the KG infection probabilities do nicely agree with the analytical prediction (the KB values), we suppose that larger deviations from the analytical expressions for the infection and outbreak probabilities as well as expected proportions of people and cities under isolation are neither due to the finite number of cities (in relation to the heterogeneity level in city sizes) nor due to the values of  $a$  and  $b$ . We rather hypothesize that the reason for the discrepancy lies in the geographic structure of Poland and Japan.

In Poland, there are due to historical reasons major socio-economic differences between the Eastern and Western part of Poland. These differences manifest beyond other also in the connectivity structure between cities, in particular in the work related mobility. In the Eastern part of Poland, these distances are of greater relevance than in the Western part, which has a very well developed transport system. Our model is not adapted to these regional differences, and therefore we expect a less good fit than for France.

The linear spatial structure of Japan as well as the accordingly adapted railway system (of the Shinkansen) influences strongly the mobility matrix of Japan (in particular because our dataset is based on railway mobility). Since our model takes into account only city sizes and not distances between cities measured in terms of geographic distances or railway connectivity our model is expected to fit less well for countries like Japan where these distances seem to play a role.

## 5.5 Comparison of strategies (U) and (P) in the general case

In the general case, where  $a$  is not necessarily equal to  $1 + b$ , we do not have analytical results on the efficiency of strategy (U) in comparison to strategy (P) and vice-versa (as given in Proposition 4.3.1). Instead we compare strategy (U) and (P) numerically. We consider the city size distributions (with a filtering according to D30+) from France, Japan and Poland and a parameter range for  $a$  and  $b$ , that covers the values of  $a$  and  $b$ , which we estimated with mobility data from France, Japan and Poland.

Furthermore, we consider three different degrees of severity of outbreaks, with the fraction of the population in quarantined cities set to 10%, 50% or 90%. Fixing this fraction determines uniquely the value  $Q_*$  and, as a consequence, also the product  $m_p := k_C p_V$  for strategy (P) and the product  $m_L := k_C L_V$  for strategy (U). It then follows from (21) and (20) that the ratio  $I_P/I_U$  does not depend on  $k_C$ . Hence, in the numerical calcula-

tions  $k_C$  can be chosen as an arbitrary positive real number, that fulfills  $\frac{m_P}{k_C} \in [0, 1]$  and  $\frac{m_L}{k_C} \leq \min_x \{\beta(x)\}$ .

Given the values of  $p_V$ ,  $L_V$ ,  $k_C$  as well as  $a$  and  $b$ , we calculate numerically the values of  $I_P$  and  $I_Q$ , i.e. the expected (asymptotic) proportion of infected individuals under strategy ( $P$ ) and ( $U$ ) conditioned on  $Q_*$  (which implies a large outbreak), and plotted  $\log(I_P/I_U)$  in Figure 8.

In these figures, we also added the estimated values of  $a$  and  $b$  for France, Japan and Poland, respectively. According to these estimates, both strategies perform approximately equally well in France and Japan, while strategy ( $U$ ) outperforms strategy ( $P$ ) in Poland. Concretely, the number of infected persons is roughly three times larger under strategy ( $U$ ) when the fraction of quarantined cities is set to 90% while it is roughly 1.5 times larger when this fraction is set to 10%.

We can observe that the function  $I_P/I_U$  exhibits intriguing patterns and is strongly influenced by the value of the fraction of quarantined cities as well as the city size distribution, see Figure 8. For Poland for instance, the curve at which both strategies perform equally well, i.e. at which  $I_P = I_U$ , exhibits a transition from a concave shape when a large fraction of cities are quarantined to a convex shape when such a fraction is small. Conversely for France, this curve does not exhibit a distinctly concave or convex shape across two of the three scenarios considered within the specified parameter range of  $a$  and  $b$ . However, we can observe for all considered city size distributions that we have a transition from a more concave to a more convex curve for decreasing fractions of quarantined cities.

## 5.6 Regional lockdown strategies during COVID-19 pandemics and estimates of empirical $R_0$ -values for SARS-Cov2 spread between cities

During autumn/winter 2020/2021, regional lockdown regulations have been applied worldwide in many countries. The stringency of containment policies depended on the number of new cases that have been detected within a region in the last days (in general one to two weeks). In several European countries, the weekly or biweekly cumulative incidences per 100.000 individuals have been recorded during the pandemic and measures have been based on these numbers. For example in Germany, the first set of restrictions have been issued at a seven-day-incidence of 35 per 100.000, followed by additional measures at an incidence of 50 and strictest measures at an incidence of 200, see Bundesregierung (Hrsg.). In this section, we aim to estimate empirical  $R_0$ -values for between-city-transmission of SARS-Cov2 under this form of regulation for Germany based on estimated individual reproduction numbers.

In autumn/winter 2020/2021, the individual reproduction number was estimated by Hotz et al. (2020) to lie between 1.3 and 1.5 based on reported cases of the Robert-Koch-institute (RKI).

Workplace-related infections have been estimated (in England and Wales in September/ December 2021) to make up about 17 % of all infections Hoskins et al. (2022). We

$$\log(I_P) - \log(I_U)$$

People under isolation:

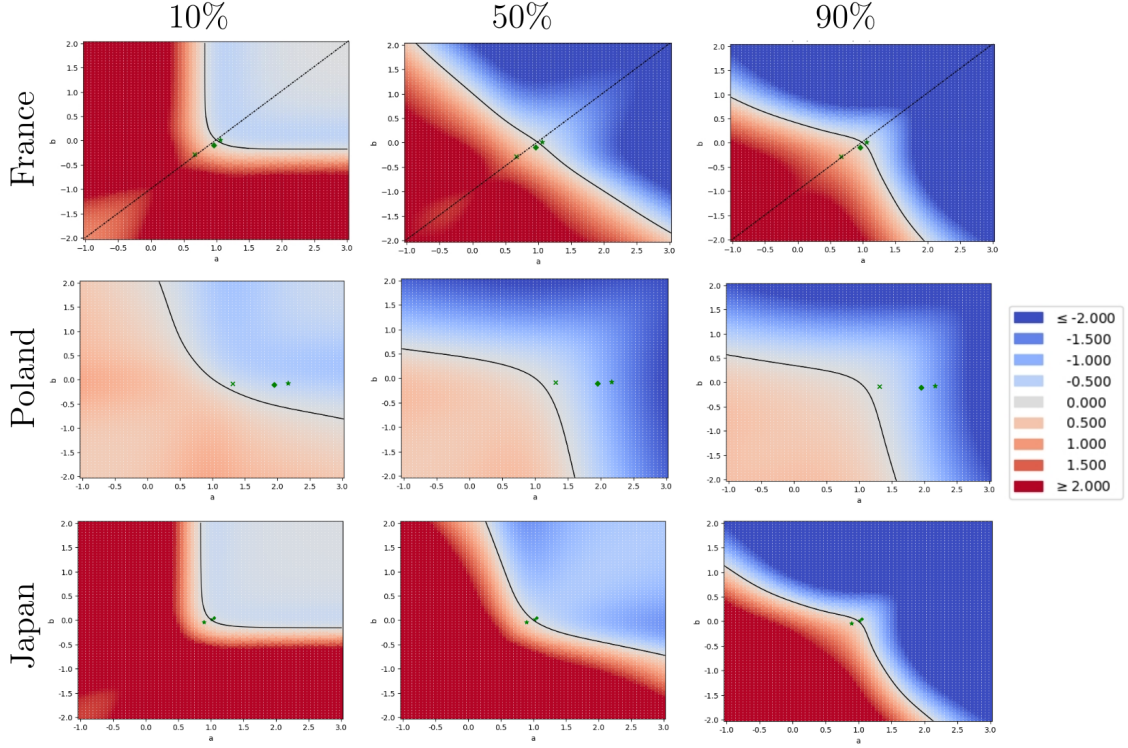


Figure 8: Logarithm of the ratio of the expected number of isolated individuals under strategy (U) vs. strategy (P) for a fixed number of infected individuals. The colour code for the values of  $\log(I_P) - \log(I_U)$  is given on the right of the figures. Green points represent estimates of  $(a, b)$  for each country,  $\times$ ,  $\bullet$ ,  $\star$ , resp. give estimated values of  $(a, b)$  for D1+, D30+ and D50+, resp. For the black line  $I_P = I_U$  and for the dashed black line  $a = b + 1$ .

assume that the proportion of workplace-related infections were not lower in Germany in autumn/winter 2020/2021, because in 2020 private activities were quite restricted in Germany. Furthermore, the pandemic in autumn/winter 2021/2022 was strongly impacted by vaccination, which was frequently mandatory for workplaces, hence the 17 % should be seen as a lower-bound. About 22 % of all persons in employment commute more than 30 km, see Destatis (2022), as well as about 55 % of all individuals living in Germany are employed, see Destatis (2024).

In the same period, the ratio of the true number of corona cases to the number of detected corona cases was estimated to be 2.5-4.5 in Germany, see Gornyk et al. (2021).

With these estimates, we arrive at a between-city-reproduction number (only based on work-related infections) of  $50 \cdot 2.5 \cdot 0.22 \cdot 0.55 \cdot 0.17 \cdot 1.3 = 3.34$  to  $50 \cdot 4.5 \cdot 0.22 \cdot 0.55 \cdot 0.17 \cdot 1.5 = 6.94$  for a city of size  $10^5$ , when commuting to other regions is prohibited from an incidence of 50, i.e. assuming that the infection is spread to other cities only in the last week before a city is put under lockdown. As a result, from an infected city, roughly 3-7 individuals in other cities get infected, potentially triggering an infection wave in those cities (cities which may not all be different). From this perspective, it comes as no surprise that the regional lockdown strategy was not successful and turned quickly into a country-wide lockdown.

## 5.7 Validity of the estimation of $R_0$

The basic reproduction number is an important characteristic of an epidemic process. In a branching process, it is the expected offspring number, i.e. the expected number of infections caused by a typical infected entity. In SIR models, and especially in the one we are considering here, it firstly defines the threshold (corresponding to  $R_0 > 1$ ) below which no large outbreak would be expected to emerge from infection clusters. In models with sufficiently well mixed populations an exponential growth is observed at the beginning of the epidemic with  $R_0$  as the per-generation infection rate. At later time points, the initial  $R_0$  fails to describe the rate of exponential growth. A typical reason for the subsequent discrepancies is the decrease in the number of susceptible entities, the cities in our case. Over time, it becomes less and less adequate to assume that the law of the size of newly infected cities is unaffected by the progression of the epidemic. We expect that this second factor plays a significant role in our models, given that the large cities tend to be contaminated sooner than the small ones, which may render the estimate of the basic reproduction number from per-generation infection numbers unreliable.

To shed light on these effects, we calculated estimates for the basic reproduction number from simulated epidemics. Since the beginning of an epidemic strongly depends on the city size of the primarily infected city, we start estimating the  $R_0$ -value only when the epidemic has been run for several generations. For this purpose, we filtered the simulations for epidemics generating a relatively large outbreak with at least 10 cities infected (within one generation). For the  $i$ -th such simulated epidemic, let  $Z^{(i)}(\ell)$  be the number of infected



## Basic reproduction number estimation

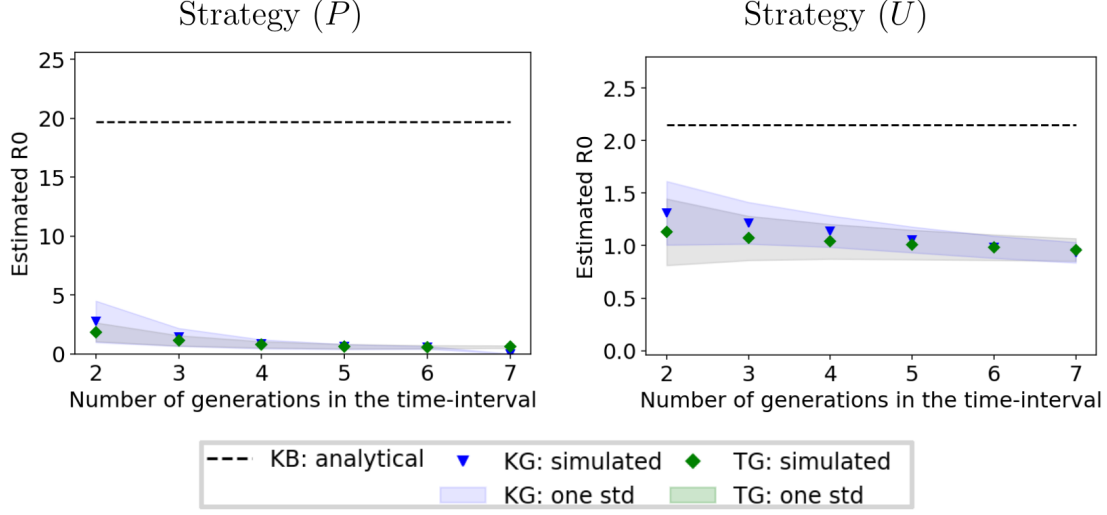


Figure 9:  $R_0$ -expected value and variations calculated from simulated epidemics, see Section 4.4, as compared to the analytical value. The considered city size distribution is the one of France filtered according to D30+. Epidemics have been simulated according to the transportation graph (TG, in green with gray shading) or to the kernel graph (KG, in blue), on the left under strategy (U) and for the right-panel under strategy (P).

cities in generation  $\ell$  and define  $T^{(i)}$  as the first generation  $g$  at which this process reaches at least 10 (i.e.  $Z^{(i)}(g) \geq 10 > \max_{\ell \leq g-1} Z^{(i)}(\ell)$ ). Given some parameter  $G \in \mathbb{N}$  to be adjusted, the  $R_0$ -value is evaluated by considering the interval of  $G$  generations after time  $T^{(i)}$ . We thus consider the subset  $\mathcal{R}_G$  consisting of all simulation indices  $i$  for which the epidemic remains ongoing in generation  $T^{(i)} + G$  for the  $i$ -th simulation. The  $R_0$ -value corresponding to  $G$  is expressed in terms of the trajectories  $: g \in \{0, \dots, G\} \mapsto Z^{(i)}(T^{(i)} + g)$  for  $i \in \mathcal{R}_G$ .

Let  $Z(\ell)$  be the random number of infected cities at generation  $\ell$  according to the branching process described in Section 3.2.3 and  $T$  the first generation at which it reaches at least 10. According to the theorem of Heyde-Seneta, there exists a random variable  $W$  such that the following equivalence holds for  $\ell$  such that  $(R_0)^\ell$  is large, on the event where the branching process survives, event that shall correspond to the occurrence of an outbreak:

$$Z(\ell) \approx W \cdot (R_0)^\ell$$

and hence, we have on this event

$$\ln[Z(T + g)] \approx \ln(W) + T \ln(R_0) + g \ln(R_0).$$

This motivates to infer the logarithm of the basic reproduction number by performing a least-square regression on the  $i$ -th trajectory for each  $i \in \mathcal{R}_G$  (for  $g \in \llbracket 0, G \rrbracket$ ). By not accounting for the  $i$ -th simulation if the outbreak has stopped before generation  $T^{(i)} + G$  (or before  $T^{(i)}$  is reached), we mimic the restriction to the event where the branching process survives. The inferred value is then denoted  $R_0^{(i)}(G)$  and we look how the distribution of  $R_0^{(i)}(G)$  over  $i \in \mathcal{R}_G$  varies with increasing  $G$  up to 9.

In Figure 9, the average over  $i$  of these estimates of  $R_0$  are depicted for various scenarios, together with intervals corresponding to one standard deviation on both side and the 5 and 95% quantiles. With values of  $G$  up to generation 7, we always keep more than 10% trajectories accounted for, (the evaluation is put to 0 in generations 8 and 9 in the left-panel for strategy ( $U$ ) due to this lack of trajectories).

For the different panels of the figure, we used the same setup as for the outbreak probabilities with the French dataset, see Section 5.4. Dataset D30+ was similarly used, as explained in Section 5.1, and we adjusted  $k_C$  (thus fitting the expected  $R_0$  value) so that the KB infection probability is equal to 0.5 for a city size of  $10^5$ . The left panel shows the estimation under strategy ( $P$ ), the right panel under strategy ( $U$ ). The estimates derived from the transportation graph (TG, in green) are displayed together with the ones from the kernel graph (KG, in blue), while the dashed line corresponds to the theoretical  $R_0$ -value computed according to Section 4.5.

In any case, the procedure for estimating the value of  $R_0$  does not produce satisfying outcomes. The inferred values do not agree with the expected one, and the inferred values are rapidly declining with increasing  $G$  (though it reduces variability in the estimation). We can also observe that the TG and KG  $R_0$ -values are extremely close, which demonstrates that the reason for the bad estimation of  $R_0$  lies in the city size distribution rather than more intricate aspects of the connection graph. This is discussed in more details in Section S.6.1 of the Supplemental Material, in which we show that the procedure could be used to infer  $R_0$ -values that align with the expected one, if the city size distribution were less heavy-tailed.

## 5.8 Indegree and Outdegree

To assess the fit between the transportation and the kernel graphs, we conducted an additional comparative analysis of the distributions of expected in- and outdegree as a function of city size. In Figure 10, we present the TG in- and outdegree distributions alongside the corresponding KG distributions based on strategy ( $U$ ) for France, Poland, and Japan.

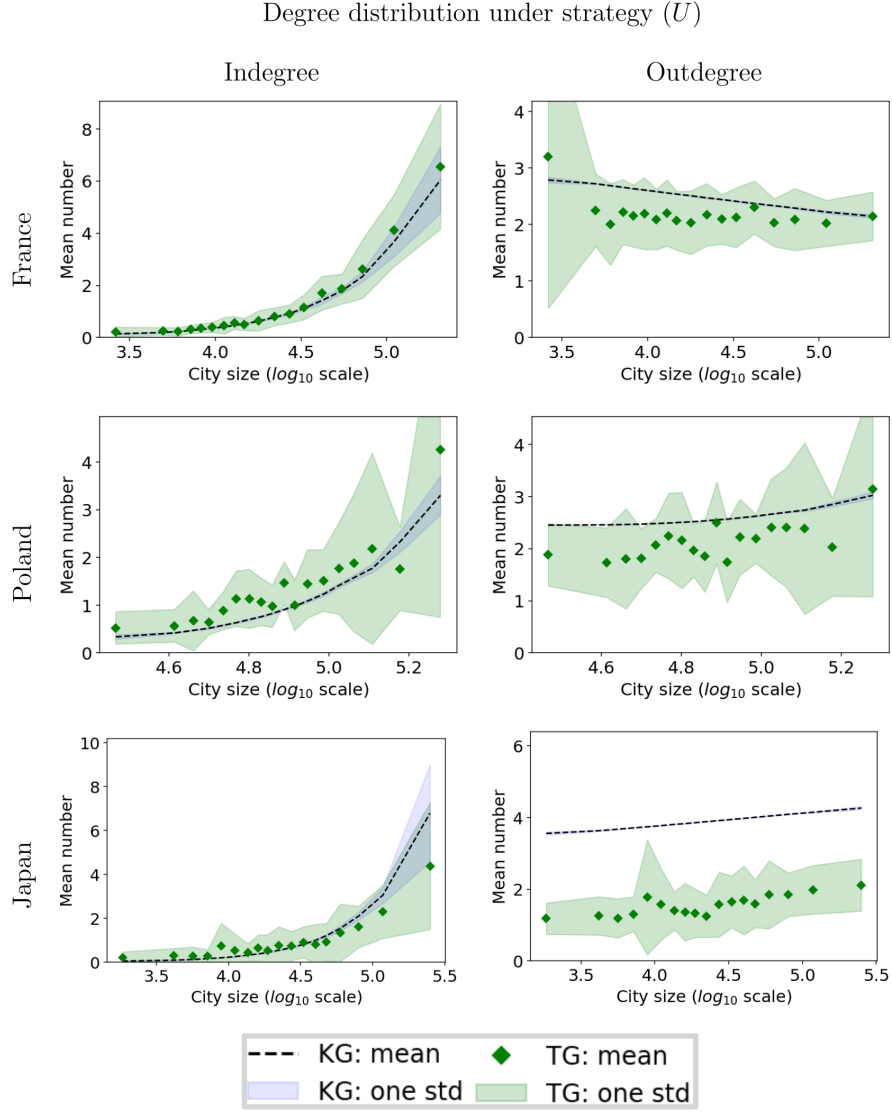


Figure 10: Comparison of the theoretical and the empirical indegrees, on the left, and outdegrees, on the right, of the epidemic graph for strategy ( $U$ ) depending on the city size for France, Poland and Japan. The  $R_0$  value is adjusted such that for cities of size  $10^5$  the theoretical infection probability of infection is 0.5, see Section 4.2.

Recalling (30), a natural proxy for the expected TG indegree of city  $i$  is given for strategy  $(P)$  by

$$\mathbf{i}_i^{(P)} = \frac{k_C p_V}{N} \cdot \left( \sum_j m_{ji} + m_{ij} \right),$$

while it is given for strategy  $(U)$  by:

$$\mathbf{i}_i^{(U)} = \frac{k_C L_V}{N} \cdot \left( \sum_j \frac{m_{ji} + m_{ij}}{x_j} \right).$$

Similarly, a natural proxy for the expected TG outdegree of city  $i$  is given for strategy  $(P)$  by  $\mathbf{o}_i^{(P)}$  equal to  $\mathbf{i}_i^{(P)}$ , while it is given for strategy  $(U)$  by:

$$\mathbf{o}_i^{(U)} = \frac{k_C L_V}{N} \cdot \left( \sum_j \frac{m_{ji} + m_{ij}}{x_i} \right).$$

Recalling (6) and (11), we deduce the following proxies  $(\mathbf{i}_i^{\kappa, (P)})_i$ ,  $(\mathbf{o}_i^{\kappa, (P)})_i$ ,  $(\mathbf{i}_i^{\kappa, (U)})_i$ , and  $(\mathbf{o}_i^{\kappa, (U)})_i$  for the kernel graph to be compared with  $(\mathbf{i}_i^{(P)})_i$ ,  $(\mathbf{i}_i^{(U)})_i$ , and  $(\mathbf{o}_i^{(U)})_i$ :

$$\begin{aligned} \mathbf{i}_i^{\kappa, (P)} &= k_C p_V \cdot (x_i^a \cdot \mathcal{Z}_{1+b} + x_i^{1+b} \cdot \mathcal{Z}_a) = \mathbf{o}_i^{\kappa, (P)}, \\ \mathbf{i}_i^{\kappa, (U)} &= k_C L_V \cdot (x_i^a \cdot \mathcal{Z}_b + x_i^{1+b} \cdot \mathcal{Z}_{a-1}), \\ \mathbf{o}_i^{\kappa, (U)} &= k_C L_V \cdot (x_i^{a-1} \cdot \mathcal{Z}_{1+b} + x_i^b \cdot \mathcal{Z}_a). \end{aligned}$$

Note that the indegree and outdegree vectors coincide (like their proxies  $(\mathbf{i}_i^{(P)})_i$  and  $(\mathbf{o}_i^{(P)})_i$ ) in the case of strategy  $(P)$ , be it for the transportation graph  $TG$  or the kernel graph  $KG$  (for the kernel branching process  $KB$  as well). This is not the case for strategy  $(U)$ , which is why we focus on strategy  $(U)$  in Figure 10. Actually, the indegree distribution under strategy  $(P)$  is also very similar to the one under strategy  $(U)$  for both the transportation graph and the kernel graph (figure not shown).

In Figure 10, we observe that the outdegrees are nearly constant (i.e. almost not dependent on the city size), while indegrees are clearly increasing in city sizes. It is striking that the degrees in the transportation graph are much more variable than in the kernel graph, for cities of similar sizes. Nonetheless, for France and Poland, the degrees in the transportation graph align well with the one in the kernel graph when averaged over the bins (recall that there are 20 bins for each country, thus 15 to 40 cities per bin). The fit is not as good for the outdegree as for the indegree under strategy  $(U)$ , with  $KG$  outdegrees consistently overestimating the  $TG$  ones. For Japan, we see that the fit of the degrees is rather good for small city sizes yet worsens as city size increases, except for the outdegree under strategy  $(U)$  where there is a strong discrepancy (again with  $KG$  outdegrees being consistently larger than  $TG$  outdegrees).

At least with the data from France and Poland, we see that the kernel approach and the chosen form of the kernel do not alter the relation between city size and the epidemic graph indegree (and by extension between city size and outdegree under strategy ( $P$ )). The reduced TG outdegree values under strategy ( $U$ ) as compared to KG ones is presumably due to the geographic structure: the transmission routes at the individual level are restricted to a smaller subset of neighboring cities. Such increased competition probably reduces the number of cities ultimately struck. It is thus expected (and can also be observed in Figure 10) that the effect is greater in Japan, given the shape of the country.

## 6 Discussion and conclusion

In this study, we were interested in the performance of containment regulations, that shall prevent the initial spread of a pathogen in a population within a country. The models we considered compromise between analytic tractability and representation of reality. We eased epidemic dynamics with respect to several aspects, which will be discussed in this section.

A key step of our analysis is to approximate the epidemic process by an infection process on a kernel graph. In the kernel model, we assume that the strength of mobility between cities only depends on the sizes of the cities (and no other parameters, like geographical proximity or the like). The probability to travel to and to travel from, resp., a city of size  $x$  is proportional to  $x^a$  and  $x^b$ , resp., that is the parameter  $a$  reflects the attractiveness of a cities and the parameter  $b$  the traveling habit of inhabitants depending on the size of the city they are living in. We estimated the parameters for France, Poland and Japan.

Interestingly, the parameter combination for France and Japan happen to be very similar, with city size distribution with a power-law coefficient close to 1.8, an estimated attractiveness  $a \approx 1$  and an estimated emissiveness  $b \approx 0$ . These values of  $a$  and  $b$  are all the more surprising that they correspond to a kind of neutral case: All contact pairs are equally likely, i.e. all individuals have roughly the same likelihood to travel independent of the size of the city they are living in (i.e.  $b = 0$ ) and the target city is chosen proportional to its number of citizens ( $a = 1$ ). On the other hand for Poland, the power-law coefficient is larger (more than 3) meaning both that the population is more evenly distributed between powiats. While the estimated emissiveness coefficient  $b$  is still quite close to 0, the attractiveness coefficient  $a$  is close to 2, meaning that attractivity of powiats is significantly biased towards larger powiats. These inferences demonstrate how various the level of city heterogeneity can be.

To check the empirical relevance of the kernel model that relies solely on the contribution of population sizes, without any specific reference to the spatial distribution of cities, we conducted simulations of epidemics which take pairwise mobility patterns between cities into account. We termed the corresponding epidemic graphs as transportation graphs (TG).

Beyond others, we calculated the infection probability (abbreviated as  $\pi$ ) and the outbreak probability (abbreviated as  $\eta$ ) as a function of city size, based on a branching approximation. We compare these theoretical probabilities to simulated probabilities that are obtained with averages of infection outcomes for 20 to 30 cities of similar size over many epidemic runs for the transportation graph. We are led to distinguish many situations, according to the country of reference, the regulation strategy (( $P$ ) or ( $U$ )), and to the rule for adjusting the scaling factor  $k_C$ .

For France and to a lesser extend for Poland, we observe a remarkably good fit of the simulated infection probabilities by the theoretical values. By comparing the simulated and theoretical proportions of infected cities and people for varying reproduction numbers, so varying scaling factor  $k_C$ , we observe that this fit is robust to the stringency of the regulation, which makes it a reasonable choice of optimization. The quality of the fit is particularly noticeable given the level of simplifications and the heterogeneity in the data. A much poorer fit of the TG simulated infection probabilities is observed for Japanese data, which indicates that the spatial structure of the country is not well-captured by the dependency on city size.

A possible explanation for the good fit could be the centralist transportation structure of France, which diminishes the impact of the geographic distance between cities. In Poland, the transportation network is in the east less developed than in the west and north. This implies that in particular in the eastern part of Poland geographical distances are more relevant. In Japan, the linear configuration of the country influences strongly the transportation network, even though cities located along the railway of the same Shinkansen line are in terms of accessibility relatively close to one another. These two effects generate a particular geometric structure that is likely to be of significant interest for inclusion in the model.

Approximations with branching processes are a key tool in our analysis. We use them to derive analytic formula for the outbreak and infection probabilities. Furthermore, we base our definition of a basic reproduction number  $R_0$  on an approximation with branching processes, which implicitly assumes an infinite reservoir of cities in which the new generation of infections can emerge.

Even though this approximation is valid only for very few generations in our setting, the derived analytical infection probabilities yield (as confirmed by our simulation studies) good approximations of the corresponding TG-infection probabilities (for French and Polish mobility networks). Our comparison of the two strategies are based on the infection probabilities, making it reasonable to assume that our results on the relative effectiveness of strategy ( $U$ ) compared to ( $P$ ) are solid, particularly for France and, to a slightly lesser degree, for Poland. The reason for the good fit is potentially that the probability for a city to get infected is depending on some random outcomes occurring within a few generations (potentially a few – backwards in time – success events characterized by a sufficiently high number of secondary infections).

The formula for the KB infection probability reflects a structural property of the epidemic graph that is independent of how the epidemic is initiated, namely the relative size of the largest forward connected component. This property presumably carries over to the TG infection probabilities when they align with the KB infection probabilities.

To evaluate the fit of our model to actual transmission patterns, we evaluate commuting data retrieved from census data. An alternative source of mobility data is given by GPS data obtained from mobile phones. An obstacle for the analysis of this kind of data are privacy restrictions as well as their frequent only commercial availability. With this kind of data, one could however investigate the effect of mobility variability in time, e.g. in winter and in summer during holidays.

Considering that many countries attempt to contain epidemic waves during a pandemic, it would be reasonable to investigate our model in more general settings, i.e. to consider epidemic scenarios that include e.g. successive waves, maybe in terms of an SIRS-like epidemic between cities, and/or vaccination. Finally, it would be valuable to explore the optimization of timing and strength of containment strategies by incorporating utility functions which factor in economic costs, health and social burden (for first steps in this direction see Schäfer et al. (2023)).

## Data availability

The data we analysed as well as the code we used for simulation is available on forgemia (a platform for data storage at Inrae):

[https://forgemia.inra.fr/aurelien.velleret/simulations\\_containment\\_strategies\\_and\\_city\\_size\\_heterogeneity.git](https://forgemia.inra.fr/aurelien.velleret/simulations_containment_strategies_and_city_size_heterogeneity.git)

Additionally some data processing code and intermediate data file are available at: <https://github.com/MOCOS-COVID19/pl-mobility-versus-size>.

## Acknowledgements

CP and AV acknowledge support from the German Research Foundation through grant PO-2590/1-1. VB, TK, CP, PS and AV acknowledge support during the JTP 2022 "Stochastic Modelling in the Life Science" funded by the Deutsche Forschungsgemeinschaft (DFG, German Research Foundation) under Germany's Excellence Strategy – EXC-2047/1 – 390685813. We thank University of Luebeck and Wroclaw University of Science and Technology for financing a visit of TK in Luebeck.

## Author contributions: CRediT

**Viktor Bezborodov:** Conceptualization, Methodology, Software, Formal analysis, Writing - Review & Editing. **Tyll Krueger:** Conceptualization, Methodology, Writing - Original Draft, Review & Editing, Visualization. **Cornelia Pokalyuk:** Conceptualization, Funding acquisition, Methodology, Writing - Original Draft, Review & Editing, Visualization. **Piotr Szymński:** Software, Formal analysis, Data Curation, Writing - Review & Editing. **Aurélien Velleret:** Conceptualization, Methodology, Software, Validation, Formal analysis, Data Curation, Writing - Original Draft, Review & Editing, Visualization.

## Declaration of generative AI and AI-assisted technologies in the writing process.

During the preparation of this work AV used YIAHO and DeepL Translation to explore alternative formulations that could enhance readability. After using this tool/service, the authors reviewed and edited the content as needed and take full responsibility for the content of the published article.

## References

- B. Maier, D. Brockmann, Effective containment explains subexponential growth in recent confirmed COVID-19 cases in China, *Science* 368 (2020). URL: <https://doi.org/10.1126/science.abb4557>.
- A. Wilder-Smith, D. Freedman, Isolation, quarantine, social distancing and community containment: pivotal role for old-style public health measures in the novel coronavirus (2019-nCoV) outbreak., *J Travel Med.* 27(2) (2020). URL: <https://doi.org/10.1093/jtm/taaa020>.
- C. I. Jarvis, A. Gimma, K. van Zandvoort, et al., The impact of local and national restrictions in response to COVID-19 on social contacts in England: a longitudinal natural experiment, *BMC Med* 19 (2021). URL: <https://doi.org/10.1186/s12916-021-01924-7>.
- Bundesregierung (Hrsg.), Konferenz der Bundeskanzlerin mit den Regierungschefinnen und Regierungschefs der Länder am 14. Oktober. 14. Oktober 2020, <https://www.bundesregierung.de/resource/blob/974430/1798920/907336cb30061987d8d14340778a662e/2020-10-14-beschluss-mpk-data.pdf?download=1>, 2020.
- T. Hale, N. Angrist, R. Goldszmidt, B. Kira, A. Petherick, T. Phillips, S. Webster, E. Cameron-Blake, L. Hallas, S. Majumdar, H. Tatlow, A global panel database of



- pandemic policies (Oxford COVID-19 Government Response Tracker), *Nat Hum Behav* 5 (2021) 529–538. URL: <https://doi.org/10.1038/s41562-021-01079-8>.
- A. J. Stier, M. G. Berman, L. M. A. Bettencourt, COVID-19 attack rate increases with city size, *Health Economics eJournal* (2020). URL: <https://doi.org/10.1101/2020.03.22.20041004>.
- J. Cao, M. Olvera-Cravioto, Connectivity of a general class of inhomogeneous random digraphs, *Random Structures & Algorithms* 56 (2020) 722–774. URL: <https://doi.org/10.1002/rsa.20892>.
- B. Bollobas, S. Janson, O. Riordan, The phase transition in inhomogeneous random graphs, *Random Structures & Algorithms* 31 (2007) 3–122. URL: <https://doi.org/10.1002/rsa.20168>.
- H. Kesten, B. P. Stigum, A Limit Theorem for Multidimensional Galton-Watson Processes, *Ann. Mathem. Stat.* 37 (1966) 1211–1223. URL: <https://doi.org/10.1214/aoms/1177699266>.
- J. Giménez-Nadal, J. Molina, J. Velilla, Trends in commuting time of European workers: A cross-country analysis, *Transport Policy* 116 (2022) 327–342. URL: <https://doi.org/10.1016/j.tranpol.2021.12.016>.
- Destatis, <https://www.destatis.de/EN/Themes/Labour/Labour-Market/Employment/Tables/commuter-1.html>, 2022. Data from Microcensus 2020 in Germany about commuters.
- INSEE, Base des aires d’attraction des villes 2020, <https://www.insee.fr/fr/information/4803954>, 2021. Data on areas of attractions in France issued from the National Institute of Statistics and Economic Studies (INSEE), accessed: 2024-07-01.
- INSEE, Mobilités professionnelles en 2017 : déplacements domicile - lieu de travail. recensement de la population - base flux de mobilité., <https://www.insee.fr/fr/statistiques/4509353>, 2020. Data on work-related mobility in France issued from the National Institute of Statistics and Economic Studies (INSEE), accessed: 2024-07-01.
- S. Beck, O. Pégaz-Blanc, A. Khamallah, La rétopolation en 2010 du zonage en aires d’attraction des villes de 2020, <https://www.insee.fr/fr/statistiques/7615286>, 2023. Data on areas of attractions in France issued from the National Institute of Statistics and Economic Studies (INSEE), accessed: 2024-07-01.
- S. Filas-Przybył, D. Stachowiak, Przeptywy ludności związane z zatrudnieniem w 2016 r, <https://stat.gov.pl/obszary-tematyczne/rynek-pracy/opracowania/przeptywy-ludnosci-zwiazane-z-zatrudnieniem-w-2016-r-,20,1.html>, 2019. Data on work-related mobility in Poland, accessed: 2024-07-01.

- MLIT, Inter-Regional Travel Survey in Japan (2015), <https://www.mlit.go.jp/common/001005633.pdf>, 2015a. Data on mobility in Japan issued from the Ministry of Land, Infrastructure, Transport and Tourism (MLIT), accessed: 2024-07-01.
- MLIT, Inter-Regional Travel Survey in Japan: O-D aggregate tables (2015), [https://www.mlit.go.jp/sogoseisaku/soukou/sogoseisaku\\_soukou\\_fr\\_000018.html](https://www.mlit.go.jp/sogoseisaku/soukou/sogoseisaku_soukou_fr_000018.html), 2015b. Data on mobility in Japan issued from the Ministry of Land, Infrastructure, Transport and Tourism (MLIT), accessed: 2024-07-01.
- L. Dijkstra, H. Poelman, P. Veneri, The EU-OECD definition of a functional urban area, <https://www.oecd-ilibrary.org/content/paper/d58cb34d-en>, 2019. doi:<https://doi.org/10.1787/d58cb34d-en>.
- J. Alstott, E. Bullmore, D. Plenz, powerlaw: A python package for analysis of heavy-tailed distributions, PLOS ONE 9 (2014) 1–11. URL: <https://doi.org/10.1371/journal.pone.0085777>.
- T. Hotz, M. Glock, S. Heyder, S. Semper, A. Böhle, A. Krämer, Monitoring the spread of COVID-19 by estimating reproduction numbers over time, 2020. URL: <https://arxiv.org/abs/2004.08557>. arXiv:2004.08557.
- S. Hoskins, S. Beale, V. Nguyen, Y. Boukari, A. Yavlinsky, J. Kovar, T. Byrne, E. Fragaszy, W. Fong, C. Geismar et al. with Virus Watch Collaborative, Relative contribution of essential and non-essential activities to SARS-CoV-2 transmission following the lifting of public health restrictions in england and wales, Epidemiol Infect 151:e3 (2022). URL: <https://doi.org/10.1017/S0950268822001832>.
- Destatis, Erwerbstätigkeit, [https://www.destatis.de/DE/Themen/Arbeit/Arbeitsmarkt/Erwerbstätigkeit/\\_inhalt.html](https://www.destatis.de/DE/Themen/Arbeit/Arbeitsmarkt/Erwerbstätigkeit/_inhalt.html), 2024. Employment data in Germany issued from the Federal Statistical Office of Germany (Destatis, i.e. Statistisches Bundesamt).
- D. Gornyk, M. Harries, S. Glöckner, M. Strengert, T. Kerrinnes, G. Bojara, S. Castell, K. Frank, K. Gubbe, J.-K. Heise et al., SARS-CoV-2 Seroprevalence in Germany - A Population Based Sequential Study in Five Regions., Dtsch Arztebl Int. 118(48) (2021) 824–831. URL: <https://doi.org/10.3238/arztebl.m2021.0364>.
- M. Schäfer, T. Götz, K. Niedzielewski, T. Krüger, An integro-differential model for the spread of diseases, 2023. URL: <https://arxiv.org/abs/2307.10087>. arXiv:2307.10087, preprint.
- M. Newman, Networks : An Introduction, Oxford University Press, 2010. URL: <https://doi.org/10.1093/acprof:oso/9780199206650.001.0001>.
- P. F. Bonacich, Power and centrality: A family of measures, Am. J. Sociol. 92 (1987) 1170–1182. URL: <https://www.jstor.org/stable/2780000>.

## S Supplementary Material

In the Supplementary Material, we provide additional figures, analyses and insights that strengthen the basis of the main study’s findings.

In Section S.1, we explain why we chose to express the infection probability in (2) with an exponential form, highlighting the theoretical reasons behind this choice. In Section S.2, we present the proof of Proposition 4.3.1, which compares the efficiency of the two strategies in the case of rank-one kernels. In Section S.4, we conduct the spectral analysis of the transfer operator, which is further divided into two parts. In Section S.4.1, we introduce the transfer operator and examine its relationship with the reproduction number (R0). In Section S.4.2, we extend our study of the spectral properties associated with the transfer operator. In Section S.5, we discuss the topic of eigenvector centrality. The theoretical basis of this notion is introduced in Section S.5.1, while we detail in Section S.5.2 the methods employed for its estimation with the data from France, Poland and Japan. Finally in Section S.6, we investigate additional influential factors affecting the outcomes of numerical evaluation.

### S.1 Justification for the exponential form of the edge probability

We provide in this Section S.1 some motivations behind our choice of formula (2) to define edge probabilities, as an approximation based on large city sizes.

Let us first note an advantage of this exponential form in that we can interpret  $p_{ij}$  as a failure probability of two independent events, occurring with probability  $p_{ij}^O$  for infections from the outside, and with probability  $p_{ij}^I$  for infections from the inside, where:

$$p_{ij}^O = 1 - \exp \left[ -\frac{k_C}{N} M_{ij} \frac{L(x_i)}{x_i} \right], \quad p_{ij}^I = 1 - \exp \left[ -\frac{k_C}{N} M_{ji} \frac{L(x_i)}{x_i} \right].$$

Indeed:  $1 - p_{ij} = (1 - p_{ij}^O) \cdot (1 - p_{ij}^I)$ .

Formula (2) can actually be interpreted as an approximation motivated by the large number of involved visits, as in the following illustrating model. Say that  $M_{ij}/(x_i x_j)$  is the rate of visits of individual  $m$  by individual  $\ell$ , for any pair  $(\ell, m)$  such that  $\ell$  is a citizen of city  $i$  and  $m$  a citizen of city  $j$ .  $L(x_i)/x_i$  corresponds to the probability that such an individual  $\ell$  has been infected before the lockdown. The effectiveness at which an infected individual transmits the disease during a visit leading to a large outbreak in city  $j$  and the duration of its infectious period is captured by the term  $k_C/N$ . A natural proxy for the probability that an outbreak is generated in city  $j$  due to a visit of  $m$  by  $\ell$  is then given by:

$$p_{ij}^v = \frac{L(x_i)}{x_i} \cdot \frac{M_{ij}}{x_i x_j} \cdot \frac{k_C}{N}.$$

Assuming these events to be independent for the pairs  $(\ell, m)$  leads to a global probability

for an infection from the outside of

$$1 - \prod_{(\ell, m) \in C_{ij}} (1 - p_{ij}^v) = 1 - (1 - p_{ij}^v)^{x_i \cdot x_j}, \quad (32)$$

where  $C_{ij}$  denotes the set of pairs  $(\ell, m)$  (which has cardinality  $x_i \cdot x_j$ ). (32) is approximated by  $p_{ij}^O$  due to  $x_i \cdot x_j$  being large. A similar reasoning leads to the probability  $p_{ij}^I$ .

## S.2 Proof of Proposition 4.3.1 and comparison of strategy efficiency under rank-one kernels

Recall our claim in Proposition 4.3.1-ii) that  $Q_U > Q_P$  when  $a = 1 + b < 1$  and the values of  $L_V$  and  $p_V$  are set according to a prescribed value  $I_\star$  common to  $I_U$  and  $I_P$ .

Instead of prescribing the values for  $I_U$  and  $I_P$ , it is more convenient to prescribe the same value  $Q_\star$  for the numbers  $Q_U$  and  $Q_P$  of people eventually under isolation. Since  $I_U, I_P, Q_U$  and  $Q_P$  are increasing functions of the threshold values, proving Proposition 4.3.1 is equivalent to showing that whatever  $Q_\star$ , it holds:

- i)  $I_U = I_P$  if  $a = 1$ ,
- ii)  $I_U < I_P$  if  $a < 1$ ,
- iii)  $I_U > I_P$  if  $a > 1$ .

In the rank-one kernel situation, (17) simplifies into:

$$\pi(x) = 1 - \exp \left[ -2K_{O, \leftarrow}(x) \int_0^\infty \pi(y) \nu_{O, \leftarrow}(dy) \right].$$

Hence, we deduce from (12) that  $\pi_U$  and  $\pi_P$  can be expressed in the form

$$\pi_\gamma(x) := 1 - \exp(-\gamma \cdot x^a),$$

that is  $\pi_U = \pi_{\gamma_U}$  with

$$\begin{aligned} \gamma_U &:= 2k_C \int_0^\infty L_V \cdot y^{a-1} \cdot \pi_U(y) \beta(dy) \\ &= 2k_C \int_0^\infty L_V \cdot y^{a-1} \cdot \pi_{\gamma_U}(y) \beta(dy), \end{aligned} \quad (33)$$

and similarly,  $\pi_P = \pi_{\gamma_P}$  with

$$\begin{aligned} \gamma_P &:= 2k_C \int_0^\infty p_V \cdot y^a \cdot \pi_P(y) \beta(dy) \\ &= 2k_C \int_0^\infty p_V \cdot y^a \cdot \pi_{\gamma_P}(y) \beta(dy). \end{aligned} \quad (34)$$

Since the function  $\gamma \mapsto \pi_\gamma$  is increasing, by (22)  $Q_U = Q_P = Q_\star$  implies  $\gamma_U = \gamma_P = \gamma_\star$  for some constant  $\gamma_\star > 0$ . Furthermore, by exploiting (33) and (34), we can express  $L_\vee$  and  $p_\vee$  in terms of  $\gamma_U$  and  $\gamma_P$  resp. We obtain the ratio  $I_U/I_P$  as a function of  $\gamma_\star$ ,  $\beta$  and  $a$ .

Let us first consider the case where  $a \geq 1$ . For ease of notations, we denote for any  $\zeta > 0$ :

$$\mathcal{Z}_\zeta^\star := \int_0^\infty x^\zeta \cdot \pi_{\gamma_\star}(x) \beta(dx).$$

By combining (33) and (34) we then deduce  $L_\vee \mathcal{Z}_{a-1}^\star = p_\vee \mathcal{Z}_a^\star$ . Then, the ratio  $I_U/I_P$  is expressed as follows:

$$\frac{I_U}{I_P} = \frac{L_\vee \mathcal{Z}_0^\star}{p_\vee \mathcal{Z}_1^\star} = \frac{\mathcal{Z}_0^\star}{\mathcal{Z}_{a-1}^\star} \cdot \frac{\mathcal{Z}_a^\star}{\mathcal{Z}_1^\star}.$$

When  $a = 1$ , we directly obtain that  $I_U = I_P$ .

Otherwise, note that  $0 < 1 \wedge (a-1) < 1 \vee (a-1) < a$ . This ratio is compared to 1 thanks to Hölder's inequality:

$$\left( \frac{\mathcal{Z}_{a-1}^\star}{\mathcal{Z}_0^\star} \right)^{1/(a-1)} > \left( \frac{\mathcal{Z}_a^\star}{\mathcal{Z}_0^\star} \right)^{1/a} \cdot 1, \quad \left( \frac{\mathcal{Z}_1^\star}{\mathcal{Z}_0^\star} \right) > \left( \frac{\mathcal{Z}_a^\star}{\mathcal{Z}_0^\star} \right)^{1/a},$$

which entails

$$\frac{\mathcal{Z}_{a-1}^\star \cdot \mathcal{Z}_1^\star}{(\mathcal{Z}_0^\star)^2} > \left( \frac{\mathcal{Z}_a^\star}{\mathcal{Z}_0^\star} \right)^{\frac{a-1}{a} + \frac{1}{a}} = \frac{\mathcal{Z}_a^\star}{\mathcal{Z}_0^\star}.$$

This inequality is equivalent to  $I_P > I_U$ , which concludes the proof in the case where  $a > 1$ .

When  $a < 1$ , we look for the shifted moments:

$$\mathcal{Z}_\zeta^\times := \int_0^\infty x^\zeta \cdot x^{a-1} \pi_{\gamma_\star}(x) \beta(dx).$$

Then, the ratio  $I_U/I_P$  is expressed as follows:

$$\frac{I_U}{I_P} = \frac{\mathcal{Z}_{1-a}^\times}{\mathcal{Z}_0^\times} \cdot \frac{\mathcal{Z}_1^\times}{\mathcal{Z}_{2-a}^\times}.$$

Note that  $0 < 1 \wedge (1-a) < 1 \vee (1-a) < 2-a$ . Thanks to Hölder's inequality, with a similar reasoning as before, we deduce this time that  $I_P < I_U$  whatever  $Q_\star$ . This concludes the proof of Proposition 4.3.1.

### S.3 Proof of Proposition 4.5.1

Recall that Proposition 4.5.1 involves the following quantities in terms of the two parameters  $a, b \in \mathbb{R}$  and of the probability measure  $\beta$  on  $\mathbb{R}_+$ .  $\mathcal{Z}_\gamma := \int y^\gamma \beta(dy)$  for  $\gamma > 0$ ,  $r_0^U = \mathcal{Z}_{a+b} + \sqrt{\mathcal{Z}_{2a-1}\mathcal{Z}_{2b+1}}$  and  $r_0^P = \mathcal{Z}_{1+a+b} + \sqrt{\mathcal{Z}_{2a}\mathcal{Z}_{2+2b}}$  (as stated in (25) and (26)). These notations were motivated by the observations that  $R_0^{(U)} = k_C L_\vee r_0^U$  (resp.  $R_0^{(P)} = k_C p_\vee r_0^P$ ) corresponds to the basic reproduction number under strategy (U) (resp. under strategy (P)). Moreover, we have assumed that  $\mathcal{Z}_{\bar{\gamma}} < \infty$ , where  $\bar{\gamma} := (2a) \vee (2+2b)$ , and that  $\delta \leq (2a-1) \wedge (2b+1)$ .

Independently of the value  $R_\star$  to which we set both  $R_0^{(U)}$  and  $R_0^{(P)}$ , we first observe that  $p_\vee \leq L_\vee \cdot \mathcal{Z}_\delta / \mathcal{Z}_{\delta+1}$  (which we generally want to prove) is actually equivalent to  $\mathcal{Z}_{\delta+1} \cdot r_0^U \leq \mathcal{Z}_\delta \cdot r_0^P$ . To deduce the later inequality, it is enough to show that:

$$\begin{aligned} \mathcal{Z}_{a+b}\mathcal{Z}_{\delta+1} &\leq \mathcal{Z}_\delta\mathcal{Z}_{a+b+1}, \\ \mathcal{Z}_{2a-1}\mathcal{Z}_{2b+1}(\mathcal{Z}_{\delta+1})^2 &\leq (\mathcal{Z}_\delta)^2\mathcal{Z}_{2a}\mathcal{Z}_{2b+2}. \end{aligned} \tag{35}$$

The inequalities (35) follow from Hölder's inequality. In general for  $\gamma > \delta$ , choosing  $q = \gamma - \delta + 1$ ,  $p = \frac{q}{q-1}$ , we note:

$$\begin{aligned} 1/p + 1/q &= 1, \quad x^{\delta+1} = x^{\delta/p} \cdot x^{(\gamma+1)/q}, \\ x^\gamma &= x^{(\gamma+1)/p} \cdot x^{\delta/q} \end{aligned}$$

which entails

$$\mathcal{Z}_{\delta+1} \leq (\mathcal{Z}_\delta)^{\frac{1}{p}} \cdot (\mathcal{Z}_{\gamma+1})^{\frac{1}{q}}, \quad \mathcal{Z}_\gamma \leq (\mathcal{Z}_{\gamma+1})^{\frac{1}{p}} \cdot (\mathcal{Z}_\delta)^{\frac{1}{q}}.$$

The inequalities (35) are deduced from the particular cases of  $\gamma$  in  $\{a+b, 2a-1, 2b+1\}$ . In these three cases,  $\delta < (2a-1) \wedge (2b+1)$  entails  $\gamma > \delta$ .

In the case where  $a = 1+b$ ,  $r_0^U = \mathcal{Z}_{2a-1} = \mathcal{Z}_\delta$  while  $r_0^P = \mathcal{Z}_{2a} = \mathcal{Z}_{\delta+1}$ , which entails Eq. (29).

This ends the proof of Proposition 4.5.1.

### S.4 Spectral analysis

#### S.4.1 Transfer operator and reproduction number

$R_0$  as defined in (23) is more directly seen as the principal eigenvalue of an integral operator  $\mathcal{T}$  which is defined as follows.  $\mathcal{T}$  is directly associated to the intensity of the PRaMes  $M_{i,\rightarrow}$ , recall Section 3.2.3.

We denote by  $\mathcal{B}(\mathbb{R}_+)$  the set of bounded measurable functions on  $\mathbb{R}_+$  and write  $\langle \mu | f \rangle := \int_0^\infty f(x)\mu(dx)$  for any  $\mu \in \mathcal{M}_1(\mathbb{R}_+)$  and  $f \in \mathcal{B}(\mathbb{R}_+)$ . Then, for any  $x \in \mathbb{R}_+$  and  $f \in \mathcal{B}(\mathbb{R}_+)$

we define

$$\begin{aligned}
\mathcal{T}f(x) &:= \langle \delta_x | \mathcal{T}f \rangle \\
&:= K_{I,\rightarrow}(x) \cdot \langle \nu_{I,\rightarrow} | f \rangle + K_{O,\rightarrow}(x) \cdot \langle \nu_{O,\rightarrow} | f \rangle \\
&= \int_{\mathbb{R}_+} \kappa(x, y) f(y) \beta(dy).
\end{aligned} \tag{36}$$

where  $\kappa$  is defined in (8).  $\mathcal{T} := K_{I,\rightarrow} \langle \nu_{I,\rightarrow} | \cdot \rangle + K_{O,\rightarrow} \langle \nu_{O,\rightarrow} | \cdot \rangle$  is another equivalent writing of the same definition. In this notation, it is clear that  $\mathcal{T}f$  is a measurable function (a priori not bounded), whereas  $\delta_x \mathcal{T}$  is a positive measure on  $\mathbb{R}_+$ .

From (23), we can interpret  $R_0$  as follows in terms of  $\mathcal{T}^k$ :

$$R_0 = \lim_{k \rightarrow \infty} \langle \delta_x | \mathcal{T}^k \mathbf{1} \rangle^{1/k},$$

where  $\mathbf{1}$  is the function uniformly equal to 1.

Indeed, denote by  $M^{(u;k)}$  the point measure on  $\mathbb{R}_+$  which points (counted with multiplicity) correspond to the sizes of the cities that get infected from city  $u$  after  $k$  generations. By considering the conditional expectation with respect to the city sizes of the first generation of cities infected by  $u$ , one shows the following equality by means of the branching property:

$$\mathbb{E}(\langle M^{(u;2)} | f \rangle | M^{(u;0)} = x) = \mathbb{E}(\langle M^{(u;1)} | \mathcal{T}f \rangle | M^{(u;0)} = x) = \langle \delta_x | \mathcal{T}^2 f \rangle.$$

By induction, for any  $k \in \mathbb{N}$ ,  $\mathcal{T}^k$  corresponds to the expectation of  $M^{(u;k)}$ , i.e.:

$$\langle \delta_x | \mathcal{T}^k f \rangle = \mathbb{E}(\langle M^{(u;k)} | f \rangle | M^{(u;0)} = x). \tag{37}$$

Evaluated for  $f = \mathbf{1}$ , (37) entails that  $\langle \delta_x | \mathcal{T}^k \mathbf{1} \rangle = \mathbb{E}_x[X_k]$ . Recalling (23), this concludes our claim that  $R_0 = \langle \delta_x | \mathcal{T}^k \mathbf{1} \rangle^{1/k}$ .

If the kernel  $\kappa$  would be symmetric and would satisfy

$$\int_{\mathbb{R}_+} \int_{\mathbb{R}_+} k(x, y)^2 \beta(dx) \beta(dy) < \infty, \tag{38}$$

then our definition would coincide with the definition of  $R_0$  as in Bollobas et al. (2007) as

$$\sup\{\|\mathcal{T}f\|_{L^2(\beta)}; f \in L^2(\beta), \|f\|_{L^2(\beta)} \leq 1\}.$$

This follows from the following Proposition S.4.2 and essentially Lemma 5.15 in Bollobas et al. (2007). Condition (38) ensures the compactness of the operator, as proved in Lemma 5.15 of Bollobas et al. (2007) and noted in Remark 3.12 of Cao and Olvera-Cravioto (2020). Without symmetry nor condition (38),  $R_0$  is defined as the spectral radius of  $\mathcal{T}$ , see in particular Theorem 3.10 in Cao and Olvera-Cravioto (2020).

The spectral radius of  $\mathcal{T}$  is identified in Proposition S.4.2. Our rank-two kernel has exactly two real eigenvalues values, the leading eigenvalue is  $R_0$ .

### S.4.2 Spectral analysis of $\mathcal{T}$

To analyse the long time behavior of  $\mathcal{T}$ , the following lemma is helpful in that it relates  $\mathcal{T}$  to a matrix operation on a two-dimensional space. For this, we recall the definition in (24) of the matrix  $W$ .

**Lemma S.4.1.** *For any  $k \in \mathbb{N}$ ,  $x \in \mathbb{R}_+$  and  $f$  a non-negative measurable function:*

$$\langle \delta_x | \mathcal{T}^k f \rangle = \begin{pmatrix} K_{I,\rightarrow}(x) & K_{O,\rightarrow}(x) \end{pmatrix} \cdot W^{k-1} \cdot \begin{pmatrix} \langle \nu_{I,\rightarrow} | f \rangle \\ \langle \nu_{O,\rightarrow} | f \rangle \end{pmatrix}.$$

*Proof.* The equality follows by induction and the definition of  $\mathcal{T}$  given in (36).  $\square$

The projection property given in Lemma S.4.1 is strongly connected to the projection of  $V^\infty$  onto  $V^2$  given in Proposition 3.2.1.

It greatly simplifies the spectral analysis of  $\mathcal{T}$ , as we can see thanks to the following proposition.

If any of the entries of  $W$  is infinite, then  $\mathcal{T}^2 \mathbf{1} \equiv \infty$  because

$$\begin{aligned} \langle \delta_x | \mathcal{T}^2 \mathbf{1} \rangle &= K_{I,\rightarrow}(x) (\langle \nu_{I,\rightarrow} | K_{I,\rightarrow} \rangle + \langle \nu_{I,\rightarrow} | K_{O,\rightarrow} \rangle) \\ &\quad + K_{O,\rightarrow}(x) (\langle \nu_{O,\rightarrow} | K_{I,\rightarrow} \rangle + \langle \nu_{O,\rightarrow} | K_{O,\rightarrow} \rangle). \end{aligned}$$

This directly implies that  $R_0 = \infty$  in this case. Therefore, in the following, we assume that all entries are finite.

If  $\beta$  is a power-law distribution with exponent  $\phi$ , this assumption translates to

$$1 + 2b - \phi < -1 \quad \text{and} \quad 2a - 1 - \phi < -1, \quad (39)$$

in the case of strategy (U) and to

$$2 + 2b - \phi < -1 \quad \text{and} \quad 2a - \phi < -1 \quad (40)$$

in the case of strategy (P). Recall that a bounded measurable function  $f$  is called an eigenfunction of  $\mathcal{T}$  if there exists some value  $\lambda$  such that  $\mathcal{T}f = \lambda f$ . Similarly, a signed measure  $\mu$  is called an eigenmeasure of  $\mathcal{T}$  if there exists some value  $\lambda$  such that  $\mu\mathcal{T} = \lambda\mu$ .  $\lambda$  is then called an eigenvalue of  $\mathcal{T}$ . If an eigenmeasure  $\mathbf{q}$  of  $\mathcal{T}$  is a probability distribution, it satisfies the property for being a quasi-stationary distribution (QSD), namely  $\mathbf{q}\mathcal{T}(dx)/\langle \mathbf{q}\mathcal{T}\mathbf{1} \rangle = \mathbf{q}(dx)$ . Denote by  $\mathbf{v}^T$  the transposition of a vector  $\mathbf{v}$ . We have the following relationships between the eigenvalues and eigenvector of  $W$  and the eigenvalues and eigenmeasures of  $\mathcal{T}$ .



**Proposition S.4.2.** *Assume that the entries of  $W$  are finite. Then  $\mathcal{T}$  has two distinct and real eigenvalues  $\lambda_0$  and  $\lambda_1$ , such that  $\lambda_0 > \lambda_1 \vee 0$  and that coincide with the ones of  $W$ . The leading eigenmeasure  $\mathbf{q}_0$  of  $\mathcal{T}$  can be chosen as a probability measure, thus as a QSD. Similarly, the leading left eigenvector of  $W$  can be chosen as  $(q_0^I \ q_0^O)$  such that  $q_0^I + q_0^O = 1$ ,  $q_0^I \wedge q_0^O \geq 0$ . The following relation holds between them:*

$$\mathbf{q}_0 = q_0^I \cdot \nu_{I,\rightarrow} + q_0^O \cdot \nu_{O,\rightarrow}. \quad (41)$$

*On the other hand, the leading eigenfunction  $h_0$  of  $\mathcal{T}$  can be chosen as a positive measurable function  $h_0$  such that  $\langle \mathbf{q}_0 | h_0 \rangle = 1$ . Similarly, the leading right eigenvector of  $W$  can be chosen as  $(h_0^I \ h_0^O)^T$  such that  $q_0^I h_0^I + q_0^O h_0^O = 1$ ,  $h_0^I \wedge h_0^O \geq 0$ . The following relationship holds between the function  $h_0$  and the vector  $(h_0^I \ h_0^O)^T$ :*

$$h_0 = \frac{h_0^I}{\lambda_0} \cdot K_{I,\rightarrow} + \frac{h_0^O}{\lambda_0} \cdot K_{O,\rightarrow}. \quad (42)$$

*In addition, there exists a function  $h_1$ , a measure  $\mathbf{q}_1$  and constant  $C > 0$  such that we have the following exact result of exponential convergence at rate  $\lambda_1/\lambda_0$ :*

$$(\lambda_0)^{-k} \langle \delta_x | \mathcal{T}^k f \rangle - h_0(x) \cdot \langle \mathbf{q}_0 | f \rangle = (\lambda_1/\lambda_0)^k \cdot h_1(x) \cdot \langle \mathbf{q}_1 | f \rangle, \quad (43)$$

*with the following bounds:*

$$|h_1| \leq C \cdot (K_{I,\rightarrow} \vee K_{O,\rightarrow}), \quad |\mathbf{q}_1|(dx) \leq C \cdot (\nu_{I,\rightarrow} \vee \nu_{O,\rightarrow})(dx).$$

*In particular,*

$$R_0 = \lim_k \langle \delta_x | \mathcal{T}^k \mathbf{1} \rangle^{1/k} = \lambda_0.$$

Before we proceed with the proof of Proposition S.4.2, let us interpret the quantities  $h_0$  and  $\mathbf{q}_0$ .

It follows from Proposition S.4.2 that  $\mathbb{E}_x[X_k] = \langle \delta_x | \mathcal{T}^k \mathbf{1} \rangle$  is asymptotically equivalent to  $(R_0)^k \cdot h_0(x)$ . This property is why it is reasonable to call  $h_0$  the survival capacity and what makes  $h_0$  relevant as an indicator of network centrality, see Section S.5.1. Furthermore, it motivates to consider the eigenmeasure  $\mathbf{q}_0$  because  $\mathbf{q}_0$  is involved in the normalization condition on  $h_0$ .

Actually, the density of  $\mathbf{q}_0$  at value  $x$  can be interpreted as the likelihood for a city randomly chosen among the infected cities at generation  $g$  to have size  $x$ , for large  $g$  in the branching approximation. More precisely, for any initially infected city  $u$  and on the event of survival of the branching approximation, we can demonstrate that the sequence of normalized random measures  $M^{(u;g)}(dx)/\langle M^{(u;g)} | \mathbf{1} \rangle$  converges to  $\mathbf{q}_0(dx)$  as  $g$  tends to infinity. In the above expression, we recall that  $M^{(u;g)}$  is the point measure on  $\mathbb{R}_+$  which

points (counted with multiplicity) correspond to the sizes of the cities that get infected from city  $u$  after  $g$  generations.

Indeed, the city sizes at generation  $g$  are prescribed by independent sampling with distributions  $\nu_{I,\rightarrow}$  and  $\nu_{O,\rightarrow}$  resp., conditionally on the numbers of cities infected from the inside and of those infected from the outside, at generation  $g$ . According to Proposition 3.2.1, these two numbers can be inferred by studying the process  $\mathbf{V}^2$ . In such setting of a discrete-type Galton-Watson processes, Kesten and P. Stigum (1966) provides a description of the relative proportions of the different types. In our case, it implies that asymptotically a proportion  $q_0^I$  of cities are infected from the inside. We also recall that on the event of survival, the number of infected cities at generation  $g$  tends a.s. to infinity with  $g$ . We then account for the next sampling of cities sizes, and recall that  $\mathbf{q}_0(dx) = q_0^I \nu_{I,\rightarrow}(dx) + (1 - q_0^I) \nu_{O,\rightarrow}(dx)$  to deduce the above claim of convergence thanks to the law of large number.

The study of the backward-in-time process is analogous. Recall that the eigenvalues of an adjoint operator are complex conjugates of the eigenvalues of the original operator. In our case, the eigenvalues of the backward operator  $\tilde{\mathcal{T}}$  simply coincide with the ones of  $\mathcal{T}$ , namely  $R_0 = \lambda_0$  and  $\lambda_1$ . On the other hand, the QSDs and the eigenvectors do not generally coincide, except in the specific case of the strategy  $P$ .

**Proof of Proposition S.4.2** Since  $W$  has positive entries, the Perron-Frobenius theorem ensures that  $W$  has two distinct real eigenvalues  $\lambda_0, \lambda_1$  of the form  $\lambda_0 > \max\{\lambda_1, 0\}$ . Also, the leading left and right eigenvectors have necessarily entries of the same sign, contrary to the corresponding eigenvectors of the second eigenvalue.

Assume that  $\mathbf{q}$  is an eigenmeasure of  $\mathcal{T}$  with eigenvalue  $\lambda$  (when  $\mathcal{T}$  is treated as an adjoint operator on measures).

Under  $\mathcal{T}$ , any non-negative measure  $\mu$  such that  $\langle \mu | K_{O,\rightarrow} \rangle$  and  $\langle \mu | K_{I,\rightarrow} \rangle$  are both finite is mapped to a measure uniquely prescribed as a linear combination of  $\nu_{O,\rightarrow}$  and  $\nu_{I,\rightarrow}$ . If either  $\langle \mathbf{q} | K_{I,\rightarrow} \rangle$  or  $\langle \mathbf{q} | K_{O,\rightarrow} \rangle$  would be infinite, then  $\mathbf{q}\mathcal{T} = \infty$ , which would contradict the fact that  $\mathbf{q}$  is an eigenmeasure of  $\mathcal{T}$ . This implies that  $\mathbf{q}$  can necessarily be expressed as follows:

$$\mathbf{q} = (q^O \quad q^I) \cdot \begin{pmatrix} \nu_{O,\rightarrow} \\ \nu_{I,\rightarrow} \end{pmatrix}.$$

From this representation and since  $\nu_{O,\rightarrow}$  and  $\nu_{I,\rightarrow}$  are not colinear, with Lemma S.4.1 it follows that  $\mathbf{q}\mathcal{T} = \lambda\mathbf{q}$  is equivalent to  $(q^O \quad q^I)$  being a left eigenvector of  $W$  with eigenvalue  $\lambda$ . In particular, recalling the Perron-Frobenius theorem the leading left eigenvector  $(q^O \quad q^I)$  of  $W$  and the leading eigenmeasure  $\mathbf{q}_0$  of  $\mathcal{T}$  (with leading eigenvalue  $\lambda_0$ ) can be chosen to be non-negative. By assuming further that  $q_0^O$  and  $q_0^I$  sum up to one and that  $\mathbf{q}_0$  is a probability measure and since  $\nu_{O,\rightarrow}$  and  $\nu_{I,\rightarrow}$  are probability measures, relationship (41) is fulfilled.

Similarly, under  $\mathcal{T}$ , any non-negative function  $f$  such that  $\langle \nu_{O,\rightarrow} | f \rangle$  and  $\langle \nu_{I,\rightarrow} | f \rangle$  are both finite is mapped to a function uniquely prescribed as a linear combination of  $K_{O,\rightarrow}$  and  $K_{I,\rightarrow}$ . Let  $\mathfrak{h}$  be an eigenfunction of  $\mathcal{T}$ . If either  $\langle \nu_{O,\rightarrow} | \mathfrak{h} \rangle$  or  $\langle \nu_{I,\rightarrow} | \mathfrak{h} \rangle$  would be infinite, then  $\mathcal{T}\mathfrak{h} = \infty$  which would contradict the fact that  $\mathfrak{h}$  is an eigenfunction of  $\mathcal{T}$ . This implies that  $\mathfrak{h}$  can necessarily be expressed as follows:

$$\mathfrak{h} = \begin{pmatrix} h^O & h^I \end{pmatrix} \cdot \begin{pmatrix} K_{O,\rightarrow} \\ K_{I,\rightarrow} \end{pmatrix}.$$

From this representation and since  $K_{O,\rightarrow}$  and  $K_{I,\rightarrow}$  are not colinear, with Lemma S.4.1 it follows that  $\mathcal{T}\mathfrak{h} = \lambda\mathfrak{h}$  is equivalent to  $\begin{pmatrix} h^O & h^I \end{pmatrix}^T$  being a right eigenvector of  $W$  with eigenvalue  $\lambda$ . Recalling Perron-Frobenius theorem, the leading eigenfunction  $h_0$  of  $\mathcal{T}$  and the leading right eigenvector  $\begin{pmatrix} h_0^O & h_0^I \end{pmatrix}^T$  can be chosen non-negative and such that  $\langle \mathfrak{q}_0 | h_0 \rangle = 1$  and  $q_0^O h_0^O + q_0^I h_0^I = 1$ . Let us denote by  $c > 0$  the constant such that  $h_0(x) = c \cdot (h_0^O K_{O,\rightarrow}(x) + h_0^I K_{I,\rightarrow}(x))$ . Then, with Lemma S.4.1,  $\langle \mathfrak{q}_0 | h_0 \rangle = 1$  translates into

$$c \cdot \begin{pmatrix} q_0^O & q_0^I \end{pmatrix} \cdot W \cdot \begin{pmatrix} h_0^O \\ h_0^I \end{pmatrix} = 1.$$

Recalling that  $\begin{pmatrix} h_0^O & h_0^I \end{pmatrix}^T$  is a right eigenvector of  $W$  with eigenvalue  $\lambda_0$  and that  $q_0^O h_0^O + q_0^I h_0^I = 1$ , it implies that  $c = 1/\lambda_0$  so that relation (42) fulfilled.

Finally, let  $\begin{pmatrix} q_1^O & q_1^I \end{pmatrix}$  be a left eigenvector of  $\mathcal{T}$  corresponding to the eigenvalue  $\lambda_1$ . It must satisfy that  $q_1^O \cdot h_0^O + q_1^I \cdot h_0^I = 0$ , because when eigenvectors of the different eigenvalues  $\lambda_0 > \lambda_1$  are considered, we have

$$\begin{aligned} \lambda_1 \cdot (q_1^O \cdot h_0^O + q_1^I \cdot h_0^I) &= \begin{pmatrix} q_1^O & q_1^I \end{pmatrix} \cdot W \cdot \begin{pmatrix} h_0^O \\ h_0^I \end{pmatrix} \\ &= \lambda_0 \cdot (q_1^O \cdot h_0^O + q_1^I \cdot h_0^I). \end{aligned}$$

Since  $h_0^O$  and  $h_0^I$  are positive, the signs of  $q_1^O$  and  $q_1^I$  are necessarily different. Similarly, any right eigenvector of  $W$  with eigenvalue  $\lambda_1$  has entries of opposite signs. Therefore, by rescaling appropriately, we can define  $\begin{pmatrix} h_1^O & h_1^I \end{pmatrix}^T$  as the unique left eigenvector of  $W$  such that  $q_1^O \cdot h_1^O + q_1^I \cdot h_1^I = 1$ . Define similarly as for the leading eigenvectors:

$$\begin{aligned} \mathfrak{q}_1 &:= q_1^O \cdot \nu_{O,\rightarrow} + q_1^I \cdot \nu_{I,\rightarrow} \\ h_1 &:= \frac{h_1^O}{\lambda_1} \cdot K_{O,\rightarrow} + \frac{h_1^I}{\lambda_1} \cdot K_{I,\rightarrow}. \end{aligned} \tag{44}$$

The spectral decomposition of  $W$  implies that for any reals  $\ell_O, \ell_I, f_O, f_I$  and  $k \in \mathbb{N}$ :

$$\begin{aligned} & (\ell_O \ \ell_I) \cdot W^k \cdot \begin{pmatrix} f_O \\ f_I \end{pmatrix} \\ &= \left[ (\lambda_0)^k \cdot (\ell_O h_0^O + \ell_I h_0^I) \cdot (q_0^O f_O + q_0^I f_I) \right. \\ & \quad \left. + \lambda_1^k \cdot (\ell_O h_1^O + \ell_I h_1^I) \cdot (q_1^O f_O + q_1^I f_I) \right]. \end{aligned}$$

Combined with Lemma S.4.1, (41), (42) and (44), it directly entails (43) and concludes the proof of Proposition S.4.2 with  $C := \max\{q_1^O, q_1^I, h_1^O, h_1^I\}$ .  $\square$

## S.5 Eigenvector centrality

### S.5.1 Notion of eigenvector centrality

In terms of the approximation by the forward in time branching process, one can get explicit formulas for a classical notion of centrality for epidemics evolving on a network, namely eigenvector centrality, which assigns to each city size  $x$  the value of the leading eigenfunction  $h_0(x)$ , see (Newman, 2010, Chapter 7), Bonacich (1987). It is a measure for the number of infections that are triggered when node  $x$  gets infected and hence, allows to compare the relative importance of the different cities during the course of an epidemic. The value is primarily of interest in situations where the goal of containing the epidemic is no longer within reach and the aim is instead to delay its progression. By targeting strict measures on cities with a high eigenvector centrality value, one wishes to target cities with a high potential for additional infections.

According to Proposition S.4.2, the leading eigenfunction  $h_0$  takes the following form:

$$h_0(x) = (R_0)^{-1} \cdot (K_{O,\rightarrow}(x) \cdot h_0^O + K_{I,\rightarrow}(x) \cdot h_0^I), \quad (45)$$

where the  $2 \times 1$  vector  $(h_0^O \ h_0^I)^T$  is the eigenvector of the  $2 \times 2$  transmission matrix  $W$ . Since  $W_{O,O} = W_{I,I}$  we arrive at the following expression for  $(h_0^O \ h_0^I)^T$  (with similar expressions for  $(q_0^O \ q_0^I)$ , the left eigenvector of  $W$ ):

$$\begin{aligned} h_0^O &:= \frac{\sqrt{W_{O,I}} + \sqrt{W_{I,O}}}{2\sqrt{W_{I,O}}}, \\ h_0^I &:= \frac{\sqrt{W_{O,I}} + \sqrt{W_{I,O}}}{2\sqrt{W_{O,I}}}, \end{aligned} \quad (46)$$

With these expressions one observes that the normalisation is such that  $(h_0^O \ h_0^I)^T$  is actually independent of the value of the thresholds  $p_\vee$  and  $L_\vee$  under strategy  $(P)$  and  $(U)$ , respectively.

The eigenvector centrality value  $h_0(x)$  can be decomposed into the two factors  $f_O(x) = (h_0^O/R_0) \cdot K_{O,\rightarrow}(x)$  and  $f_I(x) = (h_0^I/R_0) \cdot K_{I,\rightarrow}(x)$ . Since by definition  $K_{O,\rightarrow}$  and  $K_{I,\rightarrow}$  (cf (11)) depend polynomially on  $x$ , both factors are on a log scale linear functions in the city size.

### S.5.2 Estimation of eigenvector centrality

Complementary to the outbreak probability, the eigenvector centrality value provides additional insight into which cities mainly drive the epidemic. For large city sizes and large enough infection rate, outbreak probabilities cannot be distinguished. Eigenvector centralities of these cities are nonetheless still different, especially under strategy ( $P$ ), and higher centrality values actually correspond to higher risk factors (figures not shown). This lends support to the incentive to restrict the cities according to the full order of size.

Admittedly, the largest cities are in any case most likely to become infected early without strong prior regulation, so their contribution to the growth rate should not be sustained for long. However, this is all the more reason to put in place preventive restrictions in order to avoid secondary cases coming out of these cities.

In Section S.5.1, we argued that in our analytical model (with a kernel of the form (11)) the eigenvector centrality value is composed of the two factors  $f_O$  and  $f_I$  which depend on a log scale linearly on the city size. In the case of the French best fit kernel, both factors are nearly of equal magnitude, see Figure S11. In contrast, for the Polish best fit kernel, the eigenvector centrality value for large cities is predominantly influenced by the factor  $f_I$ , i.e. by infections imported by residents of large cities traveling to other areas and bringing back the disease. Conversely, for small Polish cities (those with fewer than  $10^5$  inhabitants), the eigenvector centrality value is primarily driven by the factor  $f_O$ , i.e. by infections imported into these smaller cities by visitors arriving from other locations.

Concerning Japan, the lower-panel displays very similar patterns as for France. Due to the lower quality of the kernel graph approximation for Japan, the exact values are not very reliable, yet the general trend still deserves to be remarked.

# Eigenvector centrality

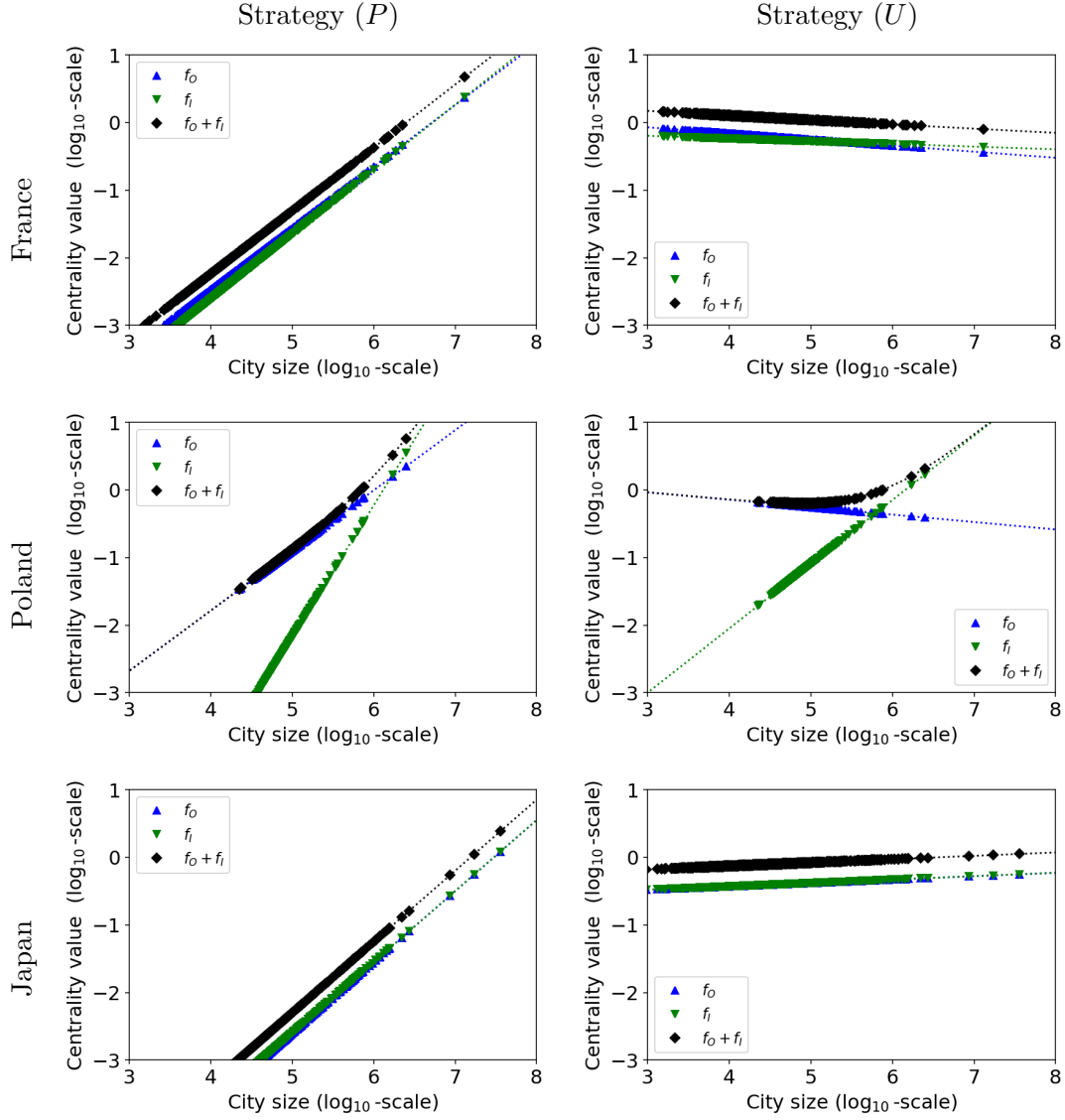


Figure S11: Decomposition of eigenvector centrality into the additive components  $f_O$  and  $f_I$  depending on city size in log-log plot, on the left under strategy (P) and on the right-panel under strategy (U), for data from France, Poland and Japan.

As expected, the heterogeneity in eigenvector centrality is much more pronounced for strategy ( $P$ ) than for strategy ( $U$ ), where the centrality value is close to a constant for Poland, slightly decreasing with population size for France, and slightly increasing for Japan. Since in France the estimated value of  $a$  is less than 1 and of  $b$  is less than 0, both attractiveness and emissivity reduce the role of large cities. Furthermore, under strategy ( $U$ ) the number of infected citizens does not increase with the city size.

As noted in Subsection S.5.1, eigenvector centrality values are independent of the threshold values, as would be outdegree with any natural normalisation. This is in stark contrast with outbreak probability, for which the inflection point (where the sigmoid function changes from being concave to convex) moves up with increasing threshold values (figures not shown). Contrary to outdegrees and eigenvector centrality values, outbreak probability makes visible the distinction between cities that are not likely to produce any outbreak and the others. On the other hand, it might be misleading in suggesting that all cities well above the inflection point are contributing equally. For strategy ( $P$ ), this suggestion is efficiently corrected by other measures like eigenvector centrality or outdegree.

## S.6 Further examination of goodness of approximations and estimates

In this section, we investigate the impact of several factors influencing the goodness of the applied approximations and estimates. In Section S.6.1, we discuss how the number of cities, size heterogeneity, and graph structures impact the estimation of the basic reproduction number. Section S.6.2 addresses the quality of KB analytical estimations of infection and outbreak probabilities, while Section S.6.3 is focused on the crucial role of data filtering methods.

### S.6.1 $R_0$ estimation: number of cities, size heterogeneity, graph structures

Recall from Section 5.7 that the  $R_0$  value could not get reliably estimated from the dynamics in the number of cities infected at each generation (even when we average over replications of outbreaks). So we investigate the effects responsible for this bad quality of the  $R_0$  estimation possibly due to (i) the too small number of cities, (ii) a tail of city size distributions that is too heavy and (iii) the specific graph structure. We check the validity of our proposed procedure for a range of power-law distributions.

Concerning (i), we anticipate that large cities are quickly hit and then isolated. This strongly reduces the number of secondary infections. To reduce this effect, we increase the number of cities by a factor 10 (without changing the city size distribution), by replicating each city size ten times. For both clarity and computational efficiency, we produce a kernel graph structure on this extended dataset, which we abbreviate as “10KG”, and compare in Figure S12 the results of the  $R_0$  estimation between the original kernel graph and the extended kernel graph. The  $R_0$  values is in both cases adjusted such that for cities of

## $R_0$ estimation for extended city size distributions

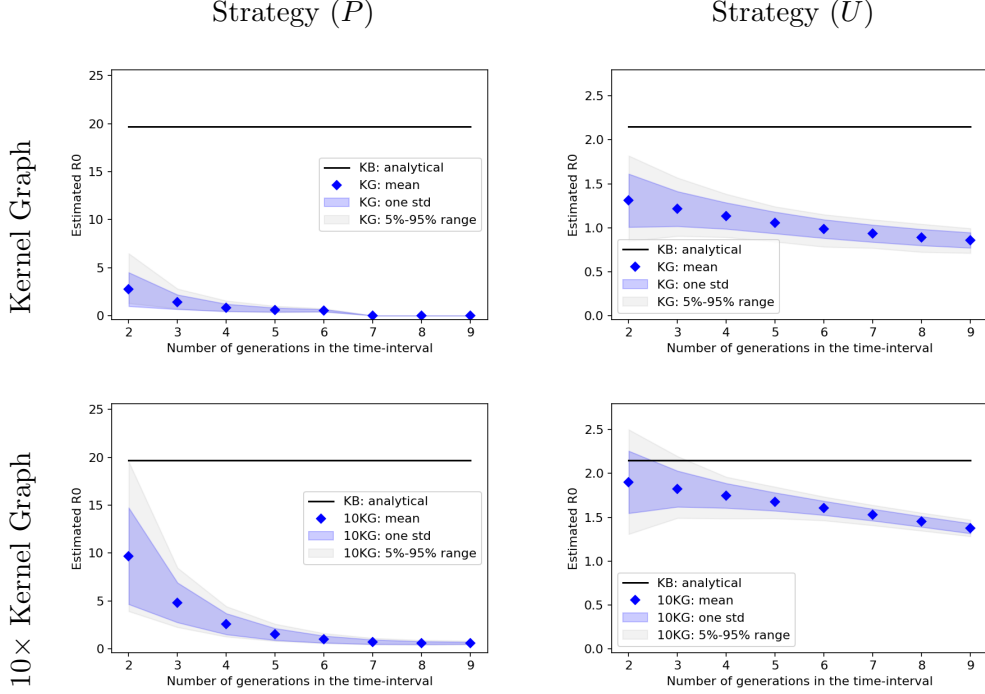


Figure S12:  $R_0$  estimation for the kernel graphs derived from the values of  $a$  and  $b$  of France (D30+) with the associated city size distributions (KG, top row) compared to the graph where these vertices are duplicated 10 times (10KG, bottom row), on the left for strategy ( $P$ ) and on the right for strategy ( $U$ ).

size  $10^5$  the theoretical infection probability is 0.5, see Section 4.2, which leads to identical values between these two graphs (and for the  $k_C$  values as well). There is a clear improvement with the extended graph, yet the estimations come close to the theoretical value only under strategy ( $U$ ) for a few generations (then still with large variations between runs). Furthermore, the decline of the estimated value with the number of generations considered is more strikingly visible. This confirms that the rapid establishment of immunity hinders the estimation of  $R_0$ .

Concerning (i) and (ii) we then consider other size distributions of 10,000 cities (of the order associated to 10KG) that are randomly sampled according to power-law distributions with various coefficients, namely  $\phi = 2, 3, 4$  and 5. In Figure S13, the corresponding estimations of  $R_0$  are compared between these different distributions, both under strategy ( $P$ ) (on



the left) and under strategy ( $U$ ) (on the right-panel), in the upper-panel with the original threshold of 10 infected cities (in a single generation, for the start of the estimation interval) and in the lower-panel with a larger threshold of 100 infected cities. As in Figure S12, the  $R_0$  values are adjusted such that for cities of size  $10^5$  the theoretical infection probability is 0.5. Since the corresponding values differ between the various sampled distributions, the estimations are rescaled by the expected value to ease the comparison. Furthermore, we set the estimated  $R_0$ -value to 0 for those generations for which less than 20 replicates (out of the 200 produced) keep a persistent outbreak over the whole interval of estimation.

We observe that the quality of  $R_0$ -estimation is also very poor with the most heterogeneous distribution, sampled according to a power-law coefficient of  $\phi = 2$ , yet much more suitable for the other distributions. The fluctuations between replicates are still very large when estimation starts with 10 infected cities. With the larger threshold of 100 infected cities, these fluctuations are largely reduced, which improves the quality of estimation though the estimator is significantly biased downwards. The increase in the number of generations produces similar effects as the one of the threshold, though not as large for the considered values.

Finally, concerning (iii), the role of the specific graph structure does not appear to be as significant as compared to the crucial role of the tail distribution, that we evaluated directly in the simplified kernel graph structure. Recall that simplifying the graph structure does not lead to a significant improvement of the estimation, as can be seen in the comparison between the transportation graph and the kernel graph (see Figure 9).

### S.6.2 Quality of the analytical estimations of infection and outbreak probabilities

We present in Figure S14 the convergence rate of the iterated procedures towards the infection/outbreak probabilities, see Section 4.1 and 4.2. For both strategies ( $U$ ) and ( $P$ ), the plots display a very clear trend of convergence (linear in log-scale) for both  $(\eta_O^k), (\eta_I^k)$  towards  $\eta_O$  and  $\eta_I$ , see (16) and (15), as well as for both (the analogously defined quantities)  $(\pi_O^k)$  and  $(\pi_I^k)$  towards  $\pi_O$  and  $\pi_I$ , see (17).

# $R_0$ estimation for various power-law distributions

## Strategy ( $P$ )

## Strategy ( $U$ )

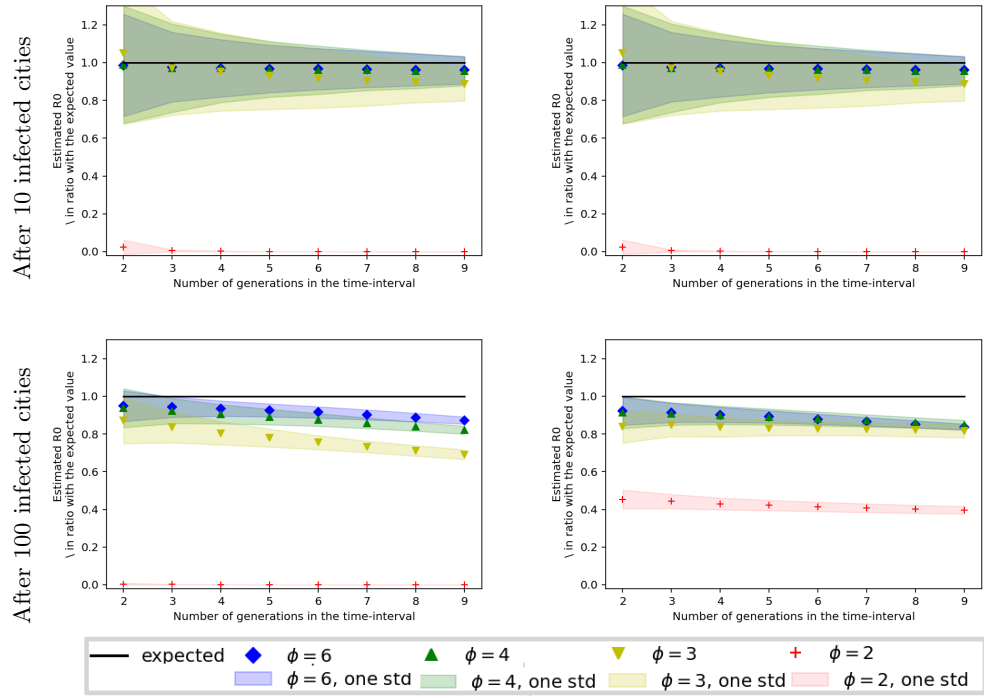


Figure S13:  $R_0$  estimation for the kernel graphs derived from the values of  $a$  and  $b$  of France (D30+) comparing city size distributions of  $10^4$  cities (of the order of 10KG) given with power-laws of coefficient 2, 3 4 and 6, on the left for strategy ( $P$ ) and on the right for strategy ( $U$ ). For the top row, the original threshold of 10 cities currently infected is considered, while for the bottom row, this threshold is set to 100 cities.

### Convergence of the analytical parameters

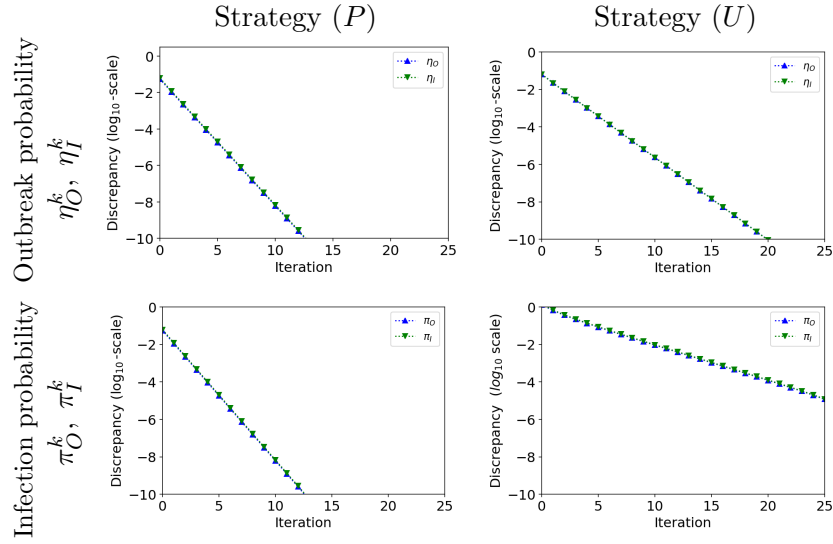


Figure S14: Convergence of  $(\eta_O^k), (\eta_I^k)$ , see (16), towards  $\eta_O$  and  $\eta_I$ , see (15), as well as of (the analogously defined quantities)  $(\pi_O^k)$  and  $(\pi_I^k)$  towards  $\pi_O$  and  $\pi_I$ , see (17), under strategy  $(P)$  (on the left) and under strategy  $(U)$  (on the right-panel). As a city size distribution  $\beta$  the empirical size distribution from France (D30+) is chosen. The upper-panel shows  $\log_{10}(|\eta_O^k - \eta_O^{30}|/\eta_O^{30})$  as well as the analogous quantity relative to  $\eta_I$  at the different iterations  $k = 0, \dots, 25$ , the lower-panel shows the analogous values for  $\pi_O$  and  $\pi_I$ . The constant  $k_C$  is chosen such that the theoretical infection probability (approximated at a large enough iteration) is 0.5.

### S.6.3 Role of the methods for adjusting the virulence parameter and for filtering the datasets

Firstly, figure S15 is an alternative way of presenting the curves displayed in Figures 3 and 6 by treating each country in a separate panel.

Figures S16 and S17 complement Figures 4 and 5 with a focus on the infection and the outbreak probabilities, respectively. Both strategies ( $U$ ) and ( $P$ ) and the three countries France, Poland and Japan are again considered with the distance restriction D30+, recall Section 5.1. The difference to Figures 4 and 5 is that the  $R_0$  value, through the parameter  $k_C$ , is adjusted according to the theoretical outbreak probability (rule  $pO$ ) instead of the theoretical infection probability (rule  $pI$ ) (the probability is set equal to 0.5 for a city of size  $10^5$ ).

We make the same observations for these Figures S16 and S17 as for the Figures 4 and 5: (i) there is a relatively good fit for Poland except for the outbreak probability under strategy ( $U$ ), consistent though less optimal compared to France; (ii) the fit is poor for Japan, simply less visible under the rule  $pO$  for the infection probability under strategy ( $U$ ) because the corresponding values are very close to 0.

However, even though the fit is similar under rule  $pO$  and  $pI$ , we would recommend a fit according to rule  $pI$ , since the outbreak probability is not fitted well under strategy ( $U$ ).

In the following Figures S18-S23 we show how the restriction on the distance affects the fits of simulated and theoretical infection and outbreak probabilities. The plots associated with datasets where no distance restrictions were applied (i.e. with the datasets D1+) are shown in Figures S18, S20 and S22, while those with a distance restriction below 50km (i.e. with the datasets D50+) are shown in Figures S19, S21 and S23, for respectively France, Poland and Japan. For reasons explained just above, we present only the results obtained under rule  $pI$ , and actually we see already under this rule that the theoretical outbreak probability is not fitted well either under strategy ( $U$ ) with these datasets D1+ and D50+.

Considering the datasets D50+ in comparison to the datasets D30+ does not lead qualitatively to different conclusions. Especially for France and for Poland, good fits are preserved (with only a slight deterioration) for scenarios that have already shown good performances for D30+, recall Figures 4 and 5.

For Japan, the fit is similarly poor as for D30+. Of note are also the levels of fluctuations, which are significantly larger than for the corresponding kernel graphs, similarly for D50+ as for D30+.

Considering the datasets D1+ instead of the datasets D30+ do generally lead to fits that are not satisfying. For France and Poland the general trend is preserved with an however much poorer fit especially for large cities.

This observation confirms our original expectation that the restriction on relatively long-distance travels is essential for infection dynamics not to be blurred by spatially correlated

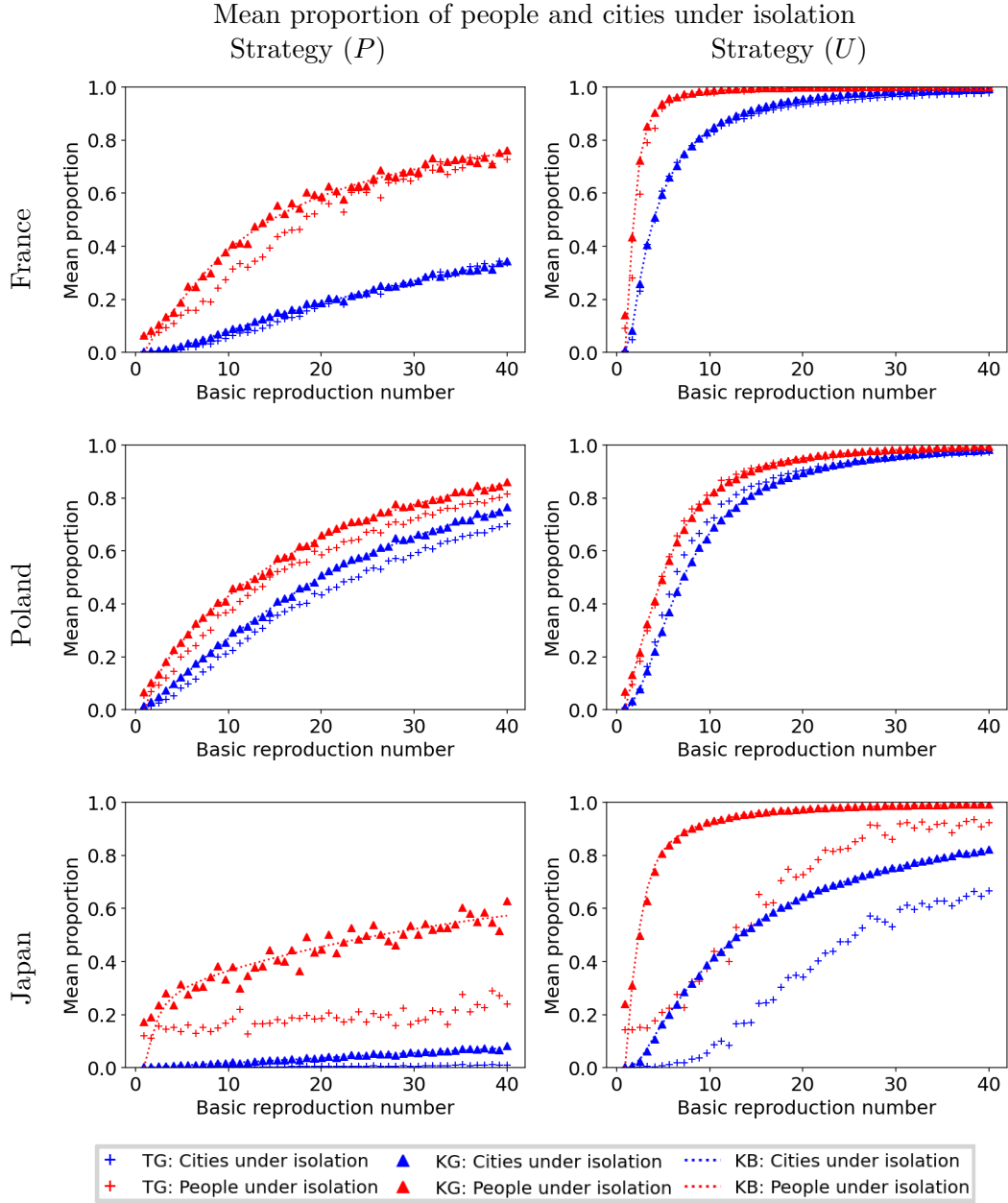


Figure S15: Comparison of the theoretical and simulated proportion of infected cities and isolated persons depending on the basic reproduction number for mobility data from France, Poland and Japan in the upper, middle and lower row, resp.

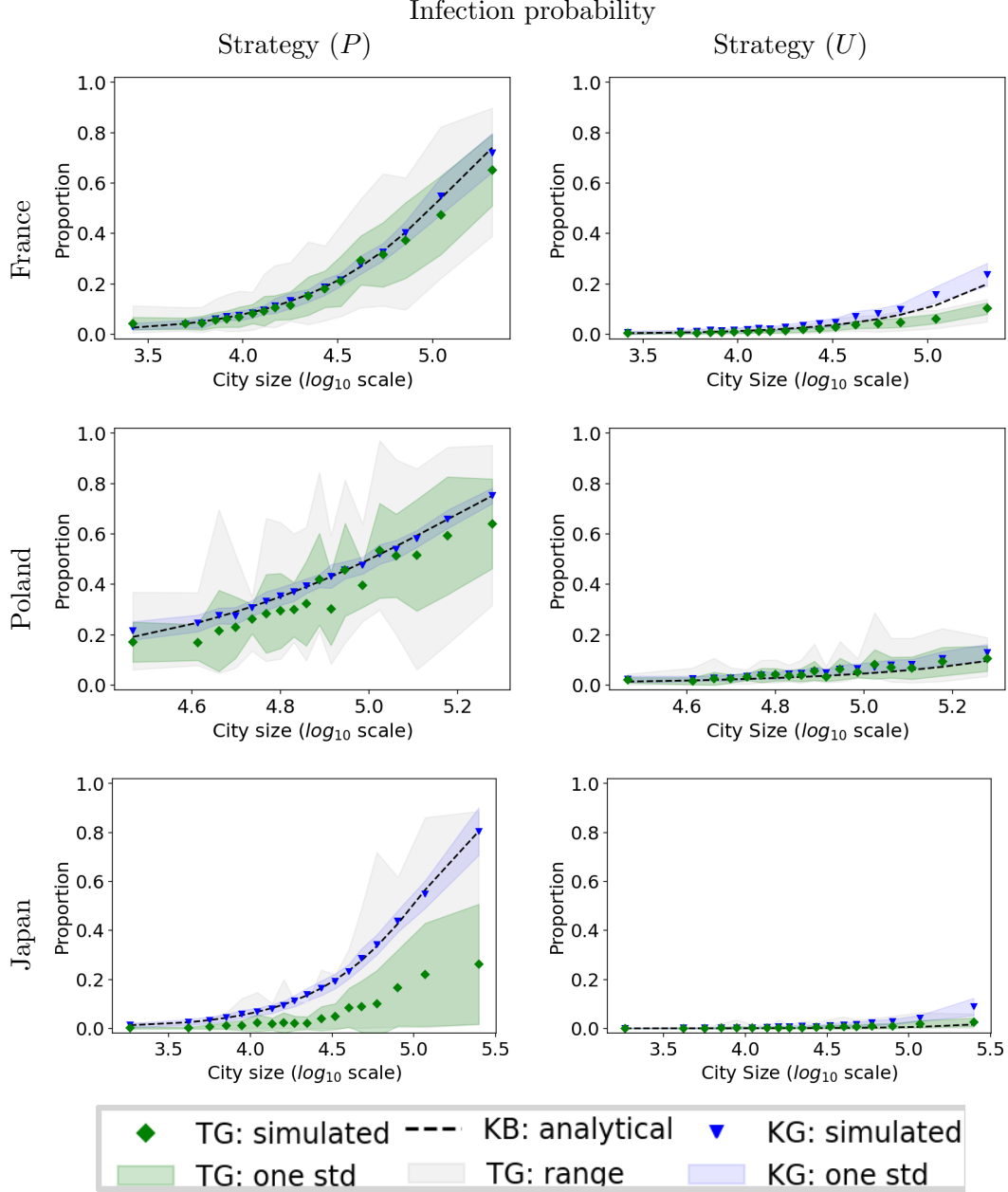


Figure S16: Comparison of simulated and theoretical infection probabilities, on the left for strategy (P) and on the right for strategy (U) for mobility data from France, Poland and Japan in the upper, middle and lower row, resp. The  $R_0$  value is adjusted such that for cities of size  $10^5$  the theoretical outbreak probability is 0.5, see Section 5.4.

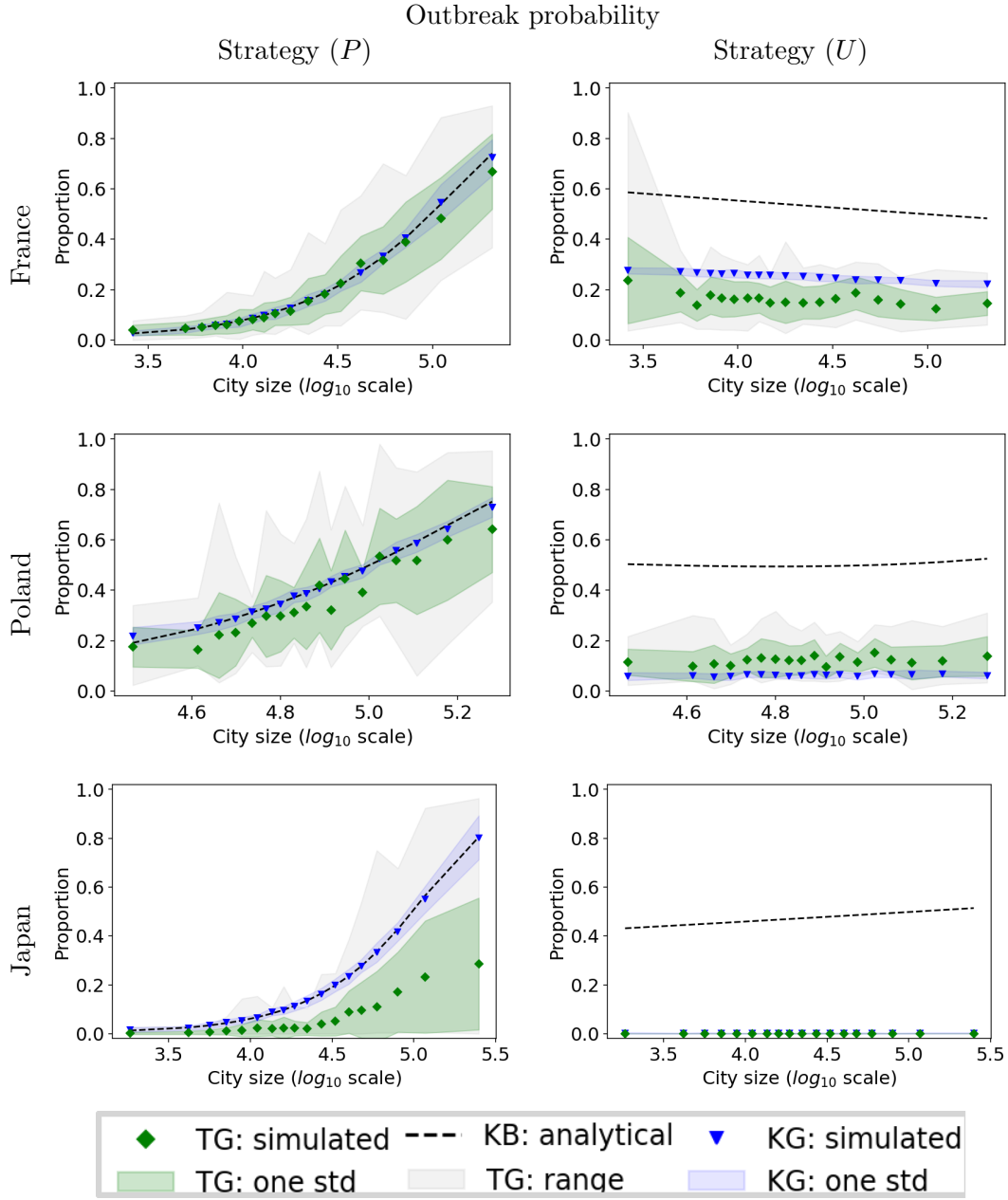


Figure S17: Comparison of simulated and theoretical outbreak probabilities, on the left for strategy ( $P$ ) and on the right for strategy ( $U$ ) for mobility data from France, Poland and Japan in the upper, middle and lower row, resp. The  $R_0$  value is adjusted such that for cities of size  $10^5$  the theoretical outbreak probability is 0.5, see Section 5.4

short-distance travels and to characterize the potential attraction effects of the largest cities. The comparison with the case of the D1+ dataset exemplifies that a very specific structure of the transportation graph is needed for the prediction with the kernel graph to inform about this spatial model. The heterogeneity in the city size distribution is not the only factor involved. The restriction on distant infection events between cities in this synthetic model isolates a very specific contribution of migrations that is captured both by the D30+ and D50+ datasets. We did not check larger values of distance restrictions because we do not see any specific interpretation of such choices, contrary to around 30-50km distances. The reduction in the migration frequency beyond these distances was previously noted in studies of work-mobility Destatis (2022).

The difference between D30+ and D50+ on the one hand and D1+ on the other hand is also a reminder that the infection probability that is inferred (especially for D30+ and D50+) only corresponds to the direct aftermath of the first wave, that is to be followed and strengthened through much more local spread of the disease. Note that the available transportation matrix (even for D1+) is not that reliable at predicting short-distance travels, while we expect the long-distance travels to be more accurately reflected by this work-related mobility. This distinction in the reliability of the data is even more pronounced in times where isolation strategies are applied preventively, due to the spontaneous change in migration behavior that is likely to happen.

There are several reasons that lead to a much worse fit of D1+ data in comparison to D30+ or even D50+ data. Notably, we observe a significant change of the attractiveness coefficient  $a$  as well as the emissivity coefficient  $b$  for D1+ data for France and Poland (while it is conserved for Japan). For short-distance travels, proximity of cities plays a stronger role than the sizes of the cities. The kernel graph model and in particular the coefficients  $a$  and  $b$  do therefore not accurately capture the dynamics of local spread. Nonetheless regarding the infection probability, the main observation is that the probability derived from the transportation graph (TG) is in general lower than the estimate derived from the analytical formula, the latter being similar to the one derived from the kernel graph (KG). This discrepancy could actually be largely compensated by making the  $R_0$  value larger for TG, then with possibly very similar relations between infection probabilities and city sizes (figures not shown for both strategy ( $U$ ) and ( $P$ ), for Poland and to a lesser extent for France). This hints at the fact that a dumping effect is produced due to the spatial correlations induced by short-distance infection events, as compared to the branching approximation. In practice, the effective  $R_0$  value appears to be reduced when comparing the estimations derived from TG to the analytical ones.

For Japan, the fit is not good for any of the considered distance restrictions, which makes it more delicate to interpret the observed discrepancies. Nonetheless, we can say that the spread is much reduced on the transportation graph as compared to the branching graph (agreeing well with the kernel graph situation also for Japanese data). Regarding the relation between the mean proportion of people under isolation as a function of the



basic reproduction number in Figure S22, there is presumably a significant contribution of the choice of the initially infected city (according to the distribution  $\nu_{O,\rightarrow}$ ). Given that the largest unit in Japan comprises around 28% of the whole population and is likely to be this first choice, the relatively high value of people under isolation is reasonable even when only a tiny fraction of cities is under isolation.

Since we observe that the proportion of people under isolation follows a similar curve as the proportion of cities under isolation with a relatively constant difference under strategy ( $U$ ) and ( $P$ ) for the D1+ dataset, we conjecture that besides this initially infected city, the infection probability is not depending much on the city size. This hints at a very strong effect of the spatial correlations in the epidemics derived from this japanese dataset. This is in contrast to the prediction derived from the branching approximation, where we observe a much larger initial slope for the proportion of people under isolation than for the one of cities under isolation.

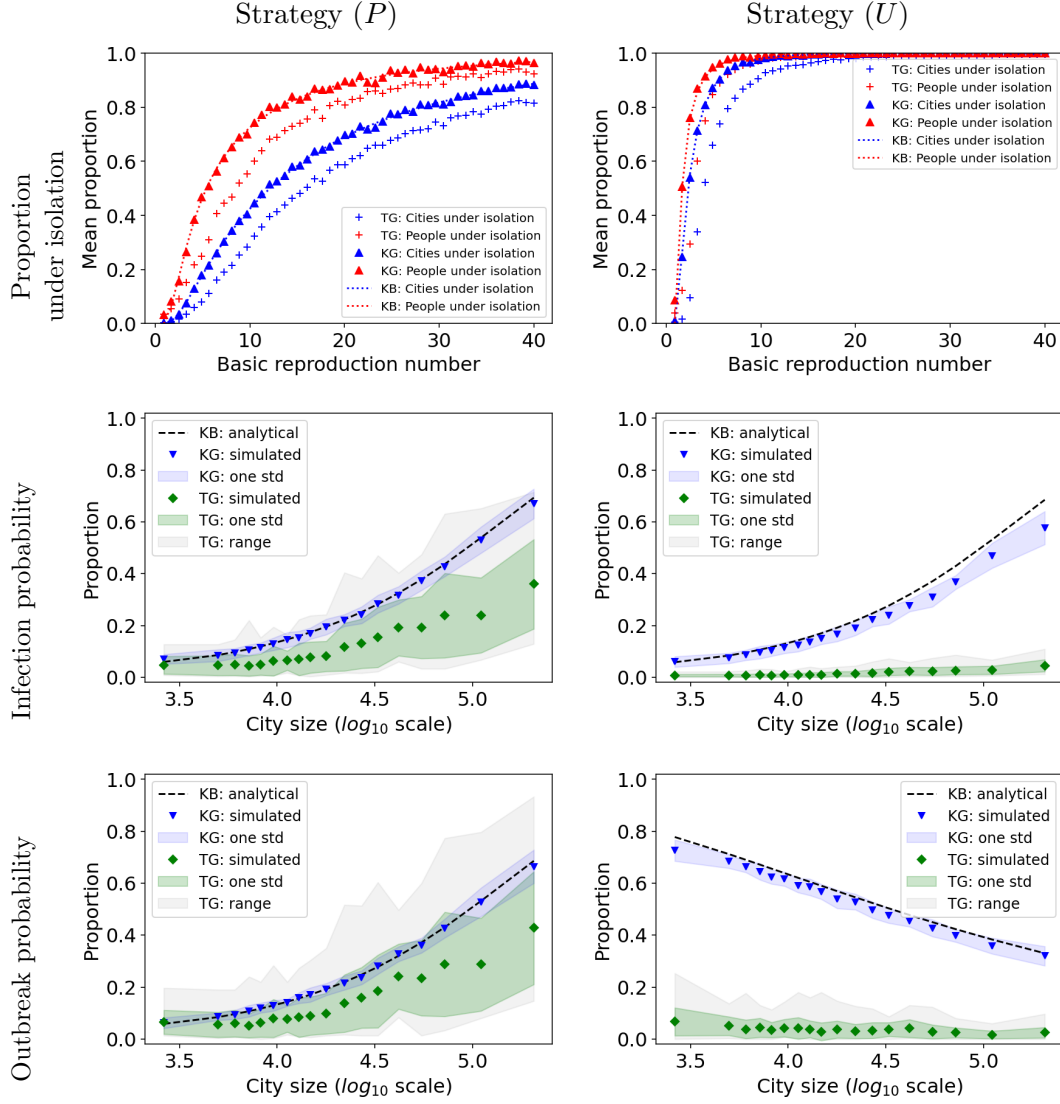


Figure S18: Comparison of infected cities and isolated cities as a function of the theoretical  $R_0$  value (top row) of simulated and theoretical infection (middle row) and outbreak probabilities (bottom row), on the left for strategy (P) and on the right for strategy (U), for France without restriction on the distance (data abbreviated as D1+). The  $R_0$  value is adjusted such that for cities of size  $10^5$  the theoretical infection probability is 0.5, see Section 5.4.

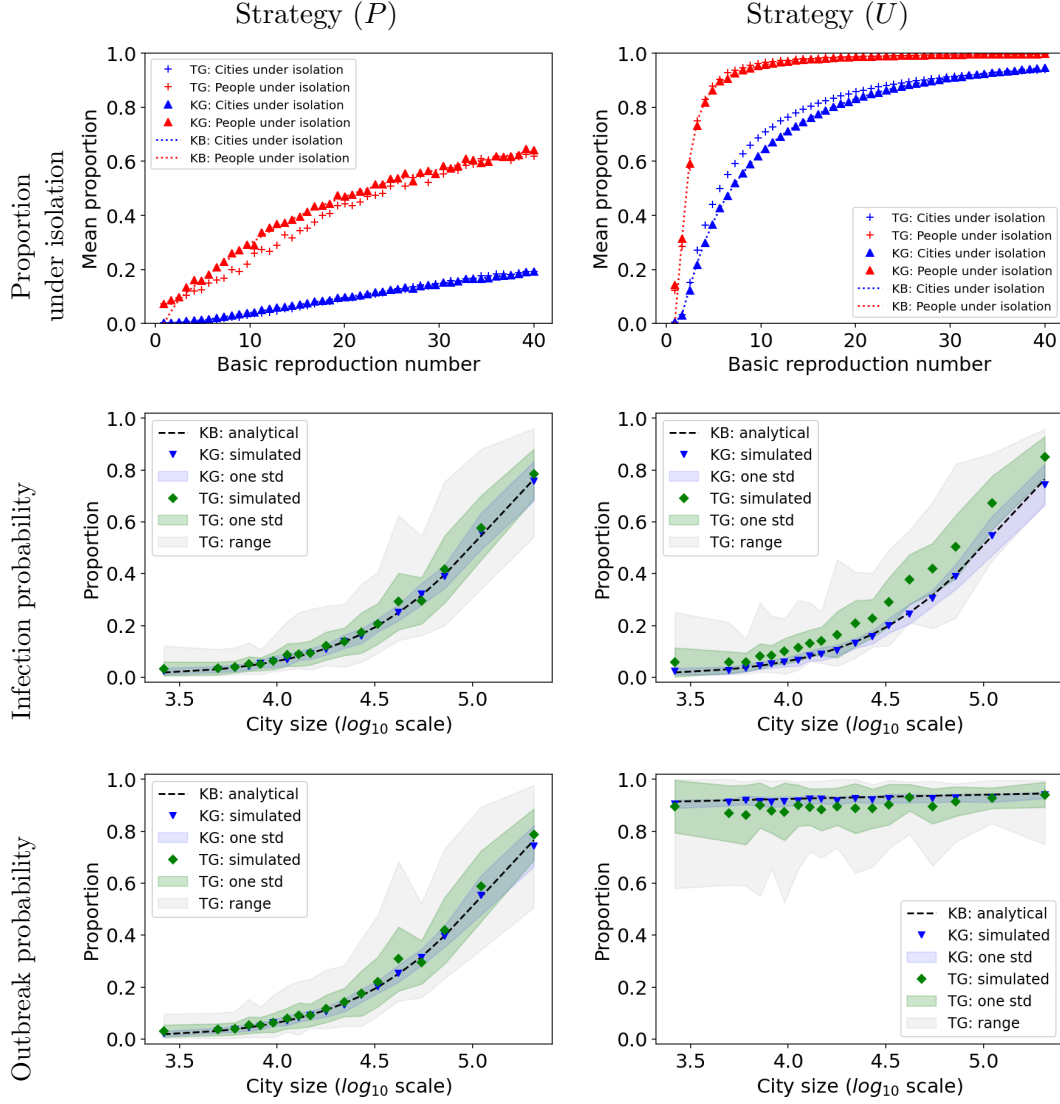


Figure S19: Comparison of infected cities and isolated cities as a function of the theoretical  $R_0$  value (top row) of simulated and theoretical infection (middle row) and outbreak probabilities (bottom row), on the left for strategy (P) and on the right for strategy (U), for France with a restriction on the distance of 50km (data abbreviated as D50+). The  $R_0$  value is adjusted such that for cities of size  $10^5$  the theoretical infection probability is 0.5, see Section 5.4.

Poland D1+

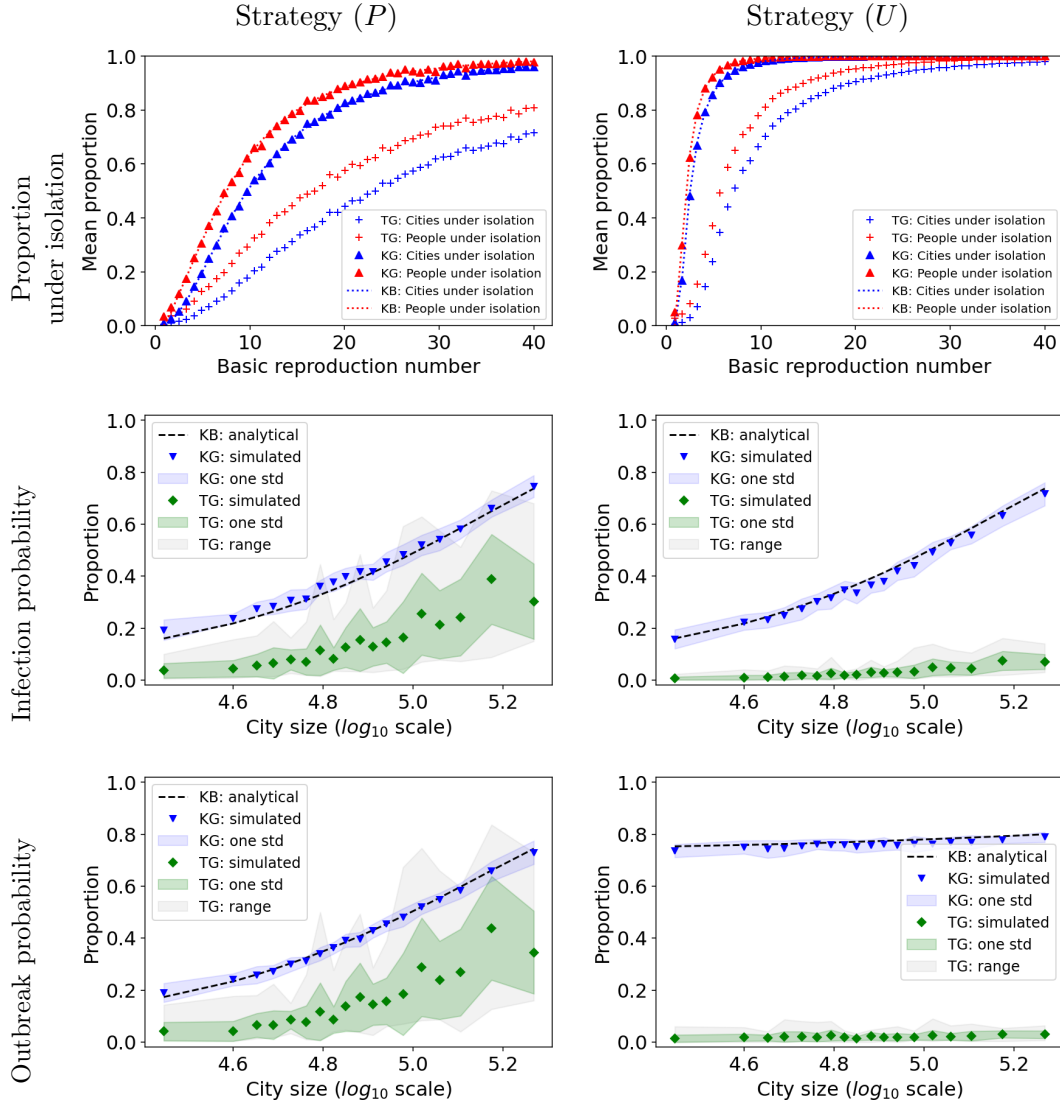


Figure S20: Comparison of infected cities and isolated cities as a function of the theoretical  $R_0$  value (top row) of simulated and theoretical infection (middle row) and outbreak probabilities (bottom row), on the left for strategy (P) and on the right for strategy (U), for Poland without restriction on the distance. The  $R_0$  value is adjusted such that for cities of size  $10^5$  the theoretical infection probability is 0.5, see Section 5.4.

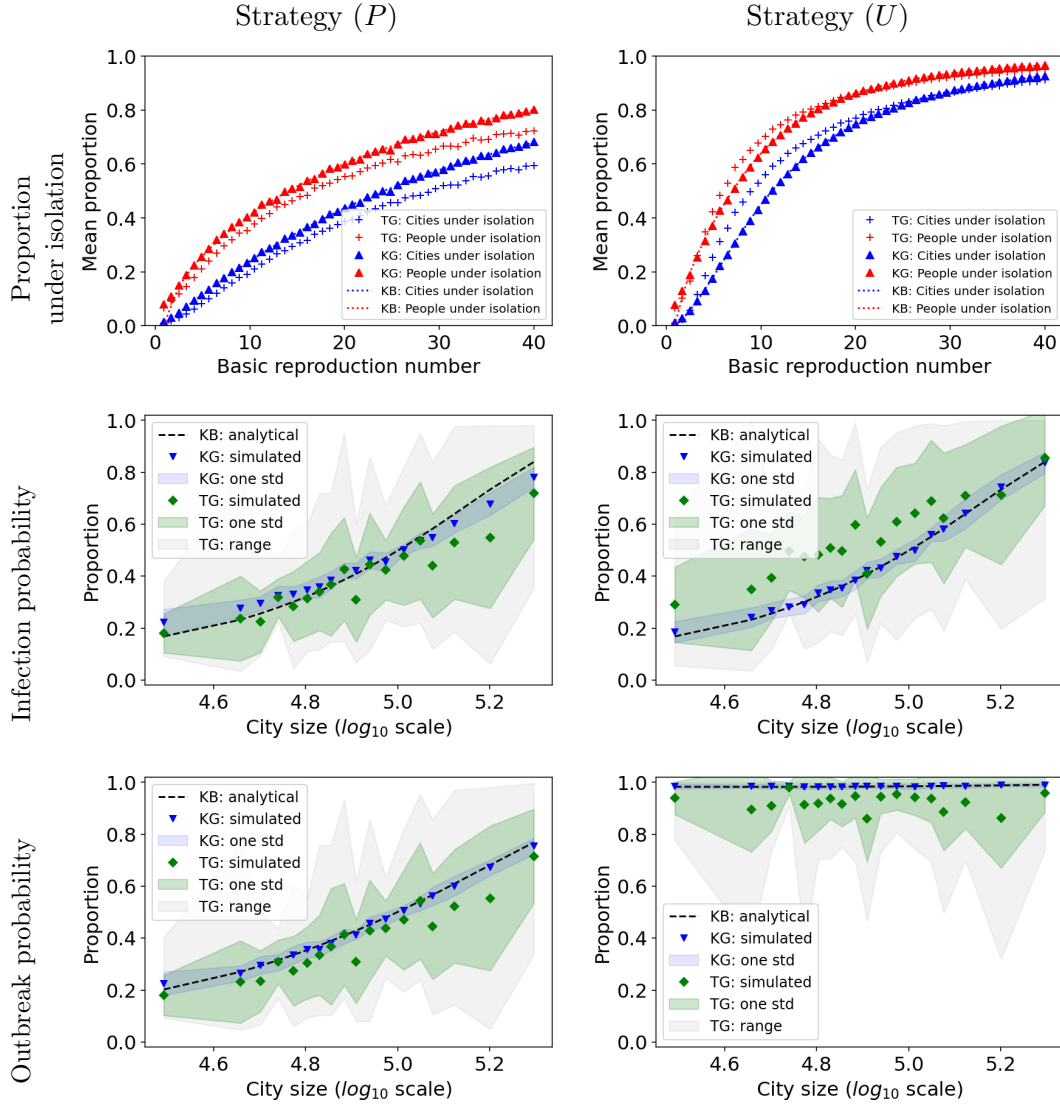


Figure S21: Comparison of infected cities and isolated cities as a function of the theoretical  $R_0$  value (top row) of simulated and theoretical infection (middle row) and outbreak probabilities (bottom row), on the left for strategy (P) and on the right for strategy (U), for Poland with a restriction on the distance of 50km. The  $R_0$  value is adjusted such that for cities of size  $10^5$  the theoretical infection probability is 0.5, see Section 5.4.

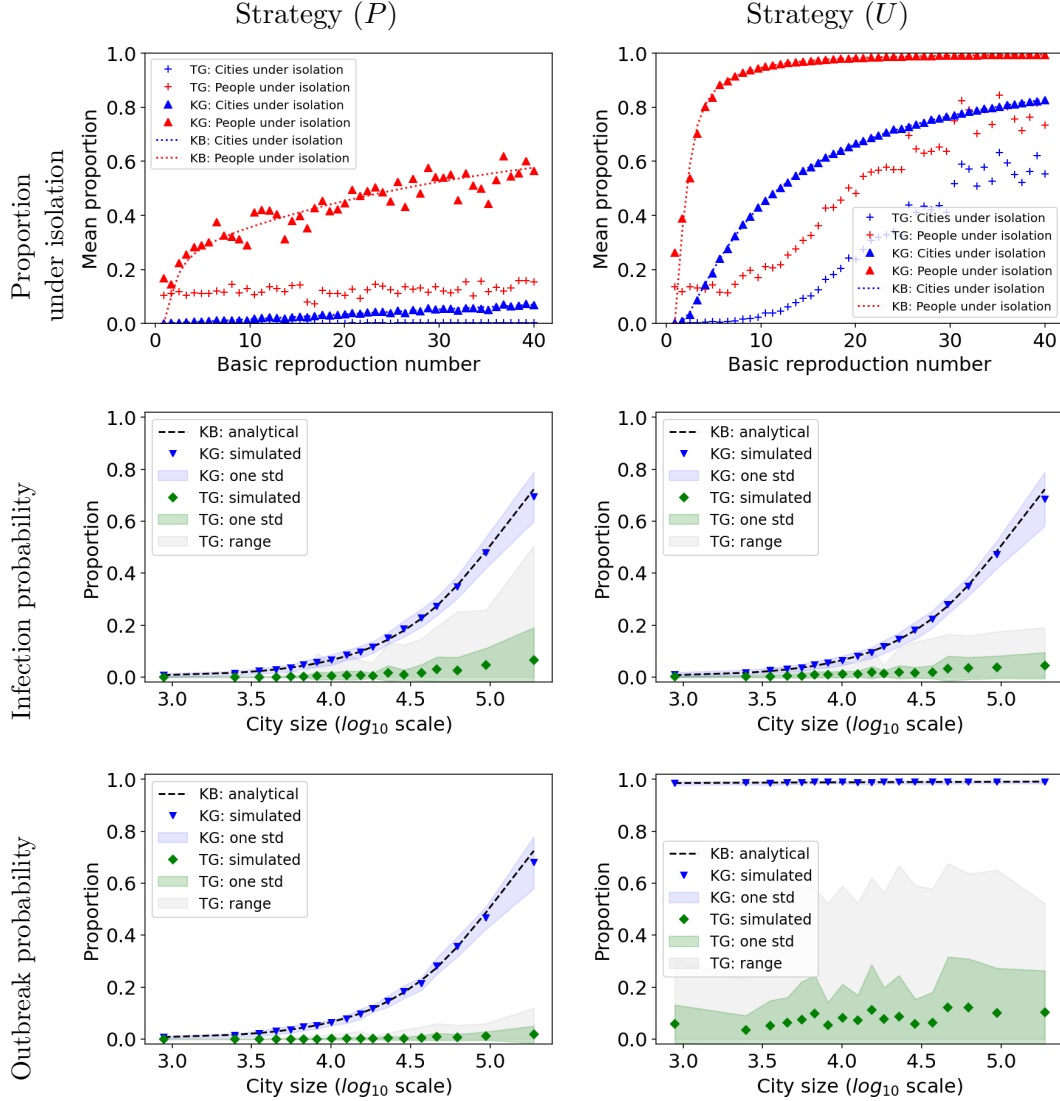


Figure S22: Comparison of infected cities and isolated cities as a function of the theoretical  $R_0$  value (top row) of simulated and theoretical infection (middle row) and outbreak probabilities (bottom row), on the left for strategy (P) and on the right for strategy (U), for Japan without restriction on the distance. The  $R_0$  value is adjusted such that for cities of size  $10^5$  the theoretical infection probability is 0.5, see Section 5.4.

Japan D50+

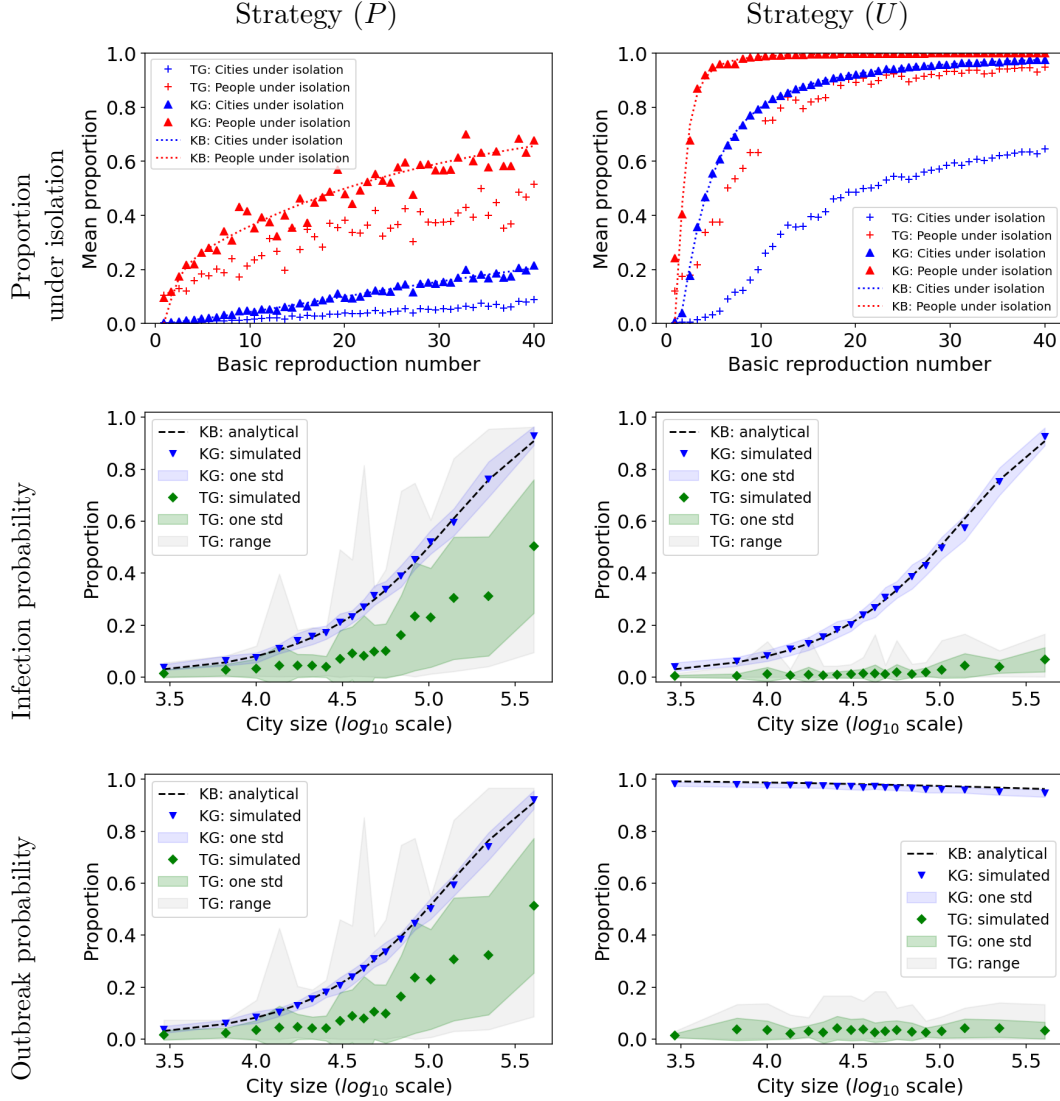


Figure S23: Comparison of infected cities and isolated cities as a function of the theoretical  $R_0$  value (top row) of simulated and theoretical infection (middle row) and outbreak probabilities (bottom row), on the left for strategy (P) and on the right for strategy (U), for Japan with a restriction on the distance of 50km. The  $R_0$  value is adjusted such that for cities of size  $10^5$  the theoretical infection probability is 0.5, see Section 5.4.